DOI:10.14753/SE.2022.2613

Functional recovery of the post-ischemic kidney after delayed contralateral nephrectomy: Pivotal role of inflammation and miRNAs

PhD thesis

Pál Tod

Doctoral School of Theoretical and Translational Medicine

Semmelweis University

Supervisors:	Péter Hamar, MD, Ph.D, D.Sc
	Gábor Szénási, C.Sc
Official reviewers:	György Losonczy, MD, PhD, D.Sc
	Csaba Kálmán Ambrus, MD, PhD
Head of the Final Examination Committee:	György Reusz, MD, Ph.D, D.Sc
Members of the Final Examination Committee:	Tamás Terebessy, MD, Ph.D
	Attila Cselenyák, Ph.D

Budapest

2021

DOI:10.14753/SE.2022.2613

Contents

DOI:10.14753/SE.2022.2613

1. Abbreviations

α-SMA: alpha-smooth muscle actin
AGO: argonaute protein
AKI: acute kidney injury
ANOVA: analysis of variance
BSA: bovine serum albumin
BUN: blood urea nitrogen
C: complement component
CCL2: chemokine C-C motif ligand 2
Cd2ap: CD2-associated protein
Cdk17: cyclin-dependent kinase 17
cDNA: complementary deoxyribonucleic acid
CKD: chronic kidney disease
Col: collagen
Crebrf: CREB3 regulatory factor
Cq: comparative quantification
DAMP: damage-associated molecular pattern
DC: dendritic cell
DN: diabetic nephropathy
ECM: extracellular matrix
ER: endoplasmic reticulum
ESRD: end-stage renal disease
FC: fold change
FN: fibronectin
GFR: glomerular filtration rate
HIF: hypoxia-inducible factor
HMGB1: high-mobility group box 1
IKKβ: IκB kinase β
IL: interleukin
IR: ischemia-reperfusion
IRAK-M: interleukin-1 receptor-associated kinase-M
IRI: ischemia reperfusion injury
JNK: c-jun NH2-terminal kinase
KIM-1: kidney injury molecule-1
KO: knock-out
LCN2: lipocalin-2
LPS: lipopolysaccharide
miRISC: microRNA-induced silencing complex
MRE: microRNA response element
miR: microRNA
mRNA: messenger RNA
miRNA: microRNA
MSC: mesenchymal stem cell
NADH: nicotinamide adenine dinucleotide
NF-κB: nuclear factor-κB
NMRI: Naval Medical Research Institute
NRF2: Nuclear factor erythroid 2–related factor
Nx: nephrectomy
PAS: periodic-acid Schiff
PDCD4: programmed cell death protein 4
PVDF: polyvinylidene difluoride
PKD: polycystic kidney disease
Plxna2: plexin A2
Pre-miRNA: precursor microRNA
Pri-miRNA: primary microRNA
PTEN: phosphatase and tensin homolog
RIPA: radioimmunoprecipitation assay

rRNA: ribosomal RNA
RNA: ribonucleic acid
ROS: reactive oxygen species
RT: reverse transcription
RT-qPCR: quantitative reverse transcription polymerase chain reaction
S: sham
TBS-T: Tris-buffer saline with Tween 20
TGF-β: transforming growth factor-β
TLR: toll-like receptor
TNF-α: tumor necrosis factor-alpha
UTR: untranslated region
UUO: unilateral ureteral obstruction
VHL: von Hippel-Lindau

2. Introduction

2.1. Acute kidney injury (AKI): definition and etiology

AKI is defined as an acute elevation of serum creatinine level (at least by 0.3 mg/dl (26.5µmol/l) within 48 hours or as a 1.5-fold increase in serum creatinine concentration from baseline (supposedly within 7 days) or as a reduction in urine output (to less than 0.5 ml/kg/h for at least 6 hours) (1). Based on the severity, AKI is categorized into three stages (Table 1).

Stage	Serum creatinine level	Urine output
1	1.5-1.9-fold elevation or at least 0.3 mg/dl (26.5µmol/l) increase from baseline	less than 0.5ml/kg/h for more than 6 hours
2	2-2.9-fold elevation from baseline	less 0.5 ml/kg/h for more than 12 hours
3	3-fold elevation or at least 1 mg/dl (353.6 µmol/l) increase from baseline	less than 0.3ml/kg/h for more than 24 hours or anuria is present for more than 12 hours

Table 1. Stages of acute kidney injury based on serum creatinine levels and urine output defined in Kidney Disease: Improving Global Outcomes (KDIGO) Clinical Practice Guideline for Acute Kidney Injury (1).

The AKI staging system depends only on serum creatinine concentration and urine output. However, the sensitivity of serum creatinine and the frequently used blood urea nitrogen (BUN) is limited to estimate glomerular filtration rate (GFR). More than half of the kidney function can be lost before detection of serum creatinine elevation (2). Furthermore, serum creatinine concentration is altered by several non-renal factors such as age, sex, muscle mass or medications, while BUN is influenced by the catabolic state, volume status or medications, among others (3). Thus, novel biomarkers would be beneficial for earlier detection and better clarification of AKI etiology.

AKI is a substantial medical burden associated with high morbidity and mortality (4). Several risk factors are known to predispose patients to develop AKI, such as age, cardiovascular diseases, sepsis and nephrotoxins (5). According to the meta-analysis of Susantitaphong et al. (6), approximately 1 in 5 adult patients and 1 in 3 children acquired KDIGO-defined AKI during hospital care worldwide. The pooled AKI-associated mortality rates were around 24% in adults and 14% in children.

The etiology of AKI can be divided into three categories: pre-renal, intrinsic AKI and post-renal. While the pre- and post-renal AKI is caused by extrarenal pathologies, intrinsic AKI is induced by kidney specific diseases. The GFR decline is associated with renal hypotension in pre-renal AKI. In post-renal AKI, an acute obstruction of urine flow is responsible for the GFR decrease. In intrinsic AKI, glomeruli can be damaged by, among others, glomerulonephritis, blood vessels occlusion by thrombosis, stenosis or the tubulointerstitium can be injured by nephrotoxic drugs or by ischemia-reperfusion injury (IRI). It has to be emphasized that renal ischemia is one of the leading causes of AKI (7).

2.2. Ischemia-induced blood flow dysregulation induces inflammation in the kidney

Under ischemic conditions, the blood supply to the kidney is severely deteriorated resulting in inadequate oxygen and nutrient supply and impaired removal of waste products (8). The kidney has high oxygen demand that requires high blood supply relative to other organs for its physiological activity, shown by the close relationship between renal blood flow and sodium transport. Hence, the kidney is highly susceptible to injuries, which interfere with oxygen supply (9). Further damage occurs during reperfusion of the ischemic renal tissue. When the blood flow is reestablished the oxygen reintroduction causes massive increases in reactive oxygen species (ROS) production in the mitochondria that leads to oxidative damage and impaired adenosine triphosphate production. The mitochondrial damage results in the release of damage-associated molecular patterns (DAMPs), which induces proinflammatory processes (see below) (10).

Renal blood flow is not equally reduced in all regions of the kidney during ischemia. Blood supply to the outer medulla is reduced more than to other regions of the kidney due to, among others, arteriolar vasoconstriction and interstitial edema induced by increased vascular permeability (11). IRI causes endothelial cell damage, and the consequent increase in endothelial chemokine expression recruits leukocytes, which secrete proinflammatory cytokines that further compromise renal blood flow and worsen inflammation by increasing vascular permeability particularly in the outer medulla (8, 12).

Damage to the proximal and distal tubular epithelium also contributes to the development of AKI in IRI (13). AKI activates the production of kidney injury molecule-

1 (KIM-1) mainly in the proximal tubules, and Lipocalin-2 (LCN2, or neutrophil gelatinase-associated lipocalin) mainly in the distal tubules (8). Both KIM-1 and LCN2 are frequently investigated as potential biomarkers (3). Our laboratory found that the ratio of urinary/plasma LCN2 concentration is a specific and sensitive marker of mild, IRI-induced AKI. Furthermore, results of experiments utilizing neutrophil-deficient animals indicated that neutrophils are not the main source of LCN2 in IRI-induced AKI in mice (14).

The most severe injury can be seen in the S3 segment of the proximal tubule, which is located in the outer medulla, and characterized by brush border loss, tubule dilatation and tubular cast deposition (8, 15). Furthermore, the severity of ischemia-reperfusion (IR)-induced AKI depends on the duration of IR. Longer IR induces more robust tubulointerstitial injury (Figure 1) (16).

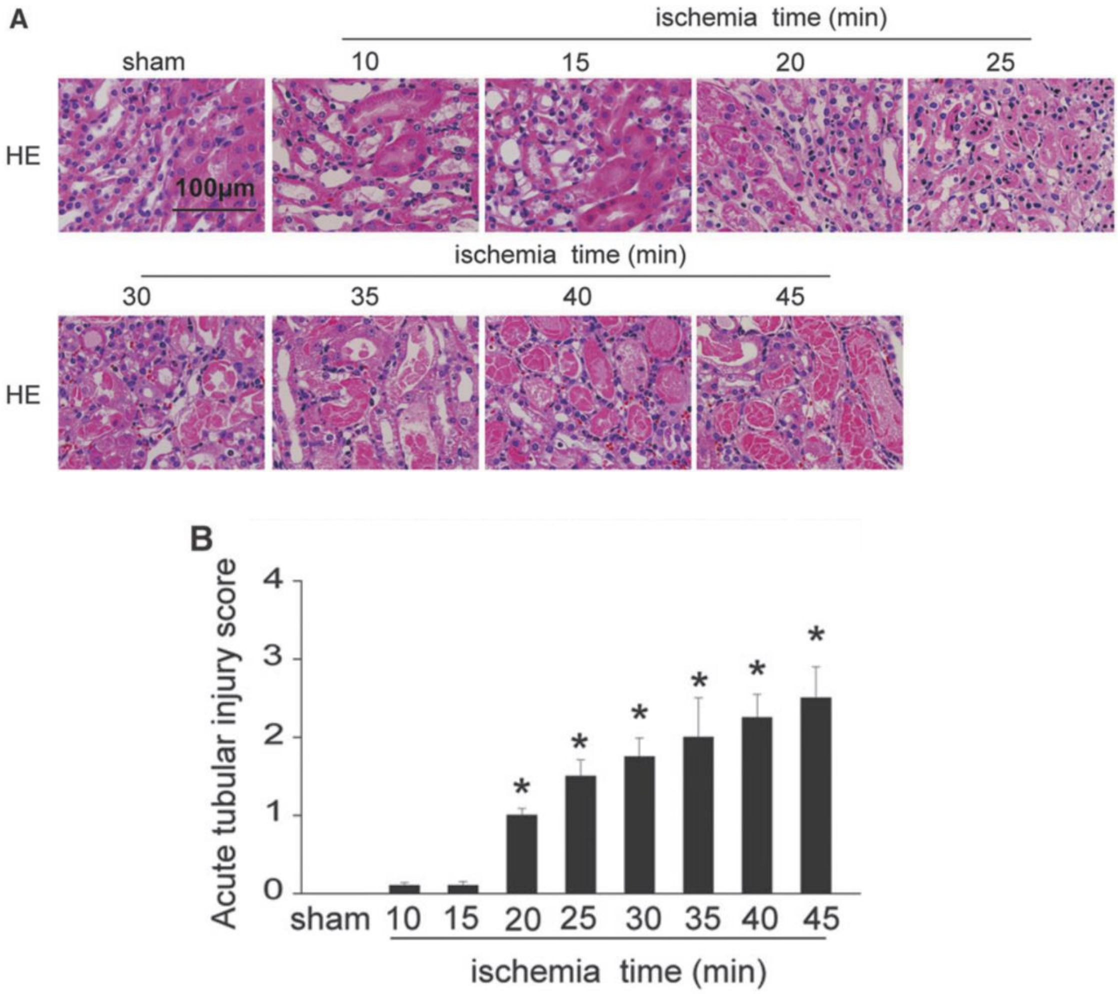

Figure 1. Correlation between tubulointerstitial injury and duration of bilateral ischemia-reperfusion injury (IRI) time 24 h after IRI. Longer periods of ischemia-reperfusion (IR) induced more severe tubulointerstitial injury (10-45 min). 10-15 min of IR did not cause observable renal injury, while more than 20 min IR led to detectable IR-induced acute tubular injury. (A) Hematoxylin-eosin (HE)-stained representative pictures of tubular injury 24 h after IR, scale bar: 100 μm. (B) Acute tubular injury score. Acute tubular injury was determined based on HE-staining comparing the sham operated animals to IR-operated mice. Sham vs. IR: *: p<0.05; Figure 1/A and B from the article of Cao et al. (17).

After the ischemic episode, the surviving tubular cells dedifferentiate, proliferate and restore the integrity of the tubular epithelium. However, the exact molecular mechanisms governing the regenerative processes and the subset of progenitor cells that are capable of differentiating are still largely unknown (18). Nevertheless, the regenerative capacity can be insufficient in areas where IRI causes more severe lesions than in other regions of the kidney. The characteristics of these areas are tubular atrophy, persistent inflammation and fibroblast/myofibroblast accumulation.

Fibroblast/myofibroblast activation leads to proliferation and connective tissue production creating scar tissue, which contracts and becomes shrunken over time (19, 20).

2.3 Tubular damage is a driving force of AKI

Tubular cells die either by apoptosis or necrosis (8). Damaged cells release various proteins and molecules, among others high-mobility group box 1 (HMGB1) protein, heat-shock proteins, histones, fibronectin (FN), which all act as DAMPs (21). DAMPs are recognized by pattern recognition receptors, like toll-like receptors (TLRs) that are localized on dendritic cells (DCs), macrophages and renal endothelial and epithelial cells, among others (21, 22). In response to IRI the affected tubular epithelial cells produce various proinflammatory cytokines, such as interleukin (IL)-6, tumor necrosis factor-alpha (TNF-α), chemokines and complement components (C), and express TLRs and complement component receptors (8).

Proinflammatory cytokines induce the expression of chemokines (chemotactic cytokines), which play an important role in leukocyte recruitment during inflammation, such as chemokine (C-C motif) ligand 2 (CCL2, or formerly known as monocyte chemoattractant protein 1, MCP-1) (23).

2.4. Macrophages play a major role in ischemia-induced AKI

Neutrophils are the first leukocytes infiltrating the kidney after IRI, although their role in AKI is controversial (24). Monocytes/macrophages infiltrate the kidney in the first 1-5 days after IRI, and start to produce various proinflammatory cytokines, like IL-1β, IL-6, TNF-α (25). Macrophages can be categorized into two subtypes, the M1 and M2, however, their exact definition is a matter of debate. Currently, M1 or M2 macrophages are not considered to be the only existing subtypes because these cells can alter their polarization state and mixed phenotypes exist in certain conditions (26). M1 macrophages produce various proinflammatory cytokines such as IL-6 or TNF-α, hence they are implicated to play a role in sustaining the proinflammatory environment and contributing to tubular damage. On the other hand, M2 subtype is thought to attenuate the inflammatory response and stimulate tissue repair. Furthermore, in IRI-induced AKI, M1 macrophages appear early (48h after the injury), while the M2 macrophages play a major role at later time points (27).

Activation of the complement system further enhances the proinflammatory processes. Complement proteins can reach the kidney via the blood stream, and the tubular epithelial cells also produce complement components. The complement system is mainly activated via the alternative pathway in rodent models of kidney IRI. Alternative pathway initiation can be autocatalytic and the complement cascade can be inhibited by complement regulators that are expressed on the glomerular, tubular epithelial and endothelial cells. However, on surfaces lacking complement regulators like pathogens or injured cells, the pathway rapidly activates resulting in the formation of membrane attack complex (C5b-C9), which causes cell lysis (28).

2.5. Hypoxia and oxidative stress are caused by ischemia

As mentioned above, disrupted microcirculation is not sufficient to fulfill oxygen demand of the kidney. The oxygen supply is compromised by endothelial cell damage and the subsequent leukocyte and platelet activation, edema formation, development of oxidative stress and the release of vasoconstrictor molecules (29).

The key regulator of the response to hypoxia at the cellular level is the hypoxia-inducible factor (HIF). HIF is a heterodimer formed by inducible subunits (HIF-1α, HIF-2α, and HIF-3α) and the constitutively expressed HIF-β subunit. In the kidney, HIF-1α is expressed in the tubular epithelial cells and in the endothelial and tubulointerstitial cells of the papilla and inner medulla, while HIF-2α is produced in the endothelial cells and tubulointerstitial fibroblast-like cells. The HIF-α subunits are sensitive to oxygen and regulated post-transcriptionally in an oxygen sensitive manner. While HIF-1α is implicated in the initial adaptation to hypoxic conditions, HIF-2α plays a role at a later phase (30, 31).

Along with hypoxia, oxidative stress is also thought to be a major pathogenic factor in AKI driven by generating ROS. (32). The key regulator of defense against oxidative stress is the Nuclear factor erythroid 2–related factor 2 (NRF2). NRF2 regulates the transcription of antioxidant genes, such as heme oxygenase 1 and members of the glutathione metabolism, and decreases the expression of pro-oxidants, such as quinonoids (33). Furthermore, the deficiency of NRF2 is proved to be deleterious in an experimental mouse model of IRI (34), underlining the importance of NRF2.

Recovery after AKI depends on multiple factors. When renal blood flow is restored, the nephrotoxic agents are eliminated and the renal parenchyma is capable of regeneration. Hence, the recovery is determined by the sum of residual deleterious effects of kidney injury and activity of repair mechanisms. In response to a mild harmful stimulus, the kidney is capable of maintaining homeostasis (renal reserve); thus, there will be no clinical signs of renal functional impairment, as the adaptive repair can recover kidney function. If the injury is severe, clinical manifestation can be seen, yet, complete resolution can still be achieved by adaptive repair. However, the maladaptive repair mechanisms may cause further damage if the repair mechanisms are incapable of restoring kidney integrity that leads to fibrosis and slow deterioration of kidneys function as also shown by elevated levels of kidney damage markers (35).

2.6. AKI to chronic kidney disease (CKD) transition

Serious AKI is not only associated with short-term adverse outcome, but is also a risk factor for the development of chronic kidney disease and end-stage renal disease (ESRD). Furthermore, there is an association between AKI and CKD, as the more severe the AKI the higher the risk that the patient will develop CKD (36).

The exact pathomechanisms of AKI-to-CKD transition are not fully understood, although several mechanisms are implicated in CKD progression, such as endothelial cell dysregulation, maladaptive repair processes in the tubular epithelial cells, excess extracellular matrix (ECM) deposition and chronic inflammation (37). Mice heterozygous for transforming growth factor-β (TGF-β) receptor knock-out (KO) in endothelial cells showed better preservation of renal blood flow and microvasculature, and less renal fibrosis than their wild-type counterparts in folic acid and unilateral ureter obstruction models (38). These data suggest that TGF-β signaling plays an important role in AKI-to-CKD transition.

Tubulointerstitial fibrosis is the main prognostic factor for CKD/ESRD, however, the exact relationship between extracellular matrix deposition and fibrosis is not yet fully understood in the development of CKD (37). Injured tubular cells, which fail to recover after the initial injury show persistent profibrotic signaling leading to fibrosis. Furthermore, these signaling pathways can transform endothelial cells and pericytes to myofibroblast, thereby, further enhancing ECM accumulation. However, these processes are not necessarily progressive, as microvascular alterations are seen only in close proximity to damaged tubules. Hence, it is though that further injury or additional mechanisms are needed for progressive ECM deposition seen in AKI-to-CKD progression (20).

Interleukin-1 receptor-associated kinase-M (IRAK-M) is an inhibitory molecule of the TLR-signaling cascade. Although renal dysfunction was similar in IRAK-M knock-out and wild-type mice in the early phase of ischemia-induced AKI, but on the long-term, loss of IRAK-M resulted in tubular atrophy, tubulointerstitial fibrosis and persistent proinflammatory macrophage accumulation and elevated proinflammatory cytokine and chemokine expression in the kidney (39).

2.7. Chronic kidney disease definition and etiology

CKD is defined by the KDIGO Clinical Practice Guideline for the Evaluation and Management of Chronic Kidney Disease (40) as structural or functional impairments of the kidney, persistent for at least 3 months that have deleterious effect on the patients' overall health. The criteria for CKD are either the presence of at least one marker of kidney damage: albuminuria (albumin excretion rate (AER) above 30 mg in 24 hours or albumin-to-creatinine ratio (ACR) above 30 mg/g), urine sediment irregularity, electrolyte and related impairments caused by tubular damage, abnormalities identified by histology or imaging, history of kidney transplantation or GFR is below 60 ml/min/1.73m^2. CKD is classified based on cause, GFR and albumin excretion (Table 2).

A

GFR categories	GFR ranges (ml/min/1.73m$^{2)}$	Description
G1	above 90	normal or high
G2	60-89	mildly decreased
G3a	45-59	mildly to moderately decreased
G3b	30-44	moderately to severely decreased
G4	15-29	severely decreased
G5	below 15	kidney failure

B

Category	Albuminuria ranges	Description
A1	below 30 mg/day (3 mg/mmol creatinine)	normal to mildly increased
A2	30-300 mg/day (3-30 mg/mmol creatinine)	moderately increased
A3	above 300 mg/day (30mg/mmol creatinine)	severely increased

Table 2. Stages of chronic kidney disease (CKD) based on glomerular filtration rate (GFR) and albuminuria defined in the KDIGO Clinical Practice Guideline for the Evaluation and Management of Chronic Kidney Disease. A) CKD stages based on GFR, B) CKD stages based on albuminuria (40).

GFR depends on the filtration capacity of a single nephron and nephron number. GFR will not decrease due to nephron loss until the nephrons are capable of increasing their filtration capacity. When the nephrons reach their maximum capacity, the loss of functioning nephrons will result in decreased GFR. Hence, CKD can be characterized by nephron loss, which ultimately will lead to ESRD (GFR less than 15 ml/min/1.73m^2), when renal replacement therapy is necessary (41).

As in the case of AKI, the diagnosis of CKD is mostly based on serum creatinine concentration. Several potential biomarkers are investigated for better diagnosis of CKD, such as uromodulin, which could reflect the number or mass of healthy nephrons. Urinary excretion of the injury marker proteins, KIM-1 and LCN2, seem to show the degree of tubular injury (42). The prevalence of CKD is estimated to be approximately between 12-15% worldwide, and most patients have stage 3 CKD (43). CKD is an ever increasing cause of death; in 1990 it was the 17th leading cause of death, while in 2017 it became the 12th as its global all age mortality rate increased by 41.5% (44). Furthermore, CKD itself is a risk factor for other causes of morbidity and mortality (45).

CKD ultimately leads to fibrosis driven by maladaptive repair and sustained injury in many cases (Figure 2), and can be described by glomerulosclerosis, tubular atrophy and tubulointerstitial fibrosis (45).

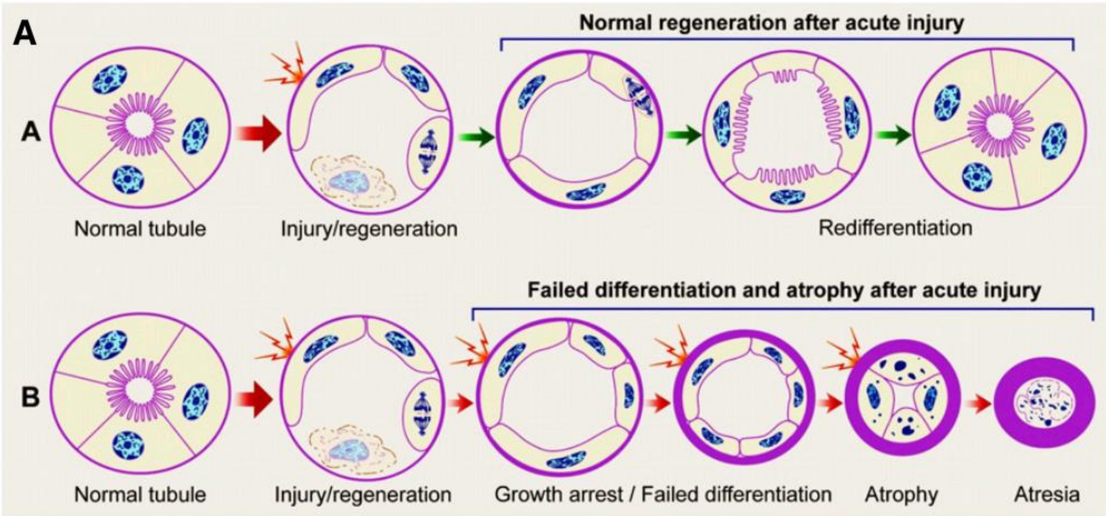

Figure 2. Schematic diagram of successful or failed recovery of the proximal tubules after acute kidney injury (AKI). A) Normal kidney regeneration after injury described as the dedifferentiation of the tubular cells, proliferation and redifferentiation leading the recovery. B) Failure of redifferentiation leads to cell growth arrest, atrophy and tubulointerstitial fibrosis. Figure 3/A from the paper of Venkatachalam MA et al. (20).

Tubular atrophy is also an important feature of CKD. Several mechanisms are hypothesized to be responsible for tubular atrophy, such as tubular cell apoptosis, cellular senescence induced by oxidative stress or decreased autophagy, hypoxia caused by abnormalities in renal microcirculation and CKD-related anemia (46).

2.8. Myofibroblasts are implicated in excess extracellular matrix production

As mentioned above, inflammation is involved in the development of renal fibrosis. Macrophages are among the first immune cells infiltrating the kidney after injury, which migrate to sites of fibrosis. The extent of macrophage accumulations near these sites corresponds to the degree of renal fibrosis. Furthermore, alpha-smooth muscle actin (α-SMA)-positive macrophages likewise co-localize with fibrotic areas in the kidney (47).

Myofibroblasts play a major role in tissue repair. They are the main extracellular matrix producing cells during wound healing or fibrosis. ECM consists of numerous proteins such as collagen (Col) 1 and -3, glycoproteins (e.g. fibronectin) and proteoglycans. However, other cells are also able to produce these proteins, such as epithelial-, endothelial and immune cells (48).

One of the main promoters of renal fibrosis is TGF-β. TGF-β directly activates and induces the migration and proliferation of mesangial and fibroblast cells, and it stimulates the expression of fibrotic genes such as collagens and FN1. Furthermore, TGF-β can promote fibrosis indirectly by inducing tubular epithelial cell and podocyte apoptosis, and transdifferentiation of various renal cells into myofibroblasts (49).

An another source of profibrotic growth factors (TGF-β and connective tissue growth factor), is tubular epithelial cells, which are arrested in G2/M phase of cell cycle after activation of the c-jun NH2-terminal kinase (JNK) signaling pathway in the injured kidney. Furthermore, the expression of fibrosis-related genes, Col1a1 and Col4a1 are also increased in G2/M arrested tubular epithelial cells. Indeed, a JNK inhibitor or contralateral nephrectomy (Nx) 3 days after the injury attenuated the profibrotic response by decreasing the number of cells arrested in G2/M phase (50).

Currently, therapeutic interventions for CKD have limited efficacy. The present clinical concept is prevention of AKI-to-CKD transition and fibrosis. The possible new treatments could target the fibrotic processes, mechanisms of cell death, autophagy, inflammation and epigenetic regulators, notably microRNAs (miRNAs), among others (51).

2.9. MicroRNAs are important regulators during AKI and CKD

MiRNAs are short, 20-25 nucleotide long, non-coding ribonucleic acids (RNAs), which post-transcriptionally regulate target genes by suppressing translation or eliciting messenger RNA (mRNA) degradation. Most of the miRNAs are transcribed by RNA polymerase II, although RNA polymerase III is also implicated in the synthesis of some miRNAs. The miRNA transcription unit can contain a single miRNA or several related miRNAs that form a cluster. If members of one such cluster possess similar seed regions, they are classified as miRNA family. MiRNA biogenesis involves the canonical and the non-canonical pathways; the majority of miRNAs are transcribed via the canonical pathway (Fig. 3). Transcription of a miRNA gene gives rise to double-stranded miRNA precursors called primary microRNAs (pri-miRNA) arranged into a hairpin structure. The next maturation step is the cleavage of pri-miRNA by the Microprocessor complex. The

Microprocessor complex consist of two major proteins: Drosha and DiGeorge syndrome critical region 8. Drosha cleaves pri-miRNAs at the base of the hairpin to produce precursor microRNAs (pre-miRNAs). Subsequently, pre-miRNAs are exported to the cytoplasm where the Dicer protein cleaves the terminal loops of pre-miRNAs to produce the mature miRNA duplex. One strand of the mature miRNA, the guide strand, is loaded into an Argonaute protein (AGO1-4 in humans), while the other (passenger strand) is discarded. The mature miRNA and the AGO protein form the microRNA-induced silencing complex (miRISC). MiRNAs identify their target mRNA by base-pairing. The target sequence is highly complementary to the miRNA seed sequence and is mainly located in the 3’ untranslated region (UTR) of the mRNAs, however, miRNAs can recognize other regions as well. If the microRNA response element (MRE) of the mRNA contains no mismatches, the targeted mRNA is degraded by the endonuclease activity of the AGO2 protein. If MRE encompasses mismatches, the targeted mRNA does not degrade but translation is inhibited by miRISC (52, 53).

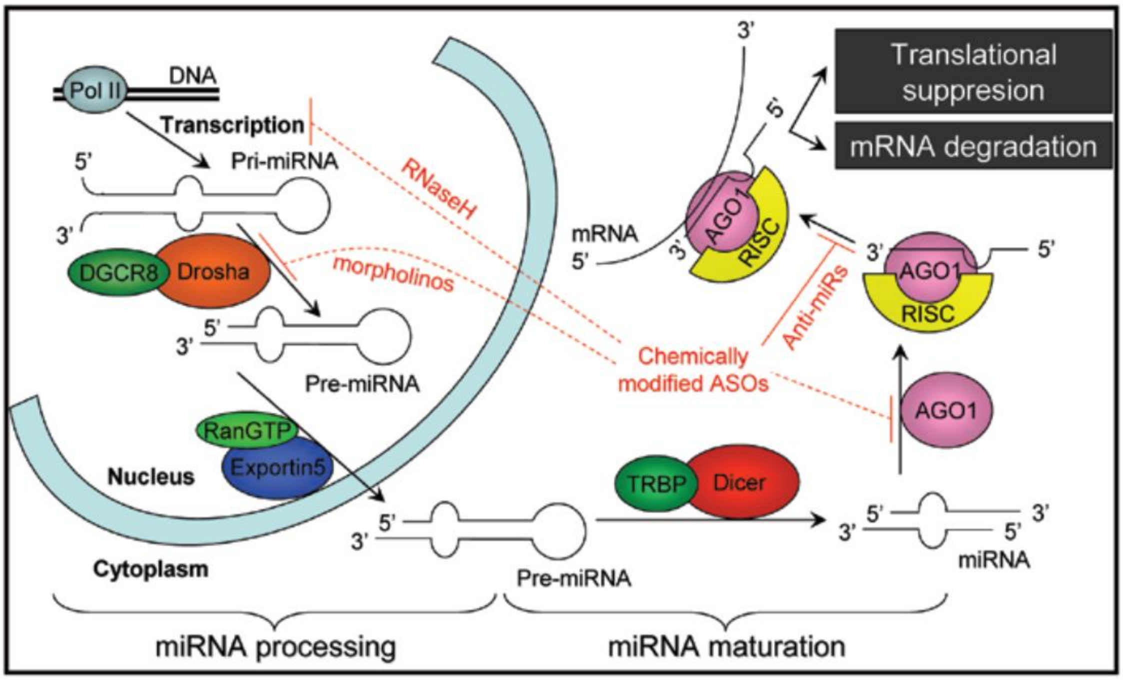

Figure 3. Schematic representation of microRNA (miRNA) biogenesis (miRNA transcription, processing and maturation) and possible points of inhibition by chemically modified antisense oligonucleotides (ASO). Transcription of miRNAs by Polymerase II (Pol II) results in a double-stranded miRNA precursors called primary miRNAs (pri-miRNA), which subsequently processed by Microprocessor complex (DGCR8: DiGeorge syndrome critical region 8 and Drosha) to form precursor miRNAs (pre-miRNAs). Pre-miRNA are exported to the cytoplasm by RanGTP (Ras-related nuclear protein-guanine-triphosphate) and Exportin 5. Mature miRNA are produced by Dicer and transactivation response element RNA-binding protein (TRBP) proteins from pre-miRNA. Mature miRNA bind to the AGO protein to form the miRNA-induced silencing complex (miRISC), which suppresses translation or induces messenger RNA (mRNA) degradation.
RNaseH: Ribonuclease H, Figure 1 from the paper of Rácz Zs. et al. (54).

Several miRNAs are implicated in kidney development (55). The conditional deletion of the miR-17-92 family are fundamental important for nephrogenesis in mice (56). Appropriate expression of miRNAs is required for normal kidney function beyond the developmental stage (57). Furthermore, miRNAs are implicated in the pathogenesis of various diseases such as acute kidney disease (58) or chronic kidney disease (59). Growing body of evidence indicates a major role for miRNAs in the regulation of tissue fibrosis, including miR-21a-5p, -146a, -155, -214 and the miR-29 and -200 family. Many of these are implicated in the regulation of TGF-β expression but further research is needed to fully identify miRNAs, which play a role in kidney fibrosis, their targets and exact functions (60, 61). These findings can help develop new biomarkers in both AKI

DOI:10.14753/SE.2022.2613

and CKD and raise hope for development of potential therapeutic treatments. Indeed, several *in vivo* studies suggest that alteration in the expression of specific miRNAs, such as induction of miR-17-5p (62), miR-21 (63) or inhibition of miR-24 (64) can be beneficial in IRI-induced AKI.

2.10. Animal models to investigate the pathophysiology of AKI and CKD

Several models have been established to investigate the pathomechanisms of and potential therapeutic interventions for AKI. Although *in vitro* models are proved to be useful tools in AKI research, *in vivo* studies are essential to explore the complex nature of AKI (Table 3). There are established animal models for pre-renal (e.g. ischemia-reperfusion) and post-renal (e.g. urinary tract obstruction) and toxin-related AKI (e.g. sepsis) (15), however, not all models are demonstrated to provide useful information for clinical translation (65).

Acute kidney disease	Pre-renal	Ischemia-reperfusion injury	Warm-ischemia
			Cold-ischemia
	Drug/toxin related	Exogen	Drugs (e.g. cisplatin)
			Overload (e.g. folic acid)
			Natural substances in herbs (e.g. aristolochic acid)
		Endogen	Pigment neuropathy
			Glycerol-induced AKI
			Warfarin-induced AKI
	Post-renal		Unilateral ureteral obstruction
	Endotoxic		Lipopolysaccharide (LPS)-induced AKI

Chronic kidney disease	Renal mass reduction		5/6 nephrectomy
	Diabetic kidney disease	Type I	Streptozotocin-induced diabetes
		Type II	Leptin receptor mutant
	Hypertension-induced kidney disease		Chronic angiotensin II infusion
	Glomerular injury	Primary glomerulonephritis	Focal segmental glomerulosclerosis
			Crescentic glomerulonephritis
			Membranous nephropathy
			Immunoglobulin A nephropathy
		Systemic diseases	Lupus nephritis
			Amyloidosis
		Hereditary glomerular injury	Alport syndrome (Col4A3 knock-out)
	Polycystic kidney diseases (PKDs)		PKD1/2 knock-out
	Chronic tubulointerstitial nephritis		Adenine overdose
	Endothelial injury	Hemolytic uremic syndrome	Shiga-toxin induced
			Complement deficiency-related
		Preeclampsia	Aortic and bilateral ovarian artery constriction
			Various genetically modified mice

Table 3. Animal models of acute kidney injury and chronic kidney disease. AKI: acute kidney disease, Col4A3: collagen 4A3 (65).

There are two major arms of IRI, the cold and warm ischemia-reperfusion. Cold IR occurs in organ transplantation and typically means longer ischemia time (up to several hours) than during warm IR (66).

Regarding the warm ischemia-reperfusion models, the bilateral and the unilateral IR subtypes can be differentiated. Furthermore, unilateral IR allows for immediate or delayed nephrectomy (15).

Bilateral IR is a frequently used method because it best characterizes IRI-induced AKI in humans. In case of bilateral IR, there is a positive correlation between ischemia time (i.e. the severity of IRI) and plasma urea or creatinine level. In C57BL/6 mice, 22-25 minutes of ischemia caused mild to moderate injury, which lasted for about one week. However, 30 min of bilateral IR results in severe AKI with a substantial mortality rate after 72 hours (15).

Unilateral IR is also frequently used, when the blood flow only to one of the kidneys is obstructed. Although the effect of unilateral IR is clinically relevant and various ischemia times allow studying different degrees of kidney injury, the researchers should be well-trained and the animals require postoperative monitoring (67). In case of unilateral IR without nephrectomy, the non-injured kidney can almost fully compensate for the loss of kidney function caused by contralateral ischemia. Furthermore, 15 min of ischemia already causes histological lesions 24 hours after the intervention, although only longer ischemia time, more than 25 min, induces persistent histological changes. However, at least 35 min of ischemia increases the expression of proinflammatory and fibrotic genes, such as TNF-α, CCL-2, IL-6, Col1a1, TGF-β at 24 hours, and these changes could last up to 35 days. Moreover, 35 min of ischemia induces cell death and progressive tubular atrophy. These data suggest a threshold ischemia time to induce long lasting, gradual deterioration of injured kidneys (68).

The contralateral kidney can be removed either at the time of surgery or later. Removal of the contralateral kidney at the time of ischemia yields a useful control tissue to which alterations in the ischemic kidney can be compared. The method is described in details by Hesketh et al. (69). They found that the severity of IRI correlated to the increase in both serum creatinine and BUN levels, and to renal histological injury, representing a gradual increase in renal impairment and damage. However, the kidney function recovered by day 7 after IR, and the kidney tubules showed signs of regeneration on day 7 compared to day 4, when intense cell proliferation could be detected. Moreover, the uninjured kidney can accelerate fibrosis in the ischemic kidney after unilateral IR (50).

Contralateral nephrectomy can be performed at a delayed time point (70). The rationale of this method is that severe, otherwise lethal renal injury can be induced with high survival rate, and the functional recovery of the injured kidney can be assessed Indeed, utilizing this experimental model, the otherwise non-functioning post-ischemic kidney regains its functional activity after contralateral nephrectomy in a few weeks.

Other experimental methods, such as unilateral ureteral obstruction (UUO), are also capable of inducing kidney fibrosis, and they also give an opportunity to study AKI-to-CKD transition. UUO induces kidney damage primarily by increasing intratubular hydrostatic pressure that causes secondary ischemia and nephron damage and subsequently leads to fibrosis in a relatively short period, approximately within 2 weeks. The pathomechanisms of UUO are comparable to those of IRI, such as tubular epithelial cell necrosis, inflammation and leukocyte infiltration, excessive ECM accumulation (71).

In mice, several factors affect the susceptibility to IRI, namely body temperature during surgery, the type of anesthesia, age, sex and strain. Older and male animals are more susceptible to IRI (65). Many factors can contribute to inconsistent results, such as incidental presence of capsular blood vessels can attenuate kidney ischemia. Hence, it is imperative to establish individual protocols in each laboratory for the mouse strain used, their age and sex and duration of ischemia (69).

Furthermore, it is known that different inbred mouse strains possess diverse susceptibility to various fibrotic stimuli and this susceptibility is organ dependent. While the most commonly used C57BL/6 and CD1 mouse strains are more prone to develop kidney fibrosis, BALB/c mouse strain is resistant. However, the fibrotic response may depend on the injury applied (72). Although the outbred Naval Medical Research Institute (NMRI) mouse strain may be susceptible to diabetic nephropathy (DN) (i.e. elevated glomerular filtration rate (hyperfiltration), a hallmark of human DN) (73), to our knowledge no such bias is reported concerning the ischemia-reperfusion induced kidney fibrosis in NRMI mice. Hence, adopting this outbred strain may be more appropriate to better characterize the molecular response to IR-induced AKI and subsequently CKD.

According to the above findings, we chose to study the molecular background of one of the clinically most promising animal models, the severe unilateral renal ischemia-reperfusion with delayed contralateral nephrectomy. Detailed knowledge of the underlying mechanisms leading to the functional recovery of the post-ischemic kidney after nephrectomy may help develop new, effective therapeutic approaches for treating AKI and impede CKD progression.

3. Objectives

Two main objectives set for the performed unilateral ischemia-reperfusion injury with delayed contralateral nephrectomy studies were to gain new, utilizable information that can be used in the clinical therapy of AKI and chronic kidney disease:

1. We aimed to study the molecular mechanisms of the functional recovery induced by delayed contralateral nephrectomy with emphasis on inflammation and fibrosis as well as on hypoxia and oxidative stress, and

2. To determine the miRNAs that potentially play role in the functional recovery of the post-ischemic kidney.

4. Methods

4.1 Animals

Male NMRI mice were used in all experiments. The animals were purchased from Toxi-Coop (Toxi-Coop Ltd., Budapest, Hungary) according to their body weight (20-25 g). Mice were housed under standard conditions with free access to standard rodent chow (Akronom Ltd., Budapest, Hungary) and tap water *ad libitum*. The animals were maintained under a 12/12 hours light/dark cycle (7 am to 7 pm) and within a temperature range of 23±2°C. All experimental protocols were approved by the Pest County Government Office and the Animal Ethics Committee of Semmelweis University (PE/EA/2202-5/2017). The Hungarian Acts XXVIII of 1998 and LXXVIII of 2018 on the protection and welfare of animals, the EU Directive 2010/63/EU for animal experiments and the 3R principle (Replace, Reduce, Refine) (74) were fully implemented in all experiments.

4.2 Experimental time-flow and group numbers

Six separate series of experiments were performed using the unilateral ischemia-reperfusion with delayed contralateral nephrectomy model (75) described by Skrypnyk N et al. (70) with some modifications: contralateral nephrectomy was performed on day 7 instead of on day 8. The experiments were terminated on the following days: 7, 8, 10, 14, 28 and 140 (Figure 4).

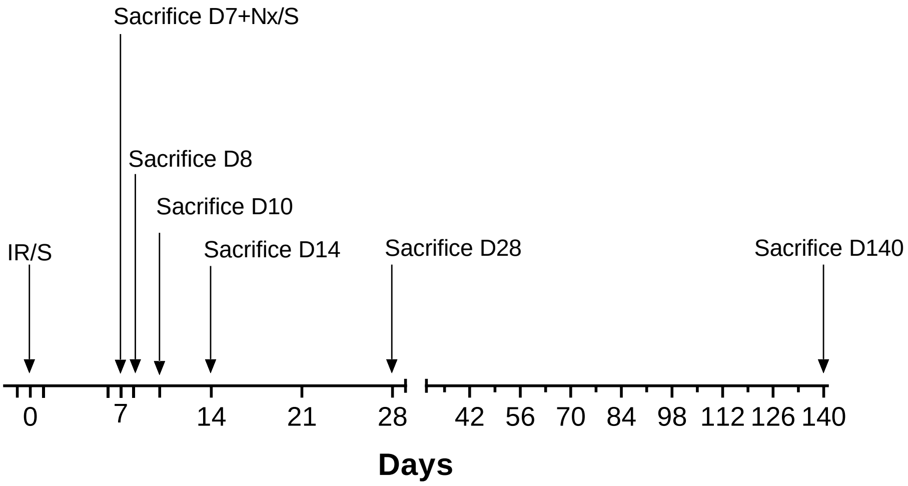

Figure 4. Outline of the studies performed. Arrows mark all major interventions. Time of blood collections are represented with major and minor ticks. IR/S: ischemia-reperfusion + sham contralateral nephrectomy; Nx/S: contralateral nephrectomy (Nx) or sham contralateral nephrectomy (S), D7-D140 denote the day of sacrifice (75).

A total of 134 animals were used (Table 4).

Study duration, (days)	Groups			
	S-S	S-Nx	IR-S	IR-Nx
7	-	-	n=8	-
8	n=6	n=6	n=9	n=10
10	n=8	n=7	n=9	n=9
14	-	-	n=8	n=7
28	-	-	n=9	n=8
140	n=5	n=6	n=4	n=15

Table 4. Number of animals in groups. S-S: sham ischemia-reperfusion (S) + sham contralateral nephrectomy (S), S-Nx: sham ischemia-reperfusion (S) + contralateral nephrectomy (Nx), IR-S: ischemia-reperfusion (IR) + sham contralateral nephrectomy (S), IR-S: ischemia-reperfusion (IR) + contralateral nephrectomy (Nx) (75, 76).

All surgical interventions were performed between 10:00 am and 5:00 pm. The animals were anesthetized with an intraperitoneal injection of a mixture of 80 mg/kg ketamine (Gedeon Richter Plc., Budapest, Hungary) and 4 mg/kg xylazine (Streuli Pharma AG, Uznach, Switzerland). The surgical area was shaved and the skin was disinfected with 70% ethanol (Molar Chemicals Ltd., Halásztelek, Hungary). Mice were placed on a heating pad (Supertech Ltd., Budapest, Hungary) and the body temperature was monitored during the operation (at the beginning of the surgery, at 10 min intervals during ischemia and at the end of the ischemia). The ischemia-reperfusion surgery was performed via exploratory laparotomy. Mice were subjected either to 30 min of warm ischemia-reperfusion using two atraumatic vascular clips (Aesculap Inc., Tuttlingen, Germany) to occlude the renal pedicles or to sham (S) surgery on the left kidney. Ischemia and successful reperfusion was confirmed by color changes of the kidney (i.e. kidney became dark red during ischemia and regained its normal color within 1-2 min after the clamps were removed). The day of the intervention was marked day 0. After 7 days contralateral nephrectomy or sham Nx was performed. Thus, the following groups were examined: sham IR-Sham Nx (S-S), sham IR-Nx (S-Nx), IR-Sham Nx (IR-S) and IR-Nx. Surgical wounds were sutured using USP 6/0 non-absorbable pseudo-monofil polyamid suture (B. Braun, Melsungen, Germany). After the surgery, morphine (1 mg/kg) was administered subcutaneously for pain alleviation. The animals were observed until full return of consciousness.

4.3 Sample collections and sacrifice

4.3.1 Blood collection

Blood samples were collected on the following days: -1, 1, 6, 8, 10, 14 and once weekly until the termination of the study. One hundred microliter of blood was collected at each time from the tail vein cut by a scalpel blade. To prevent blood clotting, samples were thoroughly mixed with 5 µl 5000 IU/ml heparin (Teva Pharmaceutical Industries, Budapest, Hungary) and immediately centrifuged at 6000 g for 2 min. Plasma was aspired and stored at - 80°C until further analysis.

4.3.2 Sacrifice

In order to prevent blood clotting 10 ml/kg heparin (500 IU/mL) was administered intraperitoneally 3 min before sacrifice. The mice were killed by cervical dislocation. Blood was collected from the chest cavity after cross-section of the inferior vena cava . Then, the animals were perfused with 10 ml ice-cold physiological saline (Fresenius Kabi, Bad Homburg v.d.H, Germany) through the left ventricle.

4.3.3 Kidney collection

Kidneys were collected at the time of nephrectomy or at the time of sacrifice. Kidneys were cut with sterile surgical blades (B. Braun, Melsungen, Germany) into three pieces. For RNA isolation the upper-third part of the kidney was immerged into 0.5 mL TRI Reagent® (Molecular Research Center Inc., Cincinnati, OH, USA) in 2 mL Cryovials (Sarstedt AG & Co. KG, Nümbrecht, Germany) and immediately submerged into liquid nitrogen and kept at -80°C for molecular analysis. A 1 mm thick cross-section of the kidney, which incorporated both the cortex and the medulla, was cut at the hilus level and fixed in 4% buffered formaldehyde (Molar Chemicals Ltd., Halásztelek, Hungary) overnight at 4°C, and then dehydrated and embedded in paraffin for histology. The remaining part of the kidney was cut into two pieces, snap frozen in liquid nitrogen and kept at -80°C until further analysis.

4.4. RNA isolation

Total RNA was isolated using TRI Reagent® according to the manufacturer's protocol. In brief, after homogenization, 0.1 ml chloroform was added to the samples and thoroughly mixed. The homogenates were allowed to separate for 3 minutes at room temperature, and then centrifuged at 12,000 g for 15 min at 4°C. The aqueous upper-layer was aspirated and the RNA was precipitated with 0.4 ml isopropanol. Samples were incubated for 30 minutes at room temperature, and then centrifuged at 12,000 g for 10 minutes at 4°C. The supernatant was discarded and the pellet was washed with 1 ml 75% ethanol, centrifuged at 7,500 g for 8 minutes at 4°C. Ethanol was discarded and the samples were washed again with 1 ml 75% ethanol, centrifuged at 12,000 g for 8 minutes at 4°C. Then, the ethanol was aspired and the RNA was air dried for 5 minutes and resuspended in ribonuclease-free water (AccuGene™ Molecular Biology Water, Lonza, Basel, Switzerland). RNA integrity was checked by electrophoretic separation on 1% agarose gel. Nucleic acid was visualized with GelRed® (Biotium, Fremont, CA, USA). RNA concentrations were measured by Nanodrop™ 2000c Spectrophotometer (Thermo Fisher Scientific, Wilmington, DE, USA).

4.5 miRNA microArray

In order to gain insight into the miRNA alterations upon IR injury, miRNA microArray analysis was performed on 20 samples from the 8-day experiment. 6-6 samples from the IR-S and IR-Nx groups and 4-4 samples from the S-S and S-Nx groups were selected based on the plasma urea levels and TNF-α and TGF-β mRNA expression (primers are listed in Table 6). The microArray was performed by Exiqon A/S (Vedbæk,

Denmark). In brief, the quality of the RNA was verified by Agilent 2100 Bioanalyzer (Agilent Technologies Inc., Santa Clara, CA, USA). Fractions of the RNA samples were pooled to gain a reference sample. 750 ng of the test and reference samples were labelled by Hy3 and Hy5 fluorescent labels utilizing miRCURY LNA™ microRNA Hi-Power Labeling Kit, Hy3™/Hy5™ (Exiqon, Denmark). Hybridization of the samples and the fluorescent dyes was performed according to the miRCURY LNA™ microRNA Array instruction manual using a Tecan HS4800™ hybridization station (Tecan, Austria). The slides were scanned using the Agilent G2565BA Microarray Scanner System (Agilent). Image analysis was executed using ImaGene® 9 (miRCURY LNA™ microRNA Array Analysis Software, Exiqon, Denmark). The quantified signals were background corrected (offset=10) and then normalized using the global Locally Weighted Scatterplot Smoothing (Lowess) regression algorithm (M-value). The data obtained were deposited in NCBI's Gene Expression Omnibus (77) and are accessible through GEO Series accession number: GSE157221.
(https://www.ncbi.nlm.nih.gov/geo/query/acc.cgi?acc=GSE157221).

MiRNAs with an average Hy3 signal intensity above 6.0 were selected for further analysis. Relative miRNA expressions were calculated as $2^{\text{M-value}}$. Fold changes (FCs) were calculated after log2 transformation as the ratio of injured to mean control right kidney expression levels.

4.6 Quantitative reverse transcription polymerase chain reaction (RT-qPCR) of mRNA and miRNA

4.6.1 RT-qPCR of mRNA targets

Reverse transcription (RT) of 1 μg of total RNA to complementary deoxyribonucleic acid (cDNA) was performed using random hexamer primers and the High Capacity cDNA Reverse Transcription Kit (Applied Biosystems, Foster City, CA, USA). All samples and reagents were kept on ice throughout the preparation of the regent mixes. Total of 20 μl reagent mix was prepared. The exact content of the mixes is described in Table 5 and the conditions of thermal cycling are specified in Table 6.

Reagents	Volume (µl)
RNA sample (1µg/µl)	12 µl
10x Reverse Transcription (RT) Buffer	2 µl
deoxyribonucleotide triphosphate mix	0.8 µl
10x RT Random Primer	2 µl
MultiScribe Reverse Transcriptase	1 µl
Nuclease-free water	2.2 µl

Table 5. Composition of reaction mix for RNA to cDNA transcription.

Step	Annealing	cDNA synthesis	Heat inactivation	Storage
Temperature	25°C	37°C	85°C	4°C
Time	10 min	120 min	5 min	∞

Table 6. The protocol applied for cDNA synthesis

The mRNA levels of the following genes were measured by real-time quantitative polymerase chain reaction: α-SMA, Col1a1, C3, fibronectin 1 (FN1), HIF-1α, HIF-2α, IL-6, LCN2, CCL2, NRF2, TGF-β,TNF-α. 18S ribosomal RNA (rRNA) was used for normalization. The sequences of the primers applied are listed in Table 7.

Target Gene	Forward Primer	Reverse Primer
18S	CTCAACACGGGAAACCTCAC	CGCTCCACCAACTAAGAACG
α-SMA	TTCCTTCGTGACTACTGCCG	GCTGTTATAGGTGGTTTCGTGG
Col1a1	GACGCATGGCCAAGAAGACA	CATTGCACGTCATCGCACAC
C3	ATCCAGACAGACCAGACCATC T	AGGATGACGACTGTCTTGCC
FN 1	CAGACCTACCCAGGCACAAC	CAGCGACCCGTAGAGGTTTT
HIF-1α	GGAGCCTTAACCTGTCTGCC	TGCTCCGTTCCATTCTGTTCA
HIF-2α	CCCTGCTGTCCTGCCTTATC	CATAGGCAGAGCGTCCAAGT
IL-6	CAAAGCCAGAGTCCTTCAGAG A	GGTCTTGGTCCTTAGCCACTC
LCN2	ACGGACTACAACCAGTTCGC	AATGCATTGGTCGGTGGGG
MCP-1	TCACTGAAGCCAGCTCTCTCT	TCTTGTAGCTCTCCAGCCTACT
NRF2	CCTCACCTCTGCTGCAAGTA	GCTCATAGTCCTTCTGTCGCT
TGF-β	CAACAATTCCTGGCGTTACCTT GG	AGATAGCAAATCGGCTGACG
TNF-α	AAATGGCCTCCCTCTCATCA	GAAAGCCCTGTATTCCGTCTCC TT

Table 7. List of the applied primers for RT-qPCR (75).

All primers were synthesized by Integrated DNA Technologies (Integrated DNA Technologies Inc., Coralville, IA, USA). Primers were purified by standard desalting. All RT-qPCR measurements were performed in 96-well PCR plates (Bio-Rad Laboratories Inc., Hercules, CA, USA) using SensiFast SYBR Green No-Rox Kit (Bioline Reagents Ltd., London, UK). Total of 2 µl/sample cDNA was amplified in duplicates in 40 cycles (for the whole amplification procedure see Table 8).

Step	Temperature	Time
Initial denaturation	95°C	120 sec
Denaturation	95°C	5 sec
Annealing, extension	60°C	20 sec
Denaturation	95°C	5 sec
Melt curve analysis	65°C→95°C, step: 0.5°C	5 sec

Table 8. The amplification procedure of RT-qPCR

Samples were measured in duplicates and expression of mRNAs were calculated using the comparative quantification (ΔΔCq) method and divided by the normalizing gene. Fold changes (FC) are given as a ratio of normalised mRNA expression to mean control mRNA expression.

4.6.2 RT-qPCR of the miRNA targets

In order to validate the results of miRNA microArray, the relevant miRNAs were measured by RT-qPCR. All samples and reagents were kept on ice throughout the preparation of the regent mixes. Total of 5 ng miRNA was transcribed into cDNA using Applied Biosystems™ TaqMan™ Advanced miRNA cDNA Synthesis Kit (Applied Biosystems, Foster City, CA, USA) according to the manufacturer's protocol. In brief, during the first phase of reaction, a polyA tail was added to the 3' end of the miRNAs, and then an adapter was ligated to the 5' end of the miRNAs. The universal RT primers recognised the extended 5' and 3' ends; hence all mature miRNAs were transcribed. The second phase of this procedure was carried out in order to enhance the detection of low-expressed miRNAs. The transcribed cDNAs were further amplified using the Universal microRNA (miR)-Amp Primers and miR-Amp Master Mix. This step equally increased the amount of each cDNA, maintaining their relative quantity.

The expression of the following 13 miRNAs was measured by RT-qPCR: mmu-miR-21a-3p, mmu-miR-21a-5p, mmu-miR-142a-3p, mmu-miR-142a-5p, mmu-miR-146a-5p, mmu-miR-199a-3p/mmu-miR-199b-3p, mmu-miR-199a-5p, mmu-miR-214-3p, mmu-miR-223-3p, mmu-miR-762, mmu-miR-2137, mmu-miR-2861, mmu-miR-3102-5p (Table 9).

No.	Annotation	No.	Annotation
1	mmu-miR-21a-3p	8	mmu-miR-214-3p
2	mmu-miR-21a-5p	9	mmu-miR-223-3p
3	mmu-miR-142-3p	10	mmu-miR-762
4	mmu-miR-142-5p	11	mmu-miR-2137
5	mmu-miR-146a-5p	12	mmu-miR-2861
6	mmu-miR-199a-3p/ mmu-miR-199b-3p	13	mmu-miR-3102-5p
7	mmu-miR-199a-5p		

Table 9. List of miRNAs validated by RT-qPCR (76).

An appropriate normalising gene (let-7g-5p) was selected using the NormFinder software v0.953 (78).

Expression of miRNA was assessed by TaqMan™ Advanced miRNA Assays and TaqMan™ Fast Advanced Master Mix (Applied Biosystems, Foster City, CA, USA). Total amount of 10 µl of reaction mix was prepared (for details see Table 10).

Reagents	Volume (µl)
miRNA sample (1µg/µl)	2.5 µl
TaqMan Fast Advanced MasterMix (2x)	5 µl
TaqMan Advanced miRNA Asssay (20x)	0.5 µl
Nuclease-free water	2 µl

Table 10. Composition of reaction mix for miRNA to cDNA transcription.

Samples were measured in duplicates and expression of miRNAs were calculated using the ΔΔCq method and divided by the normalizing gene. FCs are given as the ratio of normalised miRNA expression to mean control miRNA expression.

4.6 Plasma urea measurement

Urea concentration of plasma samples was measured without dilution in 96-well plates (Thermo Fisher Scientific Inc., Waltham, MA, USA) using Urea UV enzymatic method according to the manufacturer's protocol (Diagnosticum Inc., Budapest, Hungary). In brief, Reagent 1, containing nicotinamide adenine dinucleotide (NADH), and Reagent 2, containing Tris buffer (pH=7.6), α-ketoglutarate, urease and glutamate-dehydrogenase enzymes, were mixed in 3:1 volume ratio. In a two-step enzymatic reaction the changes induced in NADH/NAD^+ ratio altered the absorbance measured at 340 nm that correlated with the urea concentration of the plasma sample. The colorimetric detection was performed at 340 nm using Wallac VICTOR3™ Multilabel Plate Reader (PerkinElmer, Waltham, MA, USA).

4.7 Histological evaluations

4.7.1 Histology

4.7.1.1 Periodic acid-Schiff (PAS) staining

PAS staining was performed for the assessment of renal tubular injury. The following pathological changes were analyzed in the tissue: 1. bush border loss, 2. tubule dilatation, 3. cast in the tubules. The following scale was used for scoring: 0: no damage, 1: damage in 1-25% of the field, 2: 26-50% of the field, 3: 51-74% of the field, 4: 75% of the field.

4.7.1.2 Masson's trichrome staining

Interstitial fibrosis was evaluated at all time points using the method of Amman K et al. (79). Masson's trichrome method stains collagen blue, cytoplasm red and nuclei dark-black. The following scoring system was used to asses interstitial fibrosis: 0: no collagen deposition, 1: 1-25% of the field, 2: 26-50% of the field, 3: 51-75% of the field, 4: 76-100% of the field

4.7.2 Immunohistochemistry

4.7.2.1 F4/80 immunostaining

The paraffin-embedded samples were mounted on Superfrost Ultra Plus Adhesion slides (Thermo Fisher Scientific Inc., Waltham, MA, USA), deparaffinised and rehydrated in ethanol. For antigen retrieval Tris-EDTA solution (pH=9) was used. Three % bovine serum albumin (BSA, Millipore, Merck, Burlington, MA, USA) + Tris-buffer saline with Tween 20 (TBS-T) (pH=7.4-7.6) were used to prevent nonspecific protein binding. F4/80 staining was performed using rabbit monoclonal anti-mouse antibody (F4/80 (D2S9R) XP(R) Rabbit mAb #70076S, Cell Signaling, Leiden, The Netherlands). Slices were incubated for 2 hours at room temperature, and then peroxidase-labeled anti-rabbit antibody (HistolS®-MR-T, Histopathology Ltd., Pécs, Hungary) was incubated for 40 min at room temperature. Color development was performed using diaminobenzidine Quanto Chromogen (Thermo Scientific, Waltham, MA, USA). Slides were digitalized with Pannoramic Scan (3DHistech Ltd., Budapest, Hungary) with a 20x objective X 10x lens (total magnification: 200x). Images were analyzed with Fiji ImageJ software (80). The F4/80-positive and the total number of pixels was quantified in each image and their ratio was calculated.

4.8 Pathway analysis

MiRNA target network analysis was performed for those miRNAs, which were successfully validated by RT-qPCR. MiRNA-target interaction networks were created using miRNAtarget software (mirnatarget.com, Pharmahungary, Szeged, Hungary). The miRNAtarget software integrates data from the experimentally validated, manually administered miRTarBase (81) and in silico miRNA-target prediction databases, miRDB (82) and TargetScan (83), specific for Mus musculus. The following miRNA-target interaction data sources were used:

1. MiRDB v5.0 (release date: August, 2014), data were filtered for Mus musculus records on the basis of taxonomy ID

2. 'Conserved Sites context++ scores' file from TargetScan Mouse 7.2 (release date: August, 2018), where context++ scores of miRNA binding sites were summed for all transcripts, resulting total context++ scores

3. miRTarBase 8.0.

Predictions with miRDB scores and TargetScan total context++ scores ≤80 and ≥-0.2, respectively, were omitted from further analysis.

Networks were visualized by EntOptLayout plugin (version 2.1) for Cytoscape (version 3.8.0), alternately applying position and with optimization steps (84).

4.9 Western blot

Western blot analysis was performed as described by Kucsera D et al. (85). In brief, the tissue samples were homogenized in radioimmunoprecipitation assay (RIPA) buffer (Cell Signalling Technology, Danvers, MA, USA). Total of 20 μg protein was loaded onto 4-20% polyacrylamide gel, then separated with 90 V. After the separation step, the protein was transferred (Criterion Blotter, BioRad, Hercules, CA, USA) onto polyvinylidene difluoride (PVDF) membranes (BioRad, Hercules, CA, USA), then blocked with 5% BSA in 0.05% TBS-T. Membranes were incubated overnight at 4°C with the following primary antibodies dissolved in 5% BSA solution: CD2-associated protein (CD2AP) (5478, Cell Signaling Technology, Danvers, MA, USA, 1:1000 dilution) and Plexin A2 (Plxna2) (6896, Cell Signaling Technology, Danvers, MA, USA, 1:1000 dilution). The membranes were washed with 0.05% TBS-T 3 times for 10 min, and then incubated with a secondary antibody dissolved in 5% BSA solution (horseradish peroxidase-conjugated goat anti-rabbit, 7074, Cell Signaling Technology, Danvers, MA, USA, 1:2000 dilution) for 2 h at room temperature. After the incubation step with the secondary antibody, the membranes were wash 3 times for 10 min. In order to detect the corresponding bands, the membranes were incubated with enhanced chemiluminescence reagent (Clarity Western ECL Substrate or Clarity Max Western, BioRad, Hercules, CA, USA) for 5 min, after that the signal was recorded with the ChemiDoc XRS + System (BioRad, Hercules, CA, USA). Band intensity was assessed using the Image Lab Software (BioRad, Hercules, CA, USA). Total protein content were measured with the MemCode stain (24585, Pierce™ Reversible Protein Stain Kit for PVDF Membranes, Thermo Fisher Scientific, Waltham, MA, USA) as loading control.

4.10. Statistics

All results are expressed as mean±SEM. The data were analysed after base-10 logarithmic transformations if Bartlett's test indicated significant inhomogeneity of variances. Possible outliers were detected by the ROUT method (p=0.01) (86), and these data were omitted from the analysis. For comparison of scores in two groups, unpaired nonparametric Mann-Whitney U test was performed. For testing continuous variables, one-way or two-way analysis of variance (ANOVA) were performed followed by Dunnett or Tukey's post-hoc test, respectively. For data analysis and representation GraphPad Prism v8.0.2 (GraphPad Software, San Diego, CA, USA) was used.

DOI:10.14753/SE.2022.2613

5. Results

5.1 Removal of the healthy kidney restores the function of the postischemic kidney

Plasma urea concentration as a marker of kidney function did not change in mice after unilateral IR until contralateral nephrectomy. This observation suggests that a sole intact kidney can rapidly compensate for the loss of kidney function caused by unilateral IR. However, plasma urea concentration sharply increased after removal of the non-injured kidney seven days after IR, and remained elevated for the following three days, at least. This finding indicates that the injured kidney did not or hardly functioned at the time of Nx. Nevertheless, this elevation in plasma urea concentration was temporary, as it started to gradually decrease, and plasma urea concentrations were comparable to those of the sham nephrectomised mice three weeks later (28 days after IR). Furthermore, in the long-term study (see below), BUN was also normal on day 28, suggesting that in this experimental setup, the ischemic kidney needs three weeks to regain similar functional capacity to that in sham-operated mice (Fig. 5) (data from the 8- and 14-day studies are not shown).

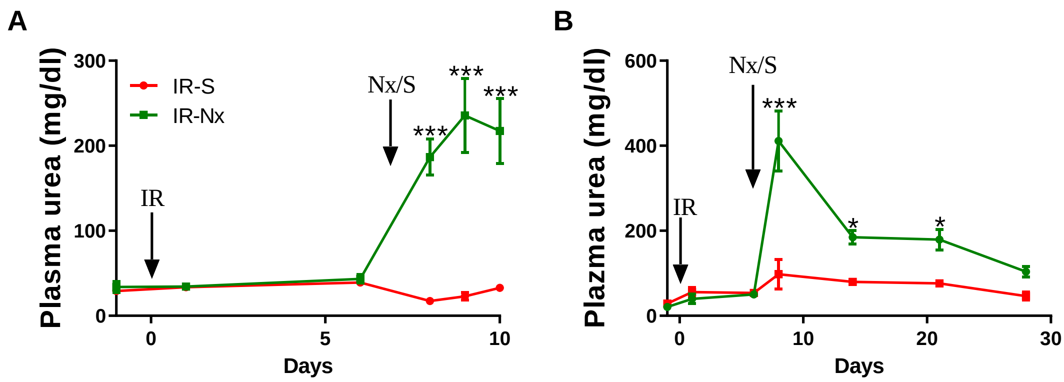

Figure 5. Kidney function after unilateral 30 min ischemia-reperfusion (IR) and subsequent sham operation (S) or contralateral nephrectomy (Nx) on day 7. Renal function was characterized by plasma urea concentration. The effect of IR was compensated by the contralateral, sham-operated kidney. Nx slowly restored the function of the post-ischemic kidney. Blood samples were taken on the days marked with nodes. (A) 10-day study; (B) 28-day study. Data are expressed as mean±SEM; two-way ANOVA for repeated measures with Tukey's post-hoc test; IR-S vs. IR-Nx groups; *: $p<0.05$, ***: $p<0.001$ (75).

The long-term study was performed in order to clarify, whether the Nx-induced improvement in kidney function is permanent or transient. In order to gain comprehensive understanding of the long-term effects of IR, the following four experimental groups were designed: sham IR-Sham Nx, sham IR-Nx, IR-Sham Nx, IR-Nx. No alterations in plasma urea concentrations were observed upon sham operation or Nx in the S-S, S-Nx and IR-S groups, but a gradual but small increase was noted in plasma urea concentrations on long-term. In contrast, in the IR-Nx group, plasma urea concentration sharply increased after Nx, and then decreased to a comparable level to that in the other three experimental groups by day 14, similarly to that seen in shorter experiments. This decrease lasted for up to day 77 with fluctuations in a narrow range. After day 77 a transient elevation was detected in plasma urea concentrations from day 112 to day 117, which diminished afterwards. However, from day 133 the plasma urea concentration began to increase sharply. One mouse died on day 139 and three others were moribund (i.e. mice were visibly fatigue, their eyes were squinted and their hair coat were rough), thus the study was terminated on the next day (day 140) (Fig. 6).

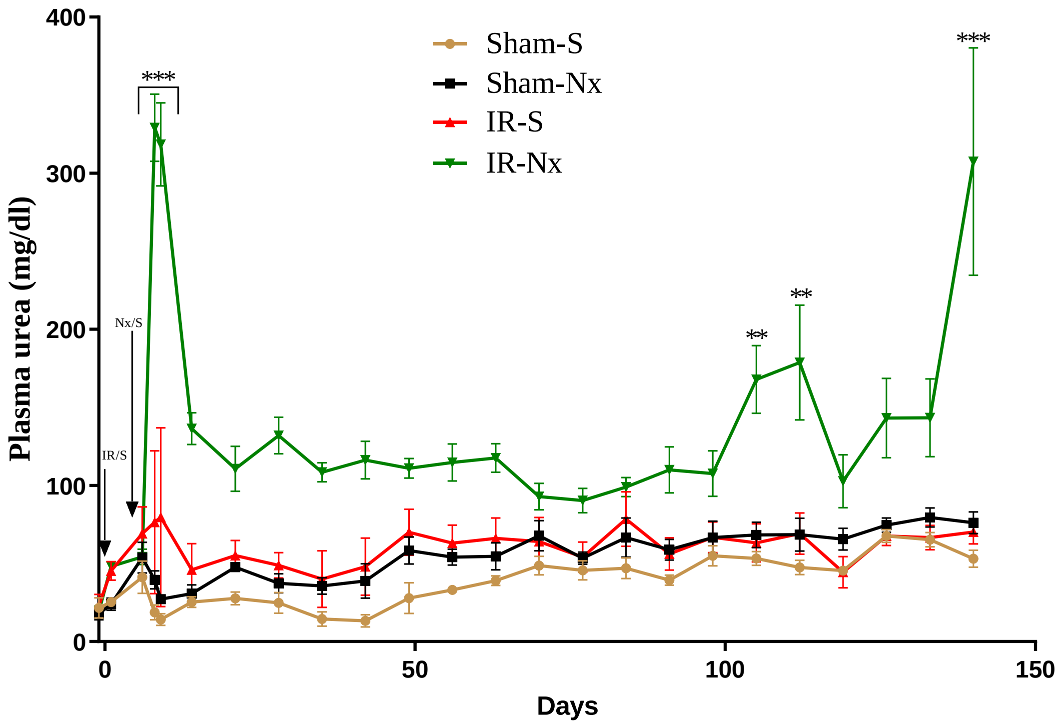

Figure 6. Kidney function after unilateral sham ischemia-reperfusion (Sham) or 30 min ischemia-reperfusion (IR) and subsequent sham contralateral nephrectomy (S) or contralateral nephrectomy (Nx) on day 7. Renal function was characterized by plasma urea concentration. Sham IR operations followed by either Nx or sham Nx did not cause pathological changes in plasma urea concentration up to day 140. After IR with sham Nx the plasma urea level remained comparable to those in the sham IR groups. Plasma urea concentration was markedly elevated after Nx on day 7 in the IR group, but few days later, it started to decrease similarly to that seen in the short-term experiments. Plasma urea concentration remained stable with small fluctuation up to 133 day, when plasma urea concentration began to increase to pathophysiological levels. Blood samples were taken on days shown by dots on the graph. Data are expressed as mean±SEM; two-way ANOVA for repeated measures with Tukey's post-hoc test; IR-Nx vs. all other groups; **: $p<0.001$, ***: $p<0.0001$ (75).

5.2 Histological analysis revealed excessive tubular injury and tubulointerstitial fibrosis in the postischemic kidneys

Periodic-acid Schiff staining was performed in order to evaluate the extent of tubular injury in the ischemic kidneys. The non-ischemic right kidney was used as control. No histological damage was seen in the right kidneys at any time points investigated. In the IR-S group marked tubular injury was observed in the postischemic kidneys (i.e. loss of the brush border, flattening of the tubular epithelial cells, tubular lumen dilatation and accumulation of PAS-positive material in the lumen of the distal tubule and collecting ducts), as soon as on day 8, along with inflammatory infiltration from day 10, and atrophy (dilated pelvis and calix surrounded by atrophic parenchyma) on day 28. Similar extent of tubular injury was seen in the IR-Nx group on day 8, however, the post-ischemic kidney started to recover from day 10, and the tubular injury markedly decreased by day 28, and no signs of further deterioration was observed on day 140. Furthermore, inflammatory infiltration and atrophy were absent in these kidneys at the time points investigated (Fig. 7/A- C).

Tubulointerstitial fibrosis was evaluated using Masson's trichrome staining. The right kidneys showed no fibrotic matrix deposition in the interstitium. In the IR-S group the postischemic kidney displayed pathological level of extracellular matrix deposition from day 8. However, upon Nx, the ECM deposition almost stalled, resulting in lower level of ECM content in the kidney on days 14 and 28 compared to the postischemic kidneys in the IR-S group. Nevertheless, the matrix deposition persisted until day 140. In this experimental setup, the ischemia seldom caused vascular damage or glomerulosclerosis (Fig. 8/A-C).

DOI:10.14753/SE.2022.2613

A

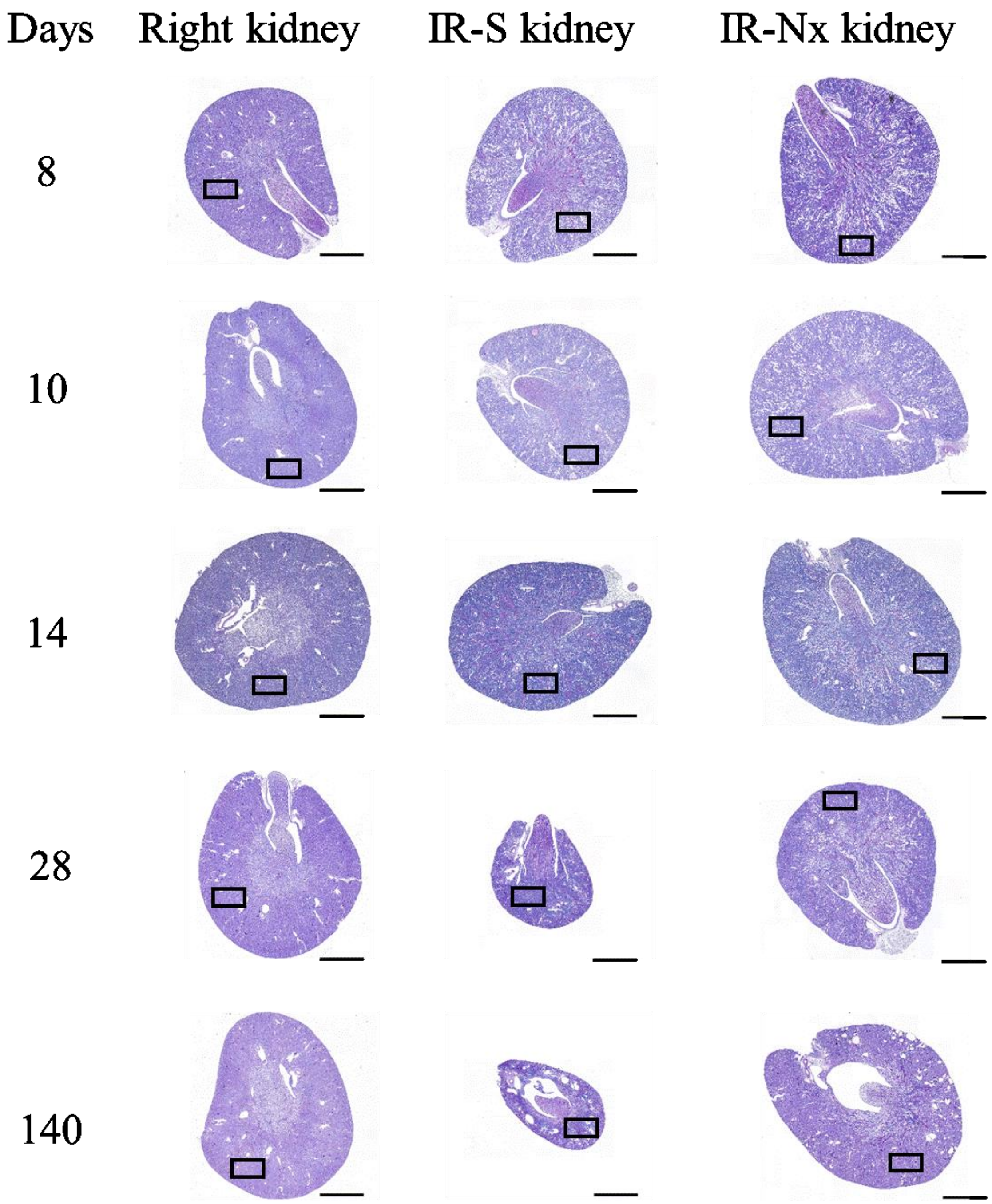

DOI:10.14753/SE.2022.2613

B

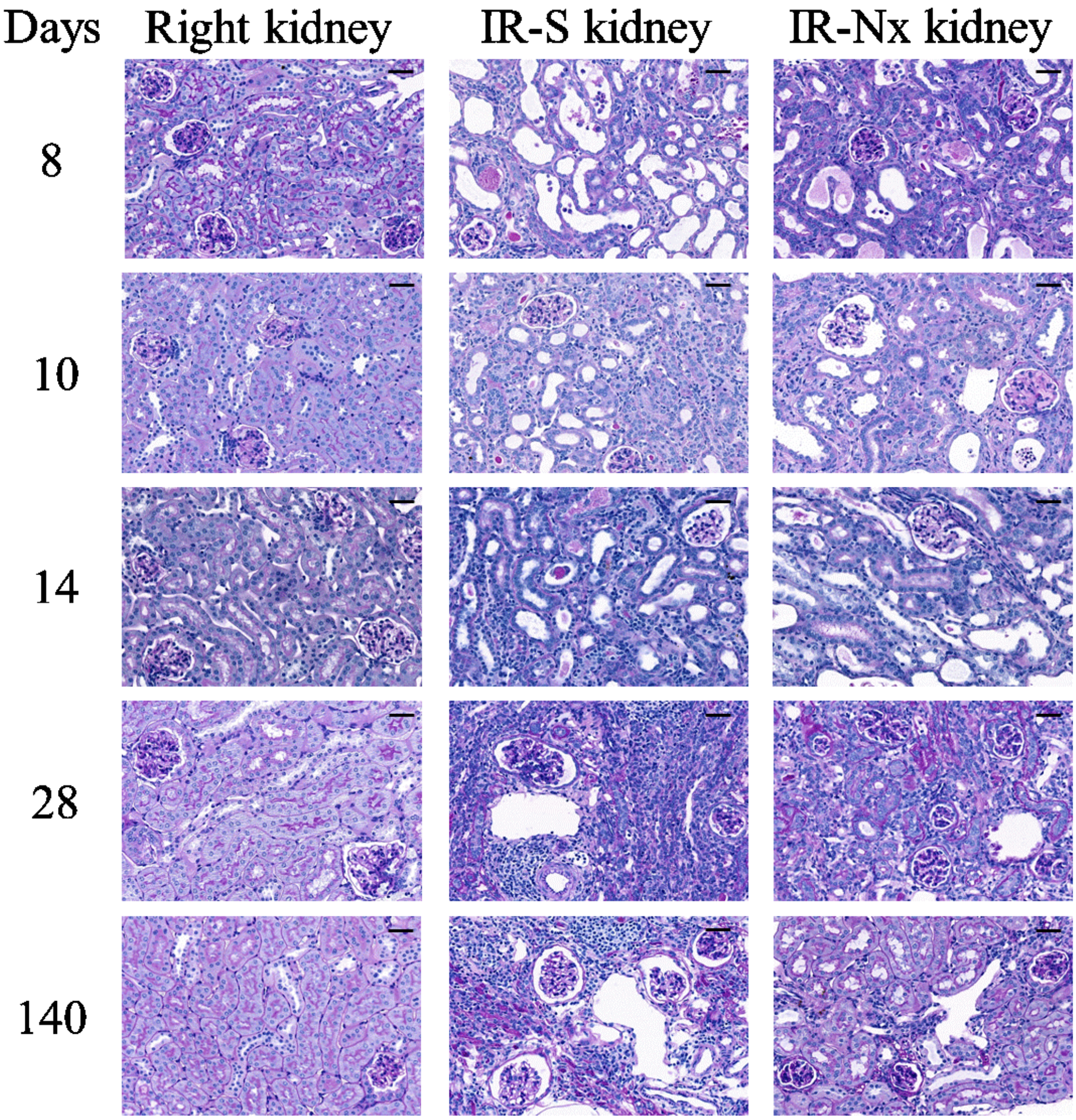

C

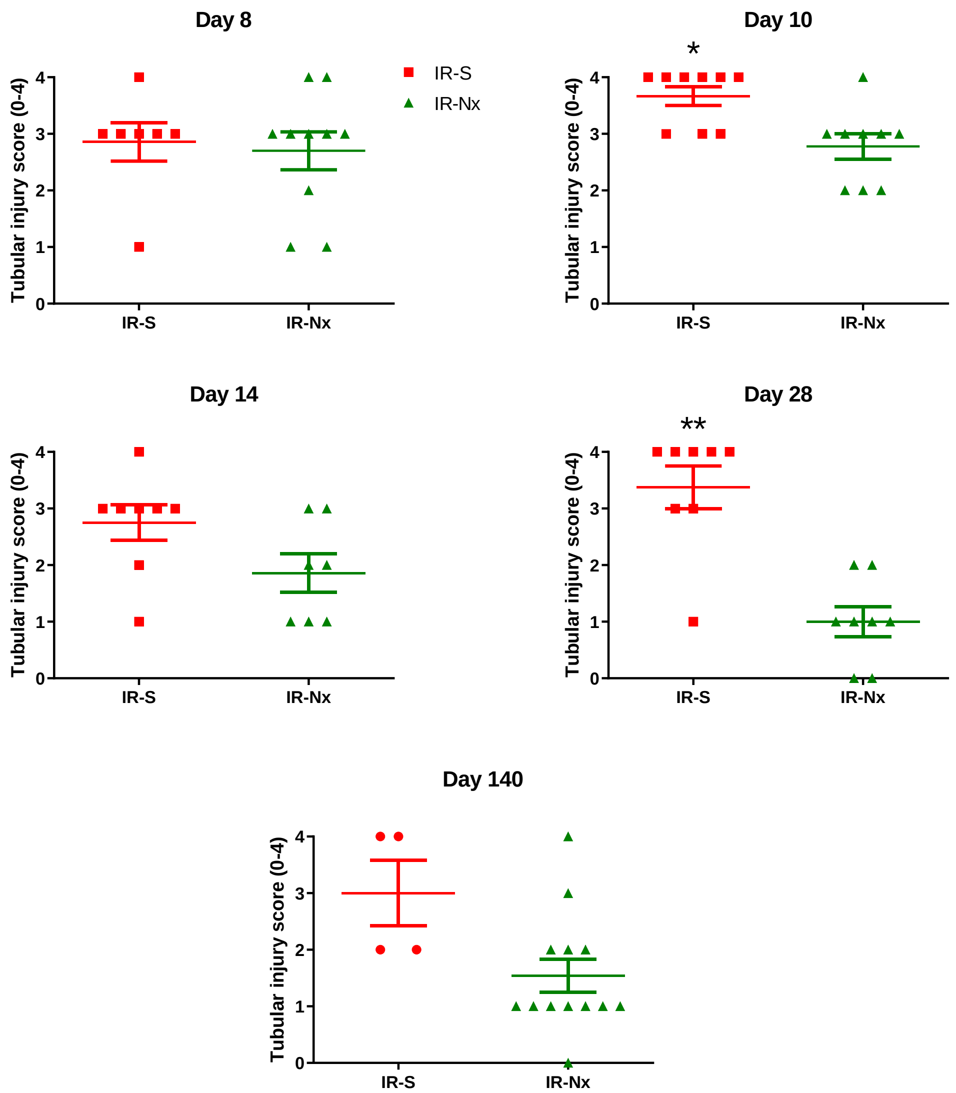

Figure 7. Kidney morphology at all investigated time points after 30 min of unilateral ischemia-reperfusion (IR) and subsequent sham operation (S) or contralateral nephrectomy (Nx) on day 7. Representative histological pictures show non-ischemic right kidneys, post-ischemic kidneys with contralateral sham surgery (IR-S group) and post-ischemic kidneys with Nx (IR-Nx) at low and high magnifications with the corresponding histology scores. (A) Periodic-acid Schiff (PAS) staining sections at low (40x) magnifications. (B) PAS staining at high magnification (800x). (C) Tubular injury scores (0-4), Scale bars: low magnification: 1000 µm, high magnification: 50 µm; Data are expressed as mean±SEM; Unpaired, nonparametric Mann-Whitney U-test; IR-S vs. IR-Nx groups, *: $p<0.05$, **: $p<0.01$, ***: $p<0.001$ (75).

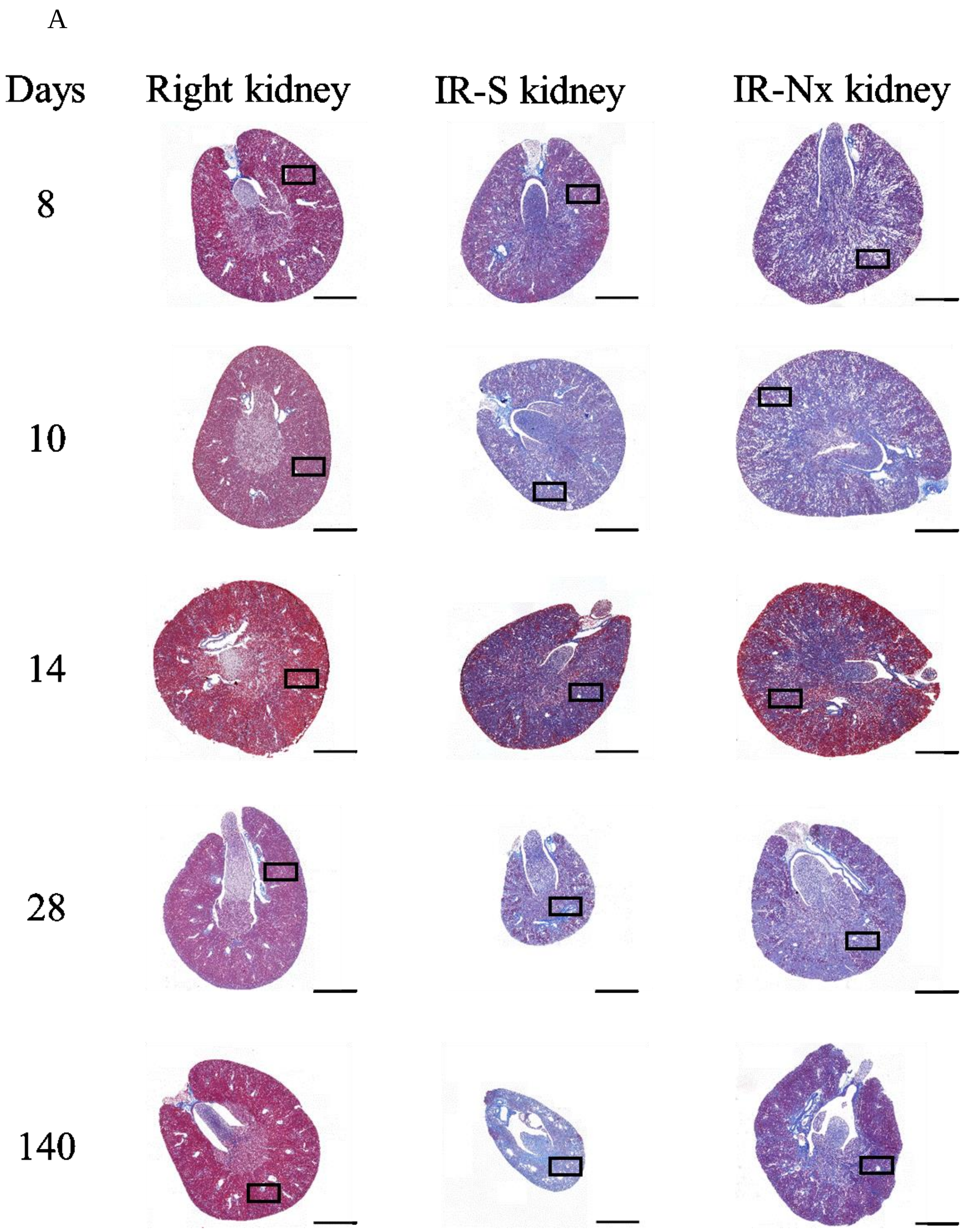
A
Days
Right kidney
IR-S kidney
IR-Nx kidney
8
10
14
28
140

B

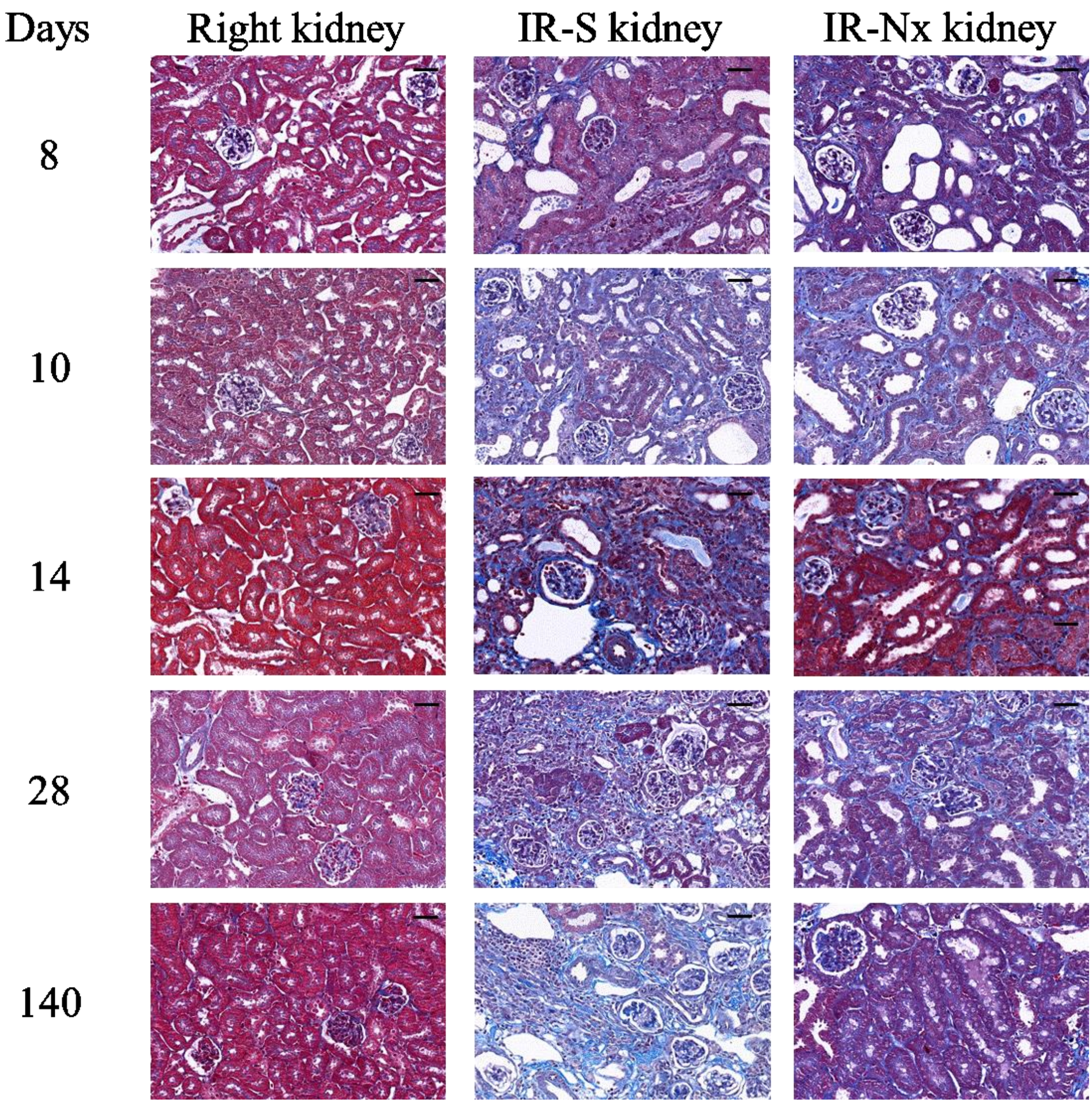

C

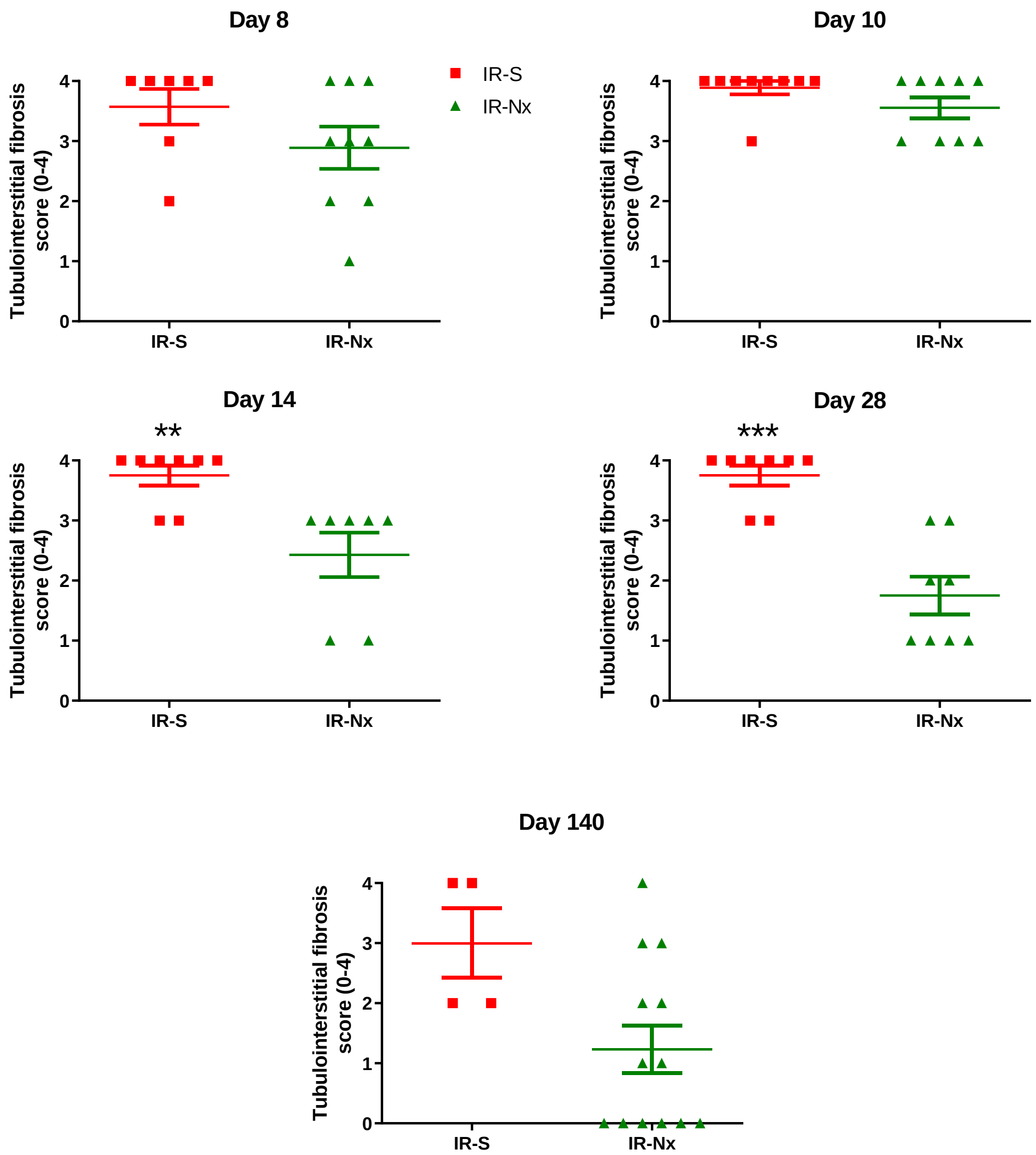

Figure 8. Extent of kidney fibrosis at all investigated time points after 30 min of unilateral ischemia-reperfusion (IR) and subsequent sham operation (S) or contralateral nephrectomy (Nx) on day 7. Representative histological pictures show non-ischemic right kidneys, post-ischemic kidneys with contralateral sham surgery (IR-S group) and post-ischemic kidneys with Nx (IR-Nx) at low and high magnifications with the corresponding histology scores. (A) Masson's trichrome-stained sections at low magnification (40x), (B) Masson's trichrome-stained sections at high magnification (800x). (C) Tubulointerstitial fibrosis scores (0-4). Scale bars: low magnification: 1000 μm, high magnification: 50 μm; Data are expressed as mean±SEM; Unpaired, nonparametric Mann-Whitney U-test; IR-S vs. IR-Nx groups, *: $p<0.05$, **: $p<0.01$, ***: $p<0.001$ (75).

5.3 Sham IR did not induce expression changes in the kidney compared to the uninjured right kidneys of IR animals

The contralateral right kidneys from the IR operated animals (S-S and S-Nx groups) were used as control tissue. To test whether the expression profile in these right kidneys is comparable to the uninjured left, sham IR operated kidneys, expression of the immune system-related TNF-α, the tubular injury marker LCN2 and the profibrotic TGF-β was measured on days 8 and 10, and compared to the right kidneys from the IR groups. No difference was observed in any gene expression in the sham-operated kidneys compared to the right kidneys from IR-S and IR-Nx groups (Fig. 9/A-F); hence no sham IR operations were performed in the 14- and 28-day long studies in accordance to the principles of 3R.

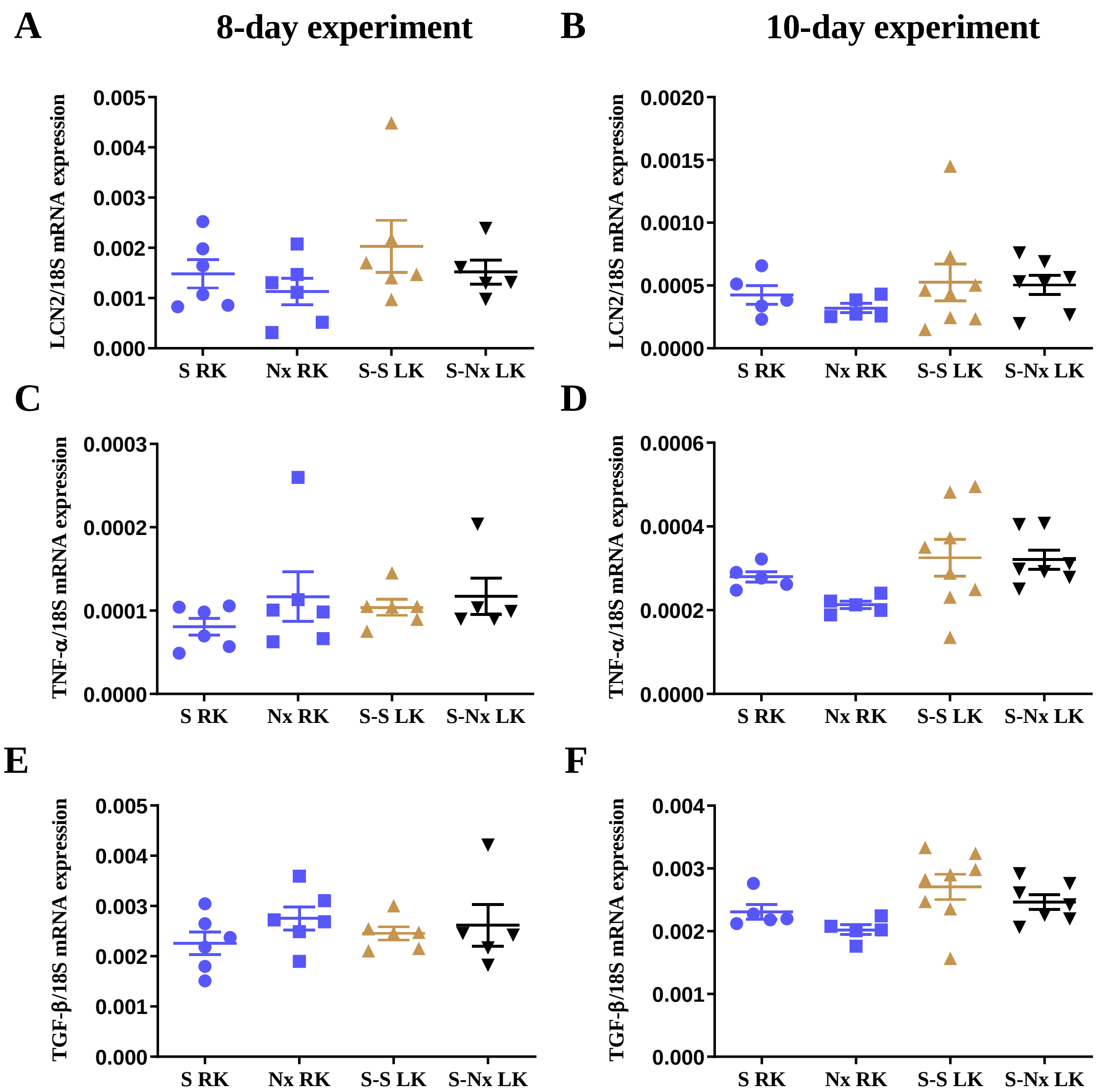

Figure 9. The mRNA expression profile normalized to 18S rRNA in the uninjured contralateral right kidneys (RK) in animals subjected to 30 min of unilateral ischemia-reperfusion and in the left kidneys (LK) after sham IR operation (S) with sham or contralateral nephrectomy (Nx) 7 days after IR. The immune system-related, tubular injury marker or profibrotic genes were similar 8 and 10 days after the initial injury. (A) Relative lipocalin-2 (LCN2) expression on day 8, and (B) day 10, (C) Relative tumor necrosis factor-α (TNF-α) expression profile on day 8 and (D), day 10, (E) Relative tumor growth factor-β (TGF- β) expression profile on day 8 and (F), day 10. Data are expressed as mean±SEM; one-way ANOVA with Tukey's post-hoc test (76).

We aimed to assess the key molecular changes, which contribute to the attenuation of kidney damage and fibrosis progression. The main focus was put on studying the molecular alterations on the first 28 days after IR. Expression of several genes was evaluated, which are potentially involved in the underlying biological processes.

5.4 Contralateral nephrectomy attenuated the tubular injury and inflammation-related mechanisms in the postischemic kidney

5.4.1. Contralateral nephrectomy was followed by downregulation of tubular injury marker lipocalin-2 and inflammation-related mRNAs in the postischemic kidney

The tubular epithelial damage marker lipocalin-2 mRNA level was markedly elevated in the postischemic IR-S kidneys in comparison to the right kidneys at the time points investigated. LCN2 peaked on day 10 (FC: 130.77±20.14) and its expression remained relatively stable up to day 28. Upon nephrectomy, LCN2 expression was lower in the IR-Nx group compared to the IR-S group from day 10, although this difference reached the level of statistical significance on day 28 only. Moreover, LCN2 expression was elevated in the postischemic kidney in the IR-Nx group compared the non-injured kidneys at all times (Fig. 10/A).

TNF-α mRNA was markedly elevated in the post-ischemic IR-S kidneys compared to the non-ischemic right kidneys. The maximum elevation of TNF-α was detected on day 28 although similar increases were seen on all other days (FC: 17.96±1.84 on day 28 and 17.74±2.27 on day 10). Unlike expression of the other three investigated proinflammatory genes, TNF-α remained high with some fluctuation throughout. Upon nephrectomy, the TNF-α upregulation was markedly attenuated in the post-ischemic IR-Nx kidney compared to the ischemic kidney in the IR-S group at all time points investigated, and the peak elevation was seen on day 10 (FC: 7.49±0.69). Despite Nx, TNF-α mRNA expression remained higher in the ischemic than in the control kidneys (Fig. 10/B).

Compared to the uninjured right kidneys, complement component 3 response was the greatest to IR (FC: 286.3±24.0, on day 10) among the proinflammatory genes studied (CCL-2, IL-6, TNF-α) in the post-ischemic IR-S kidneys. C3 mRNA gradually dropped from day 10 to 28, although it remained higher than in the control kidneys even on day 28. Nephrectomy markedly downregulated C3 expression from day 8 to day 14 compared to the postischemic IR-S kidneys with similar kinetics as in the IR-S group. Despite this Nx-induced reduction, C3 mRNA expression remained elevated compared to the non-ischemic right kidneys at all time points investigated (Fig. 10/C).

Chemokine C-C motif ligand 2 was significantly elevated upon IR in the IR-S group compared to the right kidneys on all days studied. It peaked on day 10 (FC: 124.4±22.5) and decreased by day 28. Nx markedly attenuated CCL2 expression in the IR-Nx group compared to the ischemic kidneys in the IR-S group, but no significant difference was detected between these groups on day 28. Although Nx significantly reduced CCL2 mRNA in the post-ischemic IR-Nx kidneys up to day 14, its expression was higher than in the non-ischemic right kidneys at all times (Fig. 10/D).

Interleukin-6 mRNA level was considerably increased in the post-ischemic IR-S kidneys compared to the right kidneys. In contrast to the expression of other proinflammatory genes, IL-6 expression was much higher on day 14 (FC: 28.26±5.32) than on any other days. The effect of Nx on IL-6 expression was significant on days 7 and 14 only (day 14: 19.18±4.08 vs. 8.20±2.46) in comparison to the IR-S group. Furthermore, the expression of IL-6 remained significantly elevated in the post-ischemic IR-Nx kidneys in comparison to the right kidneys at all time points (Fig. 10/E).

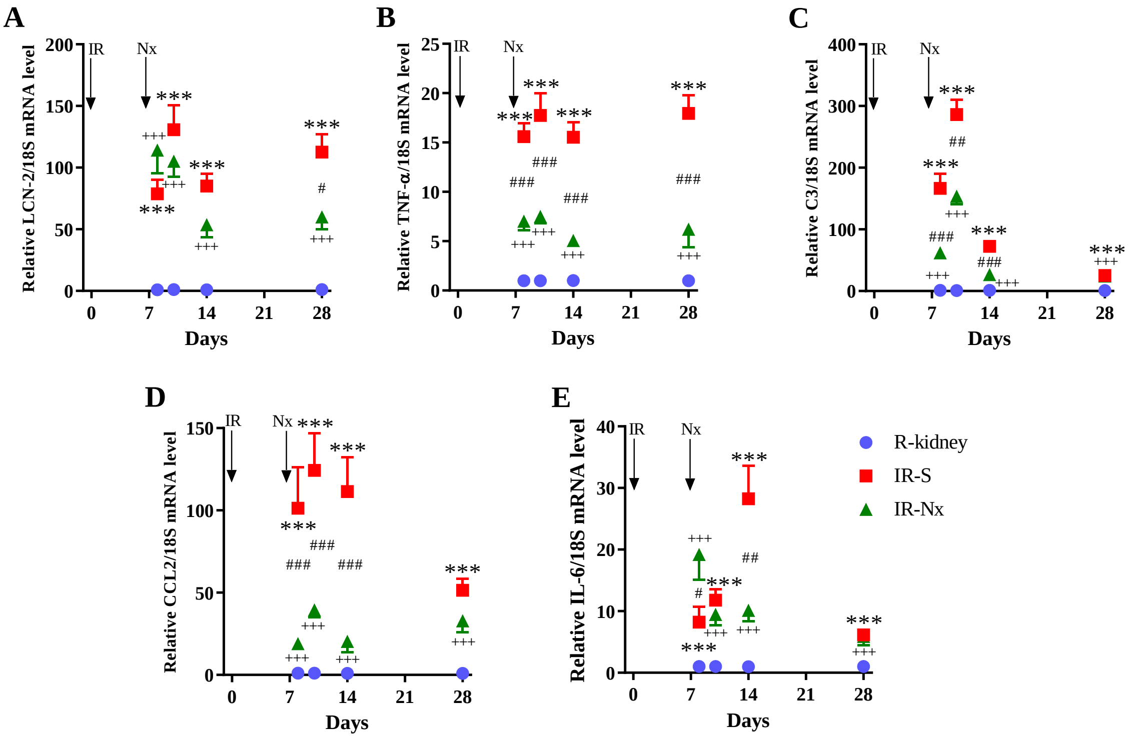

Figure 10. Expression of tubular injury-, inflammatory- and immune system-related mRNAs given as fold changes in kidneys of mice subjected to 30 min unilateral ischemia-reperfusion (IR) and sham contralateral nephrectomy (IR-S) or delayed contralateral nephrectomy (IR-Nx) 7 days later. (A) Lipocalin-2 (LCN2), (B) Tumor necrosis factor-alpha (TNF-α), (C) Complement component 3 (C3), (D) Chemokine C-C motif ligand 2 (CCL2), (E) Interleukin-6 (IL-6). Data are expressed as mean±SEM; two-way ANOVA with Tukey's post-hoc test; IR-S group vs. non-ischemic kidney: ***: $p<0.001$; IR-Nx group vs. non-ischemic kidney: +++: $p<0.001$; IR-S vs. IR-Nx: ##: $p<0.01$, ###: $p<0.001$ (75).

5.4.2 Contralateral nephrectomy markedly decreased macrophage infiltration in the postischemic kidney

Based on the strikingly altered expression of several proinflammatory- and immune system-related genes, macrophage specific immunohistochemistry was used to assess macrophage infiltration. IR caused a marked increase in the overall macrophage content in the post-ischemic IR-S and IR-Nx kidneys compared to the non-injured kidneys at all investigated time points. Similarly to the downregulation of mRNA expression of inflammatory- and immune system-related genes, Nx markedly decreased the macrophage content of the post-ischemic kidneys in the IR-Nx group compared to the IR-S group form days 10 to 28 , indicating a substantial reduction in macrophage infiltration (Fig. 11/A-C).

A

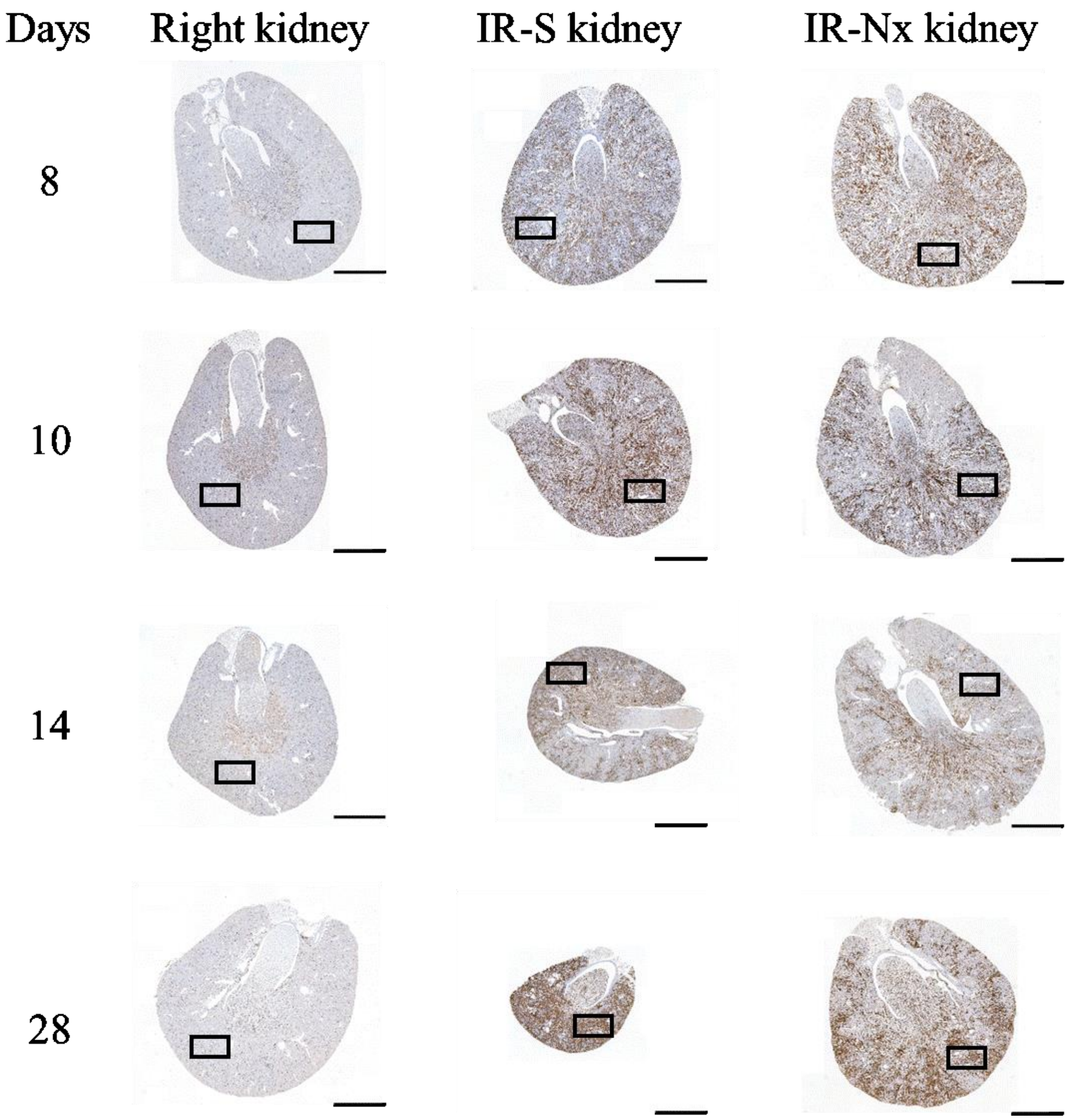

B

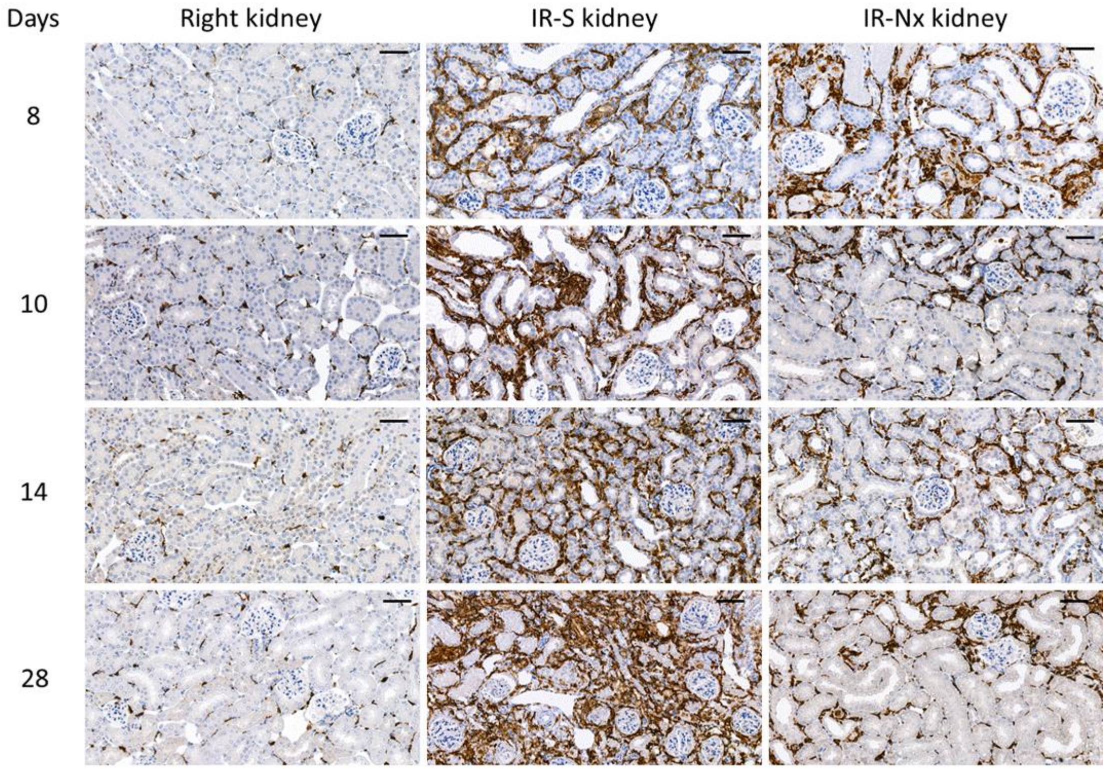

C

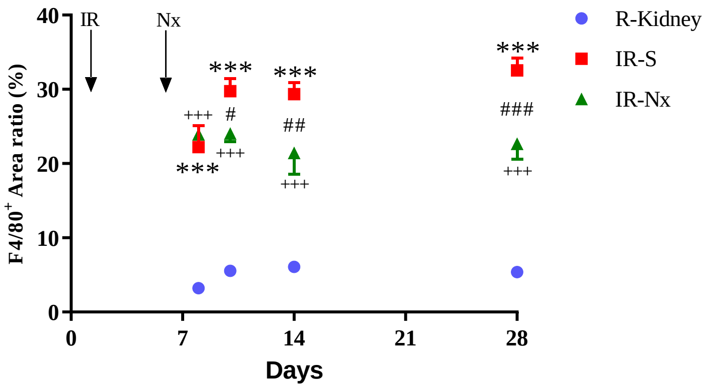

Figure 11. Macrophage infiltration following 30-min of unilateral ischemia-reperfusion (IR) and sham contralateral nephrectomy (S) or contralateral nephrectomy (Nx) 7 days later. Macrophages were visualized with macrophage-specific F4/80 immunostaining. Representative pictures show non-ischemic right-kidneys, post-ischemic kidneys with contralateral sham operation (IR-S group) and post-ischemic kidneys with Nx (IR-Nx group). (A) F4/80 staining at low magnification (40x), (B) F4/80 immunostaining at high magnification (800x). (C) Ratios of F4/80 positive and whole kidney area. Scale bars: low magnification: 1000 µm, high magnification: 50 µm. Data are expressed as mean±SEM; two-way repeated measures ANOVA with Tukey's post-hoc test; IR-S group vs. non-ischemic kidney: ***: p<0.001, IR-Nx group vs. non-ischemic kidney: +++: p<0.001; IR-S vs. IR-Nx: #: p<0.05, ##: p<0.01, ###: p<0.001 (75).

5.5 Hypoxia and oxidative stress are evident in the post-ischemic kidney

Hypoxia-inducible factor-1α mRNA level peaked on day 8 (FC: 1.70±0.18) in the post-ischemic IR-S kidney compared to the right kidney. This increased expression returned to physiological levels on days 10 and 14, but on day 28 its expression increased again. No difference was detected between the postischemic IR-Nx and the IR-S kidneys, however HIF-1α expression in postischemic IR-Nx kidneys was comparable to that in non-ischemic kidneys at all time points investigated (Fig. 12/A).

The other member of the HIF family, HIF-2α was affected differently. Upon ischemia HIF-2α was higher in postischemic IR-S kidneys than in control kidneys only on days 10, 14 and 28. The highest increase was detected on day 10 (FC: 1.67±0.18) but a similar elevation was seen on day 28 (FC: 1.66±0.18). Nx restored the expression of HIF-2α to the control level in the postischemic IR-Nx kidneys on days 10 and 14. However, on day 28 HIF-2α mRNA slightly but markedly increased in comparison to the right kidneys (FC: 1.49±0.19) and its expression was similar to that in the postischemic IR-S kidneys (Fig. 12/B).

Nuclear factor erythroid 2–related factor mRNA level was increased in the post-ischemic IR-S kidneys in comparison the non-ischemic kidneys at all time points. The peak effect of ischemia was observed on day 8 (FC: 2.39±0.27), and NRF2 mRNA level remained increased. Nephrectomy markedly decreased NRF2 expression in the IR-Nx group compared to the IR-S group except on day 10, but still remained significantly elevated compared to the right kidneys at all times (Fig. 12/C).

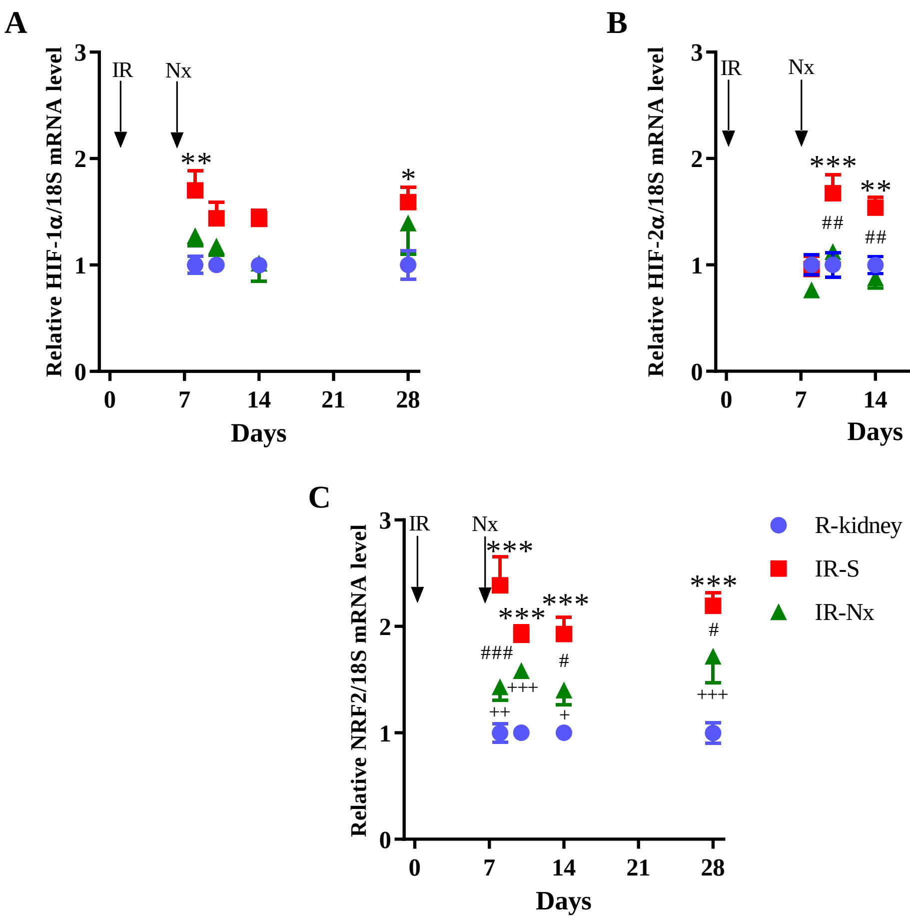

Figure 12. Expression of hypoxia- and oxidative stress-related mRNAs given as fold changes upon 30 min unilateral ischemia-reperfusion (IR) followed by sham contralateral nephrectomy (S) or contralateral nephrectomy (Nx) 7 days later. (A) Hypoxia-inducible factor-1α (HIF-1α), (B) Hypoxia-inducible factor-2α (HIF-2α), (C) Nuclear factor erythroid 2–related factor 2 (NRF2). Data are expressed as mean±SEM; two-way ANOVA for repeated measurements with Tukey's post-hoc test; IR-S group vs. non-ischemic kidney: *: p<0.05, **: p<0.01, ***: p<0.001; IR-Nx group vs. non-ischemic kidney: +: p<0.05, ++: p<0.01, +++: p<0.001; IR-S vs. IR-Nx: #: p<0.05, ##: p<0.01, ###: p<0.001 (75).

5.6 Fibrosis- and tubular injury-related gene expression was downregulated after contralateral nephrectomy

MRNA level of α-SMA was markedly increased in the post-ischemic IR-S kidneys compared to the right kidneys at all times with a peak effect on day 14 (FC: 7.60±1.41). After Nx, α-SMA expression was gradually reduced over time in the postischemic IR-Nx kidneys compared to the IR-S group, which changes reached the level of statistical significance by day 28. However, α-SMA mRNA expression remained markedly elevated in comparison to the non-ischemic kidneys at all time points (Fig. 13/A).

TGF-β expression was markedly increased in the post-ischemic IR-S kidney compared to the right kidneys at all time points investigated. TGF-β mRNA level peaked on day 10 (FC: 8.17±0.49), however, its expression progressively decreased afterwards. Although nephrectomy markedly decreased the TGF-β mRNA level in the post-ischemic IR-Nx kidneys compared to the IR-S group, its expression was still significantly elevated in comparison to the non-ischemic kidneys, at all time (Fig. 13/B).

Collagen 1a1 mRNA expression was opposite to that of α-SMA. Col1a1 mRNA level progressively increased in the IR-S group and reached a maximum on day 28 (41.03±5.39) compared to the right kidneys. Nx gradually and considerably decreased mRNA level of Col1a1 in the IR-Nx group over time in comparison to the IR-S group. However, Col1a1 expression remained elevated compared to the right kidneys at all time points investigated (Fig. 13/C).

IR caused a marked increase in fibronectin 1 mRNA expression in comparison to right kidneys at all time points investigated. FN1 mRNA peaked on day 10 (FC: 16.27±2.43) in the postischemic IR-S kidneys. Upon nephrectomy, the expression of FN1 was markedly reduced in the post-ischemic IR-Nx kidney compared to the IR-S group from day 10, but despite the gradual reduction, FN1 mRNA remained elevated in comparison to the non-ischemic kidneys at all times (Fig. 13/D).

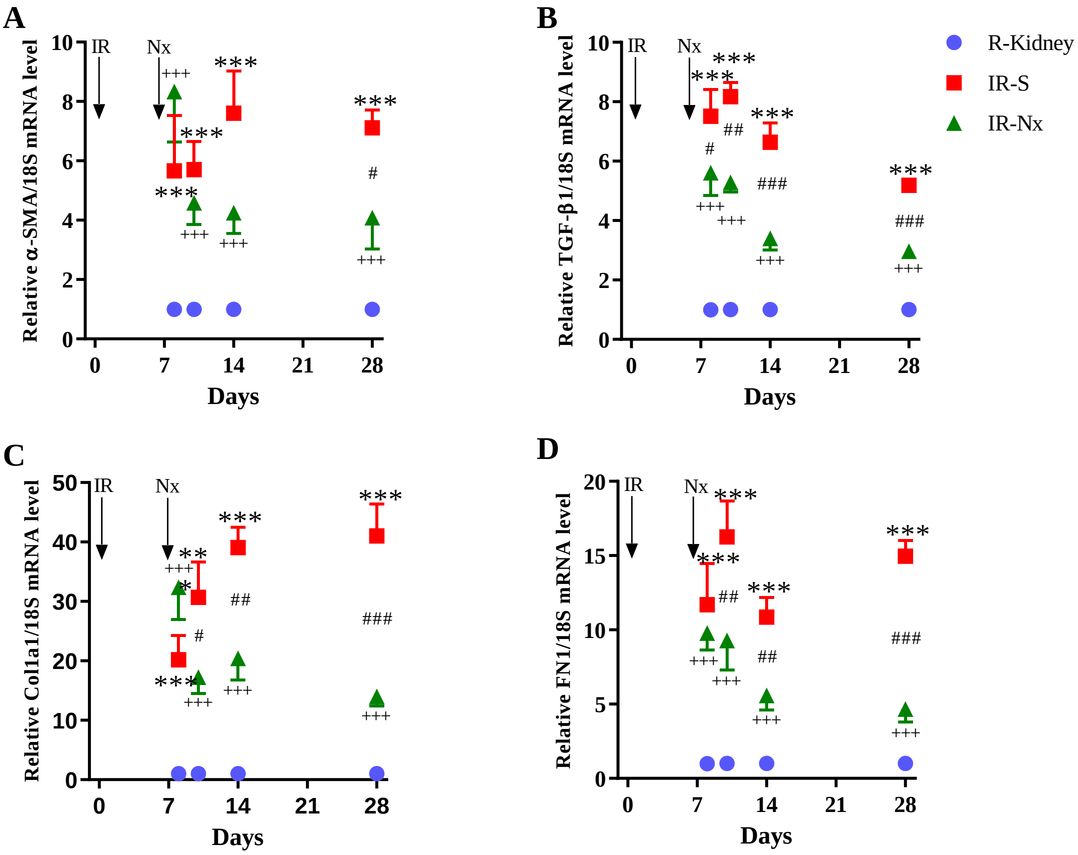

Figure 13. Fibrosis-related mRNA levels given as fold changes following 30 min unilateral ischemia-reperfusion (IR) and sham contralateral nephrectomy (S) or contralateral nephrectomy (Nx) 7 days later. (A) alpha-smooth muscle actin (α-SMA), (B) Transforming growth factor beta (TGF-β), (C) Collagen 1a1 (Col1a1), (D) Fibronectin 1 (FN1). Data are expressed as mean±SEM; two-way ANOVA for repeated measurements with Tukey's post-hoc test; IR-S group vs. non-ischemic kidney: ***: $p<0.001$; IR-Nx group vs. non-ischemic kidney: +++: $p<0.001$; IR-S vs. IR-Nx: #: $p<0.05$, ##: $p<0.01$, ###: $p<0.001$ (75).

5.7 The miArray profile of the post-ischemic kidney shows markedly altered miRNA levels

5.7.1 miRNA microArray

MiRNA microArray was performed in all four groups on day 8 to further characterize the early molecular responses and to gain insight into the regulatory mechanisms affected by unilateral nephrectomy. IR had a marked impact on miRNome (Fig. 14/A). After IR, 43 miRNAs were significantly up- and 29 downregulated with fold changes more than 1.5-fold as well as 20 miRNAs were up- and 6 downregulated with FCs more than 2-fold in the IR-S group in comparison to the S-S group (Table 11).

However, the effect of nephrectomy proved to be moderate 24 hours after Nx. None of the miRNAs upregulated and only miR-762 (FC: 0.61) and miR-2861 (FC: 0.65) were downregulated more than 1.5-fold in IR-Nx kidneys compared to the postischemic IR-S kidneys (Fig. 14/B).

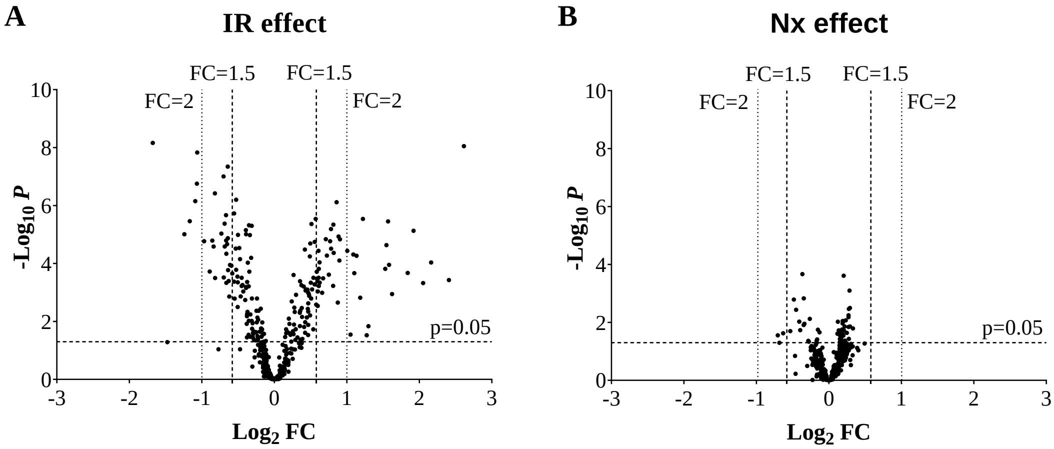

Figure 14. Results of the miRNA microArray performed by Exiqon. (A) The effect of 30 min renal unilateral ischemia-reperfusion (IR) on expression of miRNAs 8 days after IR compared to sham IR kidneys. (B) The effect of contralateral nephrectomy (Nx) in the postischemic kidney on expression of miRNAs 24 hours after Nx in comparison to the post-ischemic kidney with sham Nx. Significance levels (given as –log10 p-value) are plotted against fold changes (FCs) (given as log2). Vertical lines mark 1.5- and 2-fold FCs, horizontal lines mark the significance level ($p<0.05$) (76).

A

No.	miRNA	FC	ANOVA p-value	No.	miRNA	FC	ANOVA p-value
1	mmu-miR-21a-5p	6.13±0.63	0.0000	19	mmu-miR-5129-5p	2.07±0.82	0.0283
2	mmu-miR-2137	5.31±1.88	0.0004	20	mmu-miR-3100-3p	2.01±0.36	0.0000
3	mmu-miR-142-3p	4.48±1.31	0.0001	21	mmu-miR-17-5p	1.87±0.12	0.0000
4	mmu-miR-762	4.15±1.46	0.0005	22	mmu-miR-20b-5p	1.86±0.26	0.0001
5	mmu-miR-223-3p	3.79±0.79	0.0000	23	mmu-miR-15b-5p	1.85±0.13	0.0000
6	mmu-miR-142-5p	3.58±0.81	0.0002	24	mmu-miR-34a-5p	1.83±0.29	0.0022
7	mmu-miR-2861	3.08±0.94	0.0011	25	mmu-miR-19a-3p	1.81±0.14	0.0000
8	mmu-miR-3102-5p	2.99±0.77	0.0001	26	mmu-miR-17-3p	1.76±0.22	0.0000
9	mmu-miR-199a-5p	2.97±0.39	0.0000	27	mmu-miR-20a-5p	1.75±0.31	0.0006
10	mmu-miR-199a/199b-3p/	2.92±0.53	0.0000	28	mmu-miR-1892	1.72±0.25	0.0000
11	mmu-miR-199b-5p	2.89±0.54	0.0002	29	mmu-miR-489-5p	1.72±0.13	0.0000
12	mmu-miR-711	2.46±0.66	0.0146	30	mmu-miR-106a-5p	1.71±0.16	0.0000
13	mmu-miR-3473b	2.42±0.79	0.0300	31	mmu-miR-3095-3p	1.68±0.28	0.0002
14	mmu-miR-214-3p	2.33±0.16	0.0000	32	mmu-miR-19b-3p	1.65±0.13	0.0001
15	mmu-miR-146b-5p	2.27±0.64	0.0015	33	mmu-miR-23a-3p	1.64±0.13	0.0000
16	mmu-miR-3970	2.20±0.31	0.0001	34	mmu-miR-1894-3p	1.58±0.27	0.0010
17	mmu-miR-146a-5p	2.15±0.45	0.0002	35	mmu-miR-503-5p	1.54±0.23	0.0005
18	mmu-miR-21a-3p	2.13±0.36	0.0000	36	mmu-miR-674-5p	1.53±0.17	0.0002

No.	miRNA	FC	p-value	No.	miRNA	FC	p-value
37	mmu-miR-25-5p	1.53±0.25	0.0006	41	mmu-miR-710	1.52±0.25	0.0029
38	mmu-miR-27a-3p	1.53±0.16	0.0003	42	mmu-miR-3084-3p	1.51±0.11	0.0004
39	mmu-miR-665-3p	1.53±0.14	0.0000	43	mmu-miR-24-2-5p	1.50±0.09	0.0002
40	mmu-miR-290a-5p	1.52±0.22	0.0009				

B

No.	miRNA	FC	ANOVA p-value	No.	miRNA	FC	ANOVA p-value
1	mmu-miR-129-1-3p	0.31±0.06	0.0000	13	mmu-miR-669m-3p	0.60±0.10	0.0000
2	mmu-miR-193a-3p	0.42±0.08	0.0000	14	mmu-miR-677-3p	0.62±0.05	0.0000
3	mmu-miR-1839-3p	0.45±0.10	0.0000	15	mmu-miR-185-5p	0.62±0.06	0.0003
4	mmu-miR-150-5p	0.47±0.05	0.0000	16	mmu-miR-30e-5p	0.62±0.06	0.0000
5	mmu-miR-3961	0.48±0.06	0.0000	17	mmu-miR-378b	0.62±0.05	0.0000
6	mmu-miR-190a-5p	0.48±0.04	0.0000	18	mmu-miR-34b-3p	0.63±0.06	0.0000
7	mmu-miR-365-3p	0.51±0.09	0.0000	19	mmu-miR-505-5p	0.63±0.06	0.0000
8	mmu-miR-194-5p	0.54±0.07	0.0002	20	mmu-miR-669l-3p	0.63±0.11	0.0000
9	mmu-miR-34c-3p	0.55±0.08	0.0000	21	mmu-miR-192-5p	0.63±0.13	0.0005
10	mmu-miR-455-3p	0.56±0.04	0.0000	22	mmu-miR-30c-5p	0.64±0.03	0.0000
11	mmu-miR-187-3p	0.57±0.05	0.0000	23	mmu-miR-344h-3p	0.64±0.05	0.0000
12	mmu-miR-29c-3p	0.57±0.09	0.0003	24	mmu-miR-378a-3p/ mmu-miR-378b/ mmu-miR-378c	0.64±0.07	0.0000

No.	miRNA	FC	ANOVA p-value	No.	miRNA	FC	ANOVA p-value
25	mmu-miR-1192	0.64±0.09	0.0002	28	mmu-miR-126a-5p	0.65±0.04	0.0001
26	mmu-miR-378a-3p	0.65±0.07	0.0004	29	mmu-miR-30e-3p	0.66±0.06	0.0001
27	mmu-miR-215-5p	0.65±0.11	0.0014				

Table 11. List of differentially expressed miRNAs in the postischemic kidneys 8 days after 30 min unilateral ischemia-reperfusion based on miRNA microArray performed by Exiqon. A: MiRNAs upregulated at least 1.5-fold (50%), B: MiRNAs downregulated at least 1.5-fold (50%). Data expressed as mean±SEM; one-way ANOVA (76).

5.7.2. miRNA microArray validation by RT-qPCR

Expression of MiRNAs altered at least 2.5-fold, were attempted to validate by RT-qPCR. Furthermore, the upregulated miR-21a-3p, miR-146a-5p and miR-214-3p and the downregulated miR-762 and miR-2861 were also measured by RT-qPCR.

Expression of miRNAs in the uninjured left kidney from the S-S and S-Nx groups and in the control right kidneys were similar (Table 12).

miRNA	ANOVA p-values in the 8-day experiment	ANOVA p-values in 10-day experiment
miR-21a-3p	0.078	0.668
miR-21a-5p	0.935	0.364
miR-142a-3p	0.379	0.756
miR-142a-5p	0.086	0.523
miR-146a-5p	0.328	0.974
miR-199a-3p	0.104	0.865
miR-199a-5p	0.321	0.559
miR-214-3p	0.166	0.837
miR-223-3p	0.297	0.588

Table 12. Expression of miRNAs normalized to let-7g-5p revealed no difference among the uninjured left kidneys and right kidney in sham unilateral ischemia-reperfusion (S)+ sham contralateral nephrectomy, S + delayed contralateral nephrectomy (Nx) operated groups and the control right kidneys from 30 min unilateral ischemia-reperfusion IR+ sham Nx, IR + Nx groups 8 and 10 days after the initial intervention. The table lists the p-values of the main effect of one-way ANOVA (76).

IR altered the expression of a number of miRNAs in the IR-S and IR-Nx left kidneys in comparison to the control kidneys on day 8 (Table 13). Thus, the following section is focused on miRNA expression changes in the postischemic IR-S and IR-Nx kidneys in comparisons to the control right kidneys.

miRNA	ANOVA	S-S vs. IR-S	IR-S vs. IR-Nx
miR-21a-5p	0.000	0.000	0.347
miR-2137	0.011	0.009	0.304
miR-142a-3p	0.000	0.000	0.946
miR-762	0.900	-	-
miR-223-3p	0.000	0.000	0.309
miR-142a-5p	0.000	0.000	0.940
miR-3102-5p	0.136	-	-
miR-199a-5p	0.000	0.001	0.420
miR-199a-3p	0.000	0.000	1.000
miR-214-3p	0.000	0.000	0.896
miR-146a-5p	0.000	0.001	0.990
miR-21a-3p	0.000	0.000	0.008
miR-129-1-3p	0.174	-	-

Table 13. Comparison of the let-7g-5p normalized expression of miRNAs measured by RT-qPCR in the injured and uninjured left kidneys in the sham ischemia-reperfusion + sham contralateral nephrectomy surgery on day 8 (S-S) and 30 min unilateral ischemia-reperfusion + sham contralateral nephrectomy surgery (IR-S) groups as well as in the IR-S and 30 min unilateral ischemia-reperfusion + contralateral nephrectomy (IR-Nx) groups on day 7. The table contains the p-values of the two-way ANOVA with Tukey's post-hoc test. -: no statistical difference (76).

The RT-qPCR results were similar to those obtained by microArray for mmu-miR-21a-5p, -2137, -142-3p, 223-3p, -142-5p, -199a-5p, -199a-3p/-199b-3p, -214-3p, -146a-5p. The expression of these miRNAs similarly increased in the post-ischemic IR-S and IR-Nx kidneys in comparison to the sham IR kidneys.

However, RT-qPCR validation produced different results for miR-762, 3102-5p and miR-129-1-3p as the expression of these miRNAs did not change after IR contrary to the results of microArray. Moreover, miR-2861 could not be detected by RT-qPCR. Regarding miR-21a-3p, the microArray showed that its expression was markedly elevated in the postischemic kidneys compared to the sham IR kidneys. However, the RT-qPCR measurement revealed significant increases in the post-ischemic IR-Nx kidneys in comparison to the postischemic IR-S kidneys, which effects were not demonstrated by the microArray.

The expression of RT-qPCR validated miRNAs, except miR-2137, were measured at all time-points. To confirm that IR alone altered the expression of miRNAs, an additional time point (day 7) was included.

Mir-21a-3p was markedly elevated in the postischemic IR-S kidney compared to the non-injured kidney in all time points investigated. It peaked on day 10 (FC: 9.66±1.35), however, gradually decreased afterwards. Upon Nx, miR-21a-3p was significantly increased in the postischemic IR-Nx kidneys compared to the IR-S kidneys on day 8 (FC: 11.70±0.71), but began to decrease thereafter and no difference was observed at later time points. Furthermore, the expression of miR-21a-3p was significantly elevated in the postischemic IR-Nx kidney compared to the uninjured kidney (Fig. 15/A).

IR markedly increased the expression of miR-21a-5p in the postischemic IR-S kidneys compared to the right kidneys at all times. Its expression peaked on day 28 although a very similar elevation was observed on day 8 (FC: 8.53±0.92 and FC: 8.24±0.52, respectively). No differences were seen in the expression of miR-21a-5p between the postischemic IR-Nx and IR-S kidneys throughout the experiment, showing that despite Nx, miR-21a-5p was markedly increased in the IR-Nx group at all time points (Fig. 15/B).

IR augmented the expression of miR-142 duplex (-3p and -5p strands) in comparison to the non-injured kidneys at all time points. Both strands reached their highest level on day 28 (FCs: miR-142-3p: 22.53±2.93, miR-142-5p: 18.84±2.64). Upon nephrectomy, no difference was observed in the postischemic IR-Nx kidneys compared to the IR-S kidneys on day 8, but from day 10, the miRNA level of both strands of miR-142 significantly decreased in the IR-Nx group. However, despite these downregulations their expression was considerably higher in the postischemic IR-Nx kidneys in comparison to the right kidneys at all times and showed a progressive elevation up to day 28 (Fig. 15/C and D).

MiR-146a-5p expression was considerably upregulated in the postischemic IR-S kidneys in comparison to the right-kidneys at all time points. MiR-146a-5p expression peaked on day 10 (FC: 5.24±0.53) but started to gradually decrease afterwards. Upon Nx, miR-146a-5p expression was significantly downregulated on days 10 and 14 in the IR-Nx group compared to the IR-S group, but no difference was observed on days 8 and 28.

However, compared to the right kidney, miR-146a-5p level gradually decreased, and although a marked elevations were seen on days 8 and 10, its expression returned to the control level by day 14 (Fig. 15/E).

The expression of miR-199a duplex markedly exceeded the control level in the postischemic IR-S kidneys. MiR-199a-3p and miR-199a-5p reached the highest expression on days 10 (FCs: 5.64± 0.30) and day 28 (FC: 6.69±1.17), respectively. However, nephrectomy affected the two strands differently. Mir-199a-3p expression decreased after Nx in the IR-Nx group compared to the IR-S group and was markedly downregulated from day 14. The -5p strand showed an increasing pattern over time and a significant difference between the IR-S and IR-Nx groups was observed on day 28 only. Regardless these alterations, miR-199 expression was upregulated in the postischemic IR-Nx kidneys compared to the right kidneys at all time points (Fig. 15/F and G).

The expression pattern of miR-214 showed significant elevations in the postischemic kidneys in the IR-S group compared to the non-injured kidneys at all times. MiR-214 peaked on day 10 (FC: 7.71±0.50) and remained elevated afterwards. Upon Nx, miR-214 markedly decreased from day 14 compared to the IR-S group. However, its expression remained elevated in comparison to the right kidney at all time points (Fig. 15/H).

MiR-223-3p expression was elevated by IR in the IR-S group compared to the right kidneys at all times. The peak effect was observed on day 28 (FC: 8.62±0.90). Nx decreased miR-223-3p expression in the postischemic IR-Nx kidneys compared to the IR-S kidneys on day 14 only. As in most cases, miR-223-3p was markedly increased in the postischemic IR-Nx kidneys compared to the right kidneys at all time points (Fig. 15/I).

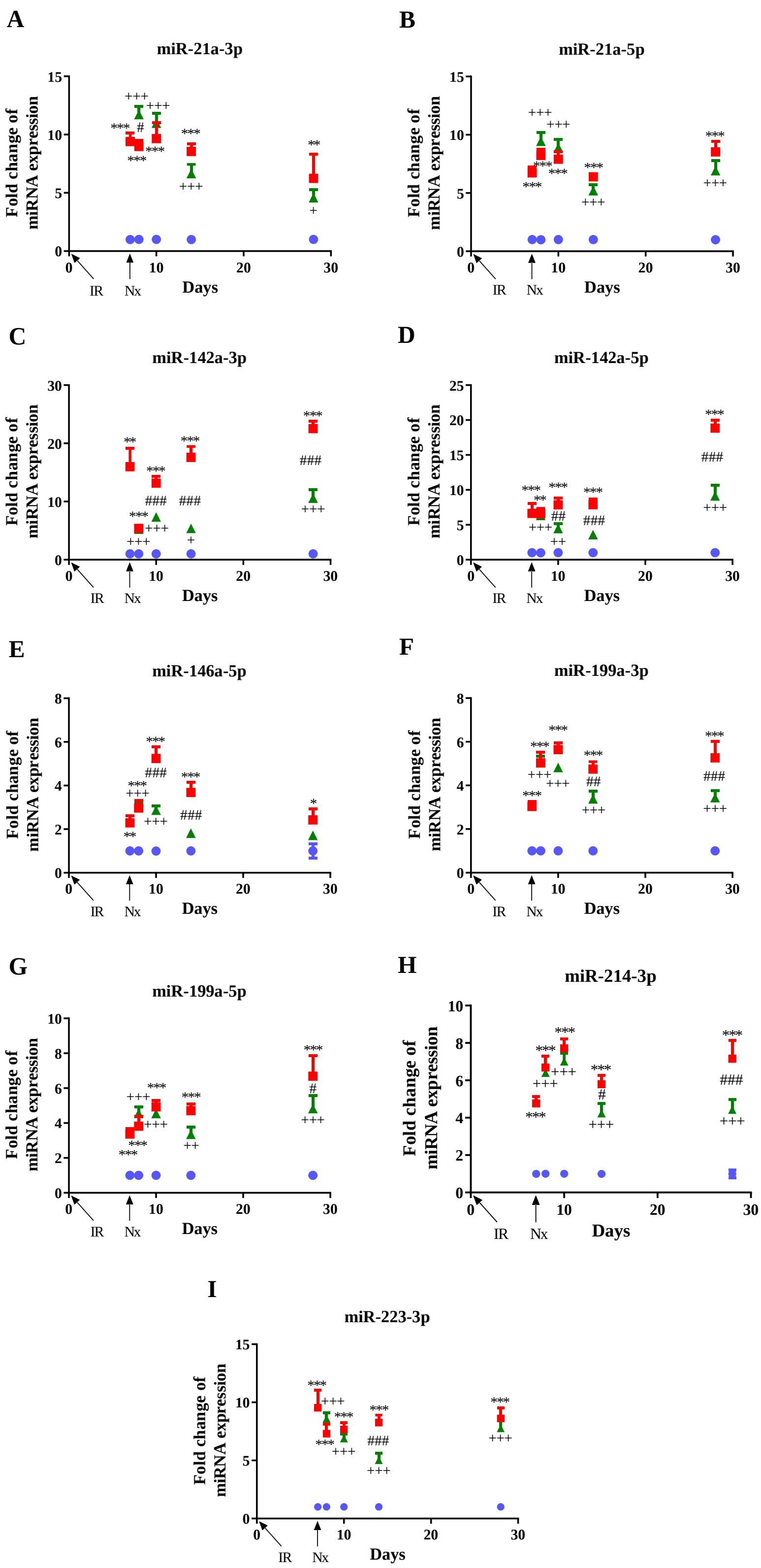

Figure 15. Changes in expression of miRNAs normalized to let-7g-5p as fold changes upon 30 min unilateral ischemia-reperfusion (IR) followed by sham contralateral nephrectomy (S) or contralateral nephrectomy (Nx) on day 7. A: miR-21a-3p, B: miR-21a-5p, C: miR-142-3p, D: miR-142-5p, E: miR-146a-5p, F: miR-199a-3p, G: miR-199a-5p, H: miR-214-5p, I: miR-223-3p. Data are expressed as mean±SEM; two-way ANOVA for repeated measurements with Tukey's post-hoc test; IR-S group vs. non-ischemic kidneys: *: p<0.05, **: p<0.01, ***: p<0.001; IR-Nx group vs. non-ischemic kidney: +: p<0.05, ++: p<0.01, +++: p<0.001; IR-S vs. IR-Nx: #: p<0.05, ##: p<0.01, ###: p<0.001 (76).

5.7.3. miRNA target prediction revealed potential miRNA targets

MiRNA-target analysis was carried out in the postischemic IR-S kidneys and in the postischemic IR-Nx kidneys separately, to gain insight into the effect of IR and Nx on the potential miRNA-target network. Expression of all validated miRNAs were included in the analysis, which were altered by IR or by Nx. The analysis revealed that several potential targets can be related to more than one miRNA regarding the effects of both IR and Nx (Fig. 16A and B). In response to IR four genes were predicted to be a target of four miRNAs: CD2-associated protein, cyclin-dependent kinase 17 (Cdk17), CREB3 regulatory factor (Crebrf) and plexin A2), and further 24 genes were predicted to be a target of three miRNAs (Table 14/A). After Nx, only one mRNA (Plxna2) was predicted to be regulated at least by 4 miRNAs and 14 genes by 3 miRNAs (Table 14/B).

A

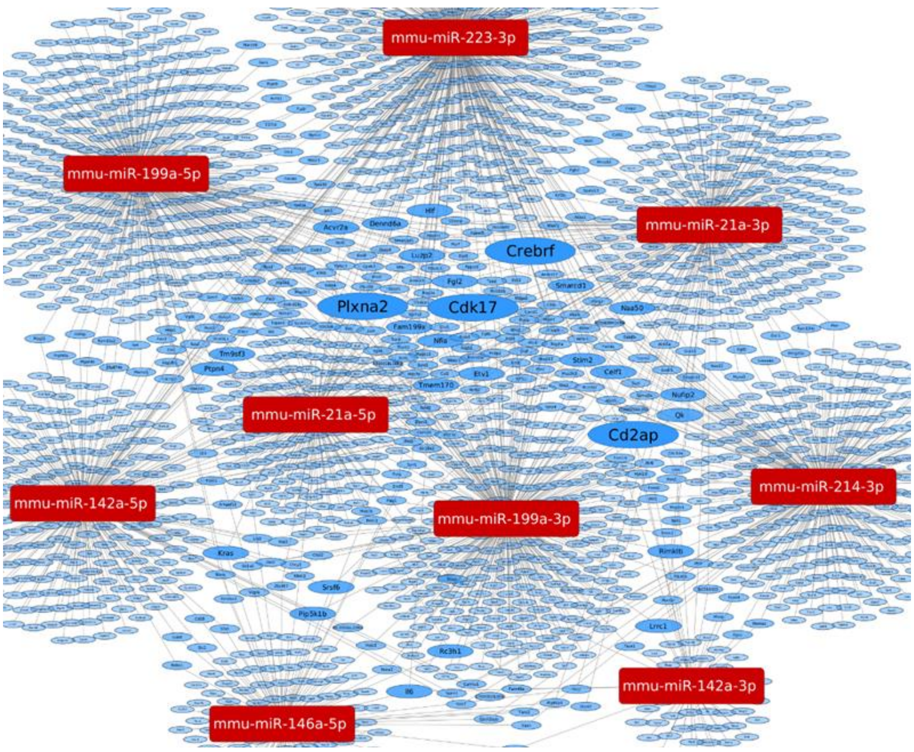

B

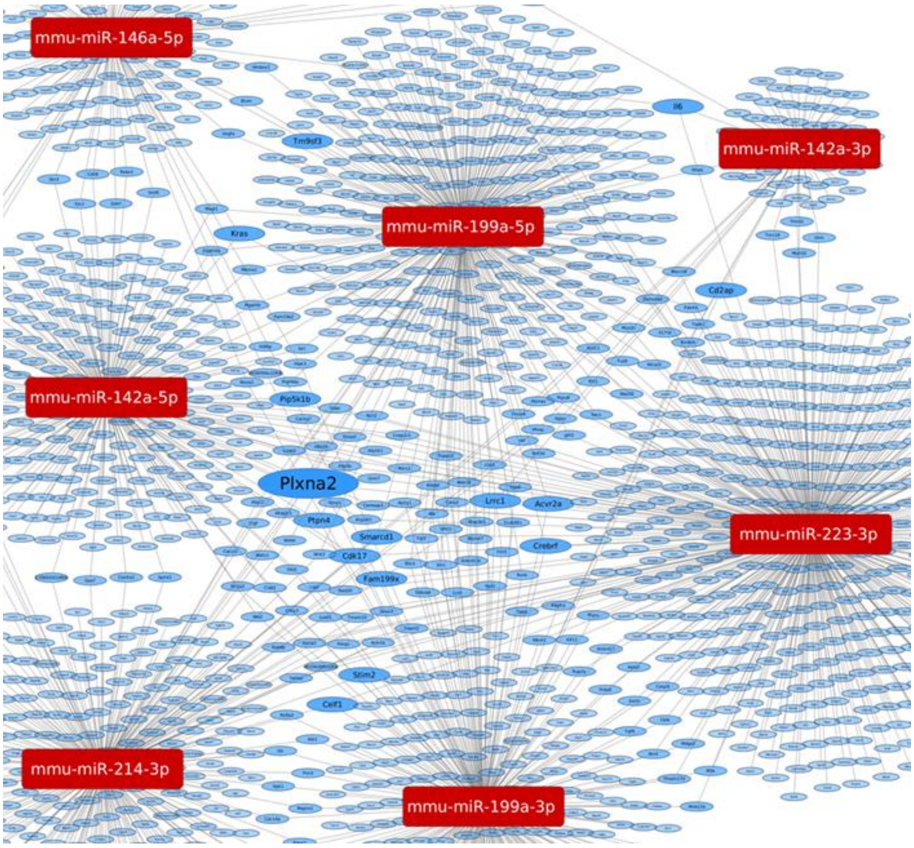

Figure 16. Visual representation of the main findings of the predicted miRNA-target network using the miRNAtarget software in postischemic kidneys. MiRNAs are represented in red boxes, and the predicted protein targets in blue ovals. The size of the hubs is proportional to the number of connections to miRNAs. A: The effect of 30 min unilateral ischemia-reperfusion (IR) on the miRNA-target network in the postischemic kidneys. B: The effect of contralateral nephrectomy on the miRNA-target network in the postischemic kidney (76).

A

No.	Gene symbol	NCBI gene description	miRNA target strength	Associated miRNAs	miRTarBase 8.0	miRDB v5.0 score	TargetScan Mouse 7.2 context++ score
1	Cd2ap	CD2-associated protein	4	mmu-miR-21a-3p	-	93.3	-
				mmu-miR-142a-3p	+	-	-
				mmu-miR-199a-3p	-	94.5	-0.603
				mmu-miR-223-3p	-	-	-0.299
2	Cdk17	cyclin-dependent kinase 17	4	mmu-miR-21a-3p	-	95.4	-0.21
				mmu-miR-142a-5p	-	93.2	-
				mmu-miR-199a-3p	-	88.3	-0.342
				mmu-miR-223-3p	-	98.8	-0.834
3	Crebrf	CREB3 regulatory factor	4	mmu-miR-21a-3p	-	90.4	-
				mmu-miR-199a-3p	-	-	-0.22
				mmu-miR-199a-5p	-	-	-0.213
				mmu-miR-223-3p	-	80.4	-
4	Plxna2	plexin A2	4	mmu-miR-142a-5p	-	91.1	-
				mmu-miR-199a-5p	-	95.5	-0.369
				mmu-miR-214-3p	-	82.4	-
				mmu-miR-223-3p	+	-	-
5	Acvr2a	activin receptor IIA	3	mmu-miR-199a-3p	-	98.6	-0.614
				mmu-miR-199a-5p	-	-	-0.306
				mmu-miR-223-3p	-	94.2	-0.436
6	Celf1	CUGBP, Elav-like family member 1	3	mmu-miR-199a-3p	-	-	-0.253
				mmu-miR-214-3p	-	81	-
				mmu-miR-223-3p	+	-	-
7	Dennd6a	DENN/MADD domain containing 6A	3	mmu-miR-21a-3p	-	94.6	-
				mmu-miR-199a-5p	-	-	-0.236
				mmu-miR-223-3p	+	-	-
8	Etv1	ets variant 1	3	mmu-miR-21a-3p	-	99.5	-
				mmu-miR-21a-5p	-	-	-0.238
				mmu-miR-142a-5p	-	92.8	-
9	Fam199x	family with sequence similarity 199, X-linked	3	mmu-miR-142a-5p	-	84.4	-
				mmu-miR-199a-3p	-	96	-0.485
				mmu-miR-223-3p	-	93.5	-
10	Fgl2	fibrinogen-like protein 2	3	mmu-miR-21a-3p	-	93.8	-
				mmu-miR-199a-3p	-	-	-0.208
				mmu-miR-199a-5p	+	-	-
11	Hlf	hepatic leukemia factor	3	mmu-miR-21a-3p	-	99.1	-
				mmu-miR-199a-5p	-	-	-0.299
				mmu-miR-223-3p	+	-	-0.584
12	Il6	interleukin 6	3	mmu-miR-142a-3p	+	-	-
				mmu-miR-146a-5p	+	-	-
				mmu-miR-223-3p	+	-	-
13	Kras	Kirsten rat sarcoma viral oncogene homolog	3	mmu-miR-142a-5p	-	92.5	-
				mmu-miR-146a-5p	-	88.6	-
				mmu-miR-223-3p	+	-	-
14	Lrrc1	leucine rich repeat containing 1	3	mmu-miR-142a-3p	-	92.9	-
				mmu-miR-199a-3p	-	-	-0.272
				mmu-miR-214-3p	-	81.7	-
15	Luzp2	leucine zipper protein 2	3	mmu-miR-21a-3p	-	97.1	-
				mmu-miR-142a-5p	-	-	-0.205
				mmu-miR-223-3p	+	-	-
16	Naa50	N(alpha)-acetyltransferase 50, NatE catalytic subunit	3	mmu-miR-21a-3p	-	99.7	-
				mmu-miR-214-3p	-	94.6	-
				mmu-miR-223-3p	-	86.6	-0.284
17	Nfia	nuclear factor I/A	3	mmu-miR-21a-5p	-	-	-0.321
				mmu-miR-199a-3p	-	-	-0.268
				mmu-miR-223-3p	-	-	-0.296
18	Nufip2	nuclear fragile X mental retardation protein interacting protein 2	3	mmu-miR-21a-3p	-	83	-
				mmu-miR-199a-3p	-	88.6	-0.33
				mmu-miR-214-3p	-	98.7	-
19	Pip5k1b	phosphatidylinositol-4-phosphate 5-kinase, type 1 beta	3	mmu-miR-142a-5p	-	-	-0.202
				mmu-miR-146a-5p	-	-	-0.236
				mmu-miR-199a-3p	-	88.7	-0.319
20	Ptpn4	protein tyrosine phosphatase, non-receptor type 4	3	mmu-miR-142a-5p	-	97.9	-
				mmu-miR-199a-3p	-	-	-0.274
				mmu-miR-199a-5p	-	-	-0.253
21	Qk	quaking	3	mmu-miR-21a-3p	-	84.5	-
				mmu-miR-199a-3p	+	-	-
				mmu-miR-214-3p	-	82.9	-
22	Rc3h1	RING CCCH (C3H) domains 1	3	mmu-miR-21a-5p	+	-	-
				mmu-miR-146a-5p	+	-	-
				mmu-miR-214-3p	-	86.3	-
23	Rimklb	ribosomal modification protein rimK-like family member B	3	mmu-miR-21a-3p	-	98.7	-
				mmu-miR-142a-3p	-	85.7	-
				mmu-miR-199a-3p	-	95.1	-
24	Smarcd1	SWI/SNF related, matrix associated, actin dependent regulator of chromatin,	3	mmu-miR-199a-5p	-	-	-0.238
				mmu-miR-214-3p	-	99.1	-
				mmu-miR-223-3p	-	-	-0.258
25	Srsf6	serine and arginine-rich splicing factor 6	3	mmu-miR-21a-3p	-	83.4	-0.287
				mmu-miR-142a-5p	-	98.7	-
				mmu-miR-146a-5p	-	88.2	-
26	Stim2	stromal interaction molecule 2	3	mmu-miR-199a-3p	-	-	-0.288
				mmu-miR-214-3p	-	80.1	-
				mmu-miR-223-3p	-	95	-
27	Tm9sf3	transmembrane 9 superfamily member 3	3	mmu-miR-146a-5p	-	85.4	-
				mmu-miR-199a-5p	-	-	-0.256
				mmu-miR-223-3p	+	-	-
28	Tmem170	transmembrane protein 170	3	mmu-miR-21a-5p	-	-	-0.492
				mmu-miR-199a-3p	-	-	-0.293
				mmu-miR-223-3p	-	-	-0.693

B

No.	Gene symbol	NCBI gene description	miRNA target strength	Associated miRNAs	miRTarBase 8.0	miRDB v5.0 score	TargetScan Mouse 7.2 context++ score
1	Plxna2	plexin A2	4	mmu-miR-142a-5p	-	91.1	-
				mmu-miR-199a-5p	-	95.5	-0.369
				mmu-miR-214-3p	-	82.4	-
				mmu-miR-223-3p	+	-	-
2	Acvr2a	activin receptor IIA	3	mmu-miR-199a-3p	-	98.6	-0.614
				mmu-miR-199a-5p	-	-	-0.306
				mmu-miR-223-3p	-	94.2	-0.436
3	Cd2ap	CD2-associated protein	3	mmu-miR-142a-3p	+	-	-
				mmu-miR-199a-3p	-	94.5	-0.603
				mmu-miR-223-3p	-	-	-0.299
4	Cdk17	cyclin-dependent kinase 17	3	mmu-miR-142a-5p	-	93.2	-
				mmu-miR-199a-3p	-	88.3	-0.342
				mmu-miR-223-3p	-	98.8	-0.834
5	Celf1	CUGBP, Elav-like family member 1	3	mmu-miR-199a-3p	-	-	-0.253
				mmu-miR-214-3p	-	81	-
				mmu-miR-223-3p	+	-	-
6	Crebrf	CREB3 regulatory factor	3	mmu-miR-199a-3p	-	-	-0.22
				mmu-miR-199a-5p	-	-	-0.213
				mmu-miR-223-3p	-	80.4	-
7	Fam199x	family with sequence similarity 199, X-linked	3	mmu-miR-142a-5p	-	84.4	-
				mmu-miR-199a-3p	-	96	-0.485
				mmu-miR-223-3p	-	93.5	-
8	Il6	interleukin 6	3	mmu-miR-142a-3p	+	-	-
				mmu-miR-146a-5p	+	-	-
				mmu-miR-223-3p	+	-	-
9	Kras	Kirsten rat sarcoma viral oncogene homolog	3	mmu-miR-142a-5p	-	92.5	-
				mmu-miR-146a-5p	-	88.6	-
				mmu-miR-223-3p	+	-	-
10	Lrrc1	leucine rich repeat containing 1	3	mmu-miR-142a-3p	-	92.9	-
				mmu-miR-199a-3p	-	-	-0.272
				mmu-miR-214-3p	-	81.7	-
11	Pip5k1b	phosphatidylinositol-4-phosphate 5-kinase, type 1 beta	3	mmu-miR-142a-5p	-	-	-0.202
				mmu-miR-146a-5p	-	-	-0.236
				mmu-miR-199a-3p	-	88.7	-0.319
12	Ptpn4	protein tyrosine phosphatase, non-receptor type 4	3	mmu-miR-142a-5p	-	97.9	-
				mmu-miR-199a-3p	-	-	-0.274
				mmu-miR-199a-5p	-	-	-0.253
13	Smarcd1	SWI/SNF related, matrix associated, actin dependent regulator of chromatin,	3	mmu-miR-199a-5p	-	-	-0.238
				mmu-miR-214-3p	-	99.1	-
				mmu-miR-223-3p	-	-	-0.258
14	Stim2	stromal interaction molecule 2	3	mmu-miR-199a-3p	-	-	-0.288
				mmu-miR-214-3p	-	80.1	-
				mmu-miR-223-3p	-	95	-
15	Tm9sf3	transmembrane 9 superfamily member 3	3	mmu-miR-146a-5p	-	85.4	-
				mmu-miR-199a-5p	-	-	-0.256
				mmu-miR-223-3p	+	-	-

Table 14. The predicted miRNA-mRNA targets produced by the miRNAtarget software in the postischemic kidneys. In case of the miRTarBase 8.0 column '+' represents available experimental evidence for the corresponding miRNA-target interaction in miRTarBase 8.0 database. In case of miRDB v5.0 score and TargetScan Mouse 7.2 context ++ score if the corresponding threshold criterion (>80 and <-0.2, respectively) is satisfied the target-prediction algorithm scores for each miRNA are given, if not, a '-' symbol is used. A) The effect of 30 min unilateral ischemia-reperfusion (IR) on the miRNA-target network. The miRNA-target network was created for mmu-miR-21a-duplex, -142a-duplex, -146a-5p, -199a-duplex, -214-3p, and -223-3p. B) The effect of contralateral nephrectomy, performed 7 days after IR, on the miRNA-target network. The miRNA-target network was established on the basis of the same miRNAs, except miR-21a-duplex, as miR-21a-duplex was not regulated by nephrectomy. (76).

5.7.4. MicroRNA target validation

Based on the predicted miRNA-target connections, Plxna2 and Cd2ap protein levels were measured in the post-ischemic kidneys on day 10 (3 days after Nx) to verify the miRNA-target functional connection. Regarding Cd2ap protein expression, no difference was measured in the post-ischemic IR-S and IR-Nx kidneys in comparison to the sham-operated kidney (Fig. 17/A). In comparison to the sham-operated left kidney, Plxna2 protein content was markedly elevated in the post-ischemic IR-S kidneys , but no difference was seen in the IR-Nx group compared to the IR-S or uninjured kidney (Fig 17/B).

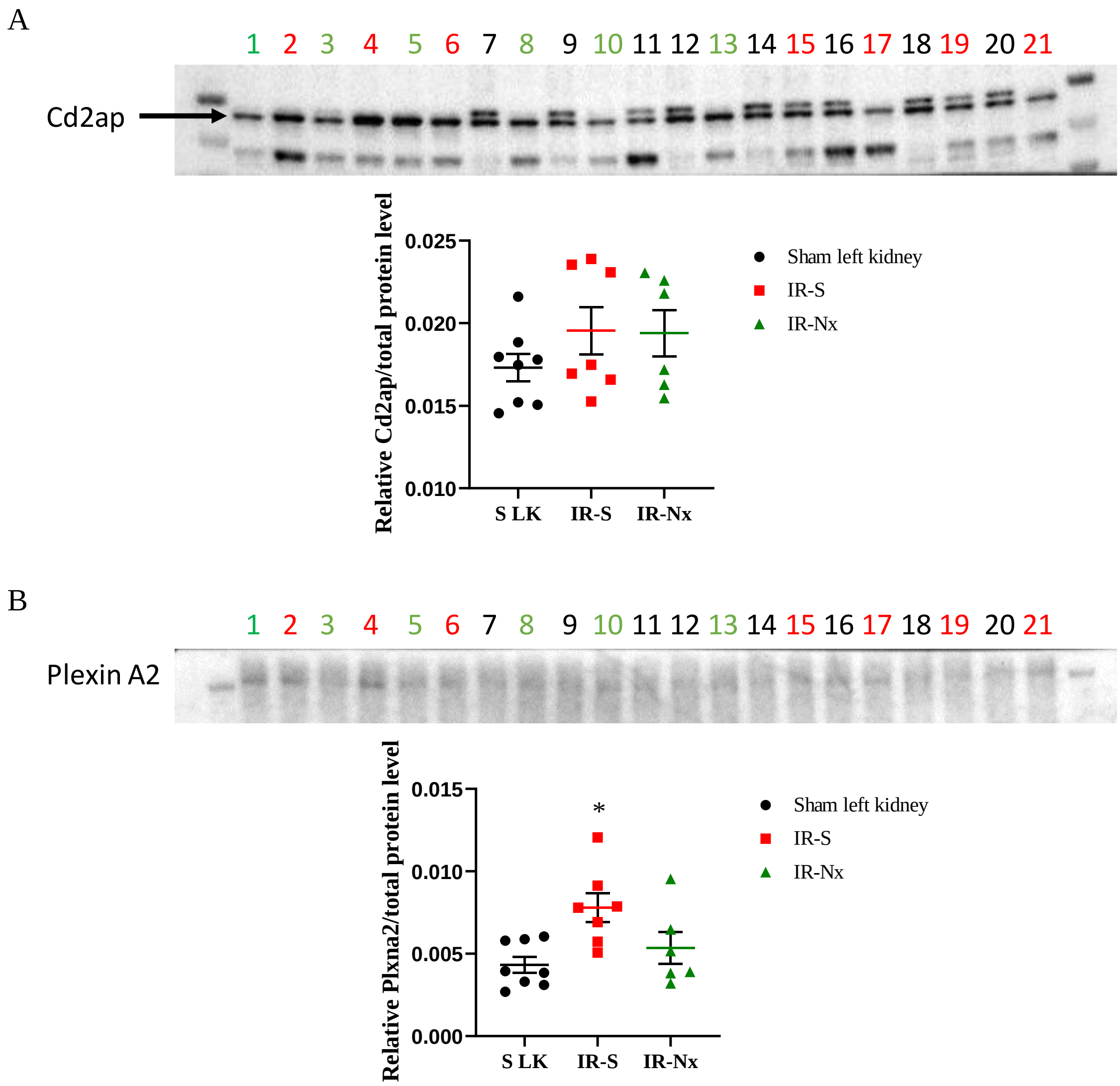

Figure 17. CD2-associated protein (Cd2ap) and plexin A2 (Plxna2) protein levels 10 days after 30 min unilateral ischemia-reperfusion (IR) and sham contralateral nephrectomy (S) or contralateral nephrectomy (Nx) 7 days later. A: Western blot images and optical density analysis of Cd2ap. B: Western blot images and optical density analysis, of Plexin A2. Optical density analysis showing the target protein level relative to total protein amount. Data are expressed as mean±SEM; one-way ANOVA with Tukey's post-hoc test, IR-S group vs non-ischemic left kidney: *: $p<0.05$ (76).

6. Discussion

6.1. Delayed contralateral nephrectomy restored the functional capacity of the postischemic kidney

It has been demonstrated that 30 min of unilateral kidney ischemia-reperfusion caused a long-lasting kidney injury in mice indicating that this experimental setup is a robust, reproducible method for investigating AKI/CKD. In the presence of an uninjured contralateral kidney, the injured kidney was not functional and underwent accelerated fibrosis resulting in considerable atrophy, shrinkage and scaring within 4 weeks. However, upon delayed contralateral nephrectomy at one week after injury, the injured kidney regained its almost full functional capacity in one to two weeks. However, the effects of this functional restoration of the injured kidney were transient, as the progression of chronic kidney disease and development of renal failure in about 20 weeks were not abolished. The downregulation of proinflammatory, hypoxic, oxidative stress and fibrotic mechanisms were the most important among the principal processes responsible for the functional recovery of the postischemic kidney.

Some similar studies were performed previously. Besides the above mentioned methodological study of Skrypnyk et al. (70), the same authors found that treating mice with the antioxidant pyridoxamine before IR improved long-term functional recovery of the postischemic kidney, decreased acute tubular damage and, in long-term (28 days), pyridoxamine reduced interstitial fibrosis in the postischemic kidney. Even if pyridoxamine was administered 24 hours after IR, the extent of fibrosis was markedly reduced, although the renal function did not improve (87). In another related study in rats, Polichnowski et al. (88) described that Nx performed 2 weeks after unilateral IR increased renal blood flow and subsequently elevated GFR in the postischemic kidneys, as well as increased expression of HIF-1α and improved tubular epithelial regeneration. Furthermore, delayed Nx decreased the level of tubulointerstitial fibrosis and partly restored the capillary density in the injured kidneys. However, these studies did not evaluate the time course of molecular responses to contralateral nephrectomy and did not investigate long-term outcome.

Another study was conducted to investigate the relationship of severe (32 and 60 min) unilateral ischemia-reperfusion with delayed contralateral nephrectomy and the degree of renal injury in C57BL/6 mice in order to compare renal recovery after AKI in humans and rodents (89). Nx was performed on day 12 and 26 (2 days before sacrifice) to examine the function of the post-ischemic kidney. It was found that both serum creatinine and BUN were markedly elevated in these mice compared to the sham or unilateral IR without Nx animals. These results are comparable to our findings since we also observed an increase in serum urea concentration even 3 days after Nx, while we detected a decrease in BUN 7 days after Nx. Furthermore, the same study found that GFR (measured transcutaneously) was reduced after 60 min but not after 30 min unilateral IR compared to sham-operated animals 12 days after the injury. The GFR was comparable in all 3 groups on day 26. After Nx, GFR was very low in both IR groups compared to the sham-operated animals on day 14 post-operative, however on day 28 mice, which underwent 32 min IR showed no difference in their GFR compared to the sham-operated animals but after 60 min IR the GFR was greatly reduced. These results indicate that the kidney can recover after 32 min IR but 60 min IR virtually completely abolished kidney function.

In our long-term study, the effect of IR was hidden by enhanced function of the non-ischemic kidney as demonstrated by normal plasma urea level. Upon nephrectomy, plasma urea concentration increased sharply, but only temporarily. Although there were small fluctuations and transient elevations in plasma urea concentration it started to increase again only 20 weeks after IR. Our results are comparable to those of Chancharoenthana et al. (90). who found markedly elevated serum creatinine and proteinuria along with reduced hematocrit in CD-1 outbred mice 20 weeks after a 50-min unilateral IR and contralateral nephrectomy one week later.

6.2. Persistent tubular injury after severe ischemia-reperfusion

Expression of the immune system-related TNF-α, profibrotic TGF-β and the tubular injury marker LCN2 genes was similar in the sham IR, sham Nx groups, and in the non-injured, right kidneys, removed on day 7, suggesting that experimental procedures caused no measurable injury and had negligible inflammatory and profibrotic effects on the kidneys.

Unilateral IR induced a marked increase in the expression of the tubular epithelial cell injury marker LCN2 one week after ischemia. Contralateral nephrectomy progressively reduced LCN2 mRNA in the postischemic IR-Nx kidneys compared to the

IR-S group, although LCN2 remained elevated in comparison to the right kidneys at least up to 28 days. Since LCN2 production is thought to be distal tubule specific in the kidney (8, 14), its elevated expression up to 28 days indicate distal tubular injury in the postischemic kidneys even if the contralateral kidney is removed. On the other hand, the expression of LCN2 remained persistently elevated in the postischemic IR-S kidneys during the period investigated, suggesting unabated injury over a long period, and, in consequence, the kidney histology showed massive atrophy. However, there can be other sources of LCN2 in the mouse kidney after IR, as the infiltrating macrophages also produce LCN2, in rats (91) and mice after IRI-induced AKI (92). We have also found a massive macrophage infiltration in postischemic IR-Nx kidneys that was attenuated by nephrectomy in the postischemic IR-S kidneys. These data warrant further research to fully elucidate the exact sources of LCN2 in this experimental model and their potential contribution to the restoration of kidney function.

6.3. Delayed nephrectomy significantly reduced inflammation in the postischemic kidney

IR provoked a massive proinflammatory response in the kidney already in the first week. The expression of C3, IL-6, CCL2 and TNF-α reached their highest expression on day 10, except IL-6 which peaked on day 14. However, the elevation of C3, IL-6 and CCL2 proved to be transient, as mRNAs of these genes began to decrease on day 14 (except IL-6) and further declined by day 28. On the contrary, increased expression of TNF-α remained elevated up to day 28. These data suggest that CCL2 and IL-6 along with C3 signaling seems to be less important in maintaining the progression of chronic kidney disease that ultimately ends up in renal failure.

CCL2 plays a role in the recruitment and activation of macrophages in IRI (93). Indeed, in parallel with the elevated CCL2 expression, a marked macrophage infiltration was observed in the postischemic IR-S kidneys. Although contralateral nephrectomy significantly reduced CCL2 expression, it remained higher than in the right kidneys. In parallel with this observation, macrophage infiltration dropped in the postischemic IR-Nx kidneys, but did not return to the level of the uninjured kidneys. Hence, reduced macrophage infiltrations in the postischemic kidneys can be, at least partly, attributed to decreased CCL2 production after contralateral nephrectomy. The question whether an M1-to-M2 macrophage polarization took place was beyond the scope of our study.

However, Kim et al. (94) found evidence that macrophages are predominantly M1 type in the early phase of IRI, and they were subsequently replaced by M2 macrophages in the kidney. Thus, based on the extent of macrophage infiltration and persistent proinflammatory cytokine expression in the postischemic IR-S kidney, and the attenuation of these factors in the IR-Nx group, it is implied that an M1-M2 macrophage switch might have occurred after Nx. However, further research is needed to gain conclusive evidence.

Both tubular cells and the infiltrating macrophages can be the sources of TNF-α in the postischemic IR-S kidney in the early phase of AKI (8). However, as tubular atrophy developed over time, seen in the PAS stained sections, macrophages may take over the role of tubular epithelial cells as the primary source of TNF-α, explaining the constitutively elevated TNF-α expression in the IR-S group. Nephrectomy partly reduced CCL2 expression and macrophage infiltration, which may contribute to the decrease in TNF-α production in the postischemic IR-Nx kidneys.

Upregulation of complement component 3 was the most prominent change among the investigated proinflammatory genes. C3 has long been implicated in kidney injury. Indeed, C3a or C5a receptor and double KO mice were protected from the deleterious effects of IRI. They developed less severe histological alterations and reduced level of inflammatory response (95). Pharmacological inhibition of the complement system also alleviated the effect of IRI by downregulating proinflammatory processes (96). Furthermore, the complement system is also implicated in the development of renal fibrosis. C3 expression by tubular epithelial cells was increased already 3 days after UUO. Compared to normal mice, tubulointerstitial fibrosis and proinflammatory signaling was reduced in C3 KO animals, supposedly because of prominent M2 macrophage polarization in the early stages of injury (97). A further study confirmed that M1 macrophages are the main source of C3, moreover, C3 is implicated in M1 polarization. C3 and C3a receptor blockade alleviated the proinflammatory environment upon UUO (98). Thus, this series of studies suggest that the highly elevated C3 expression favors polarization of macrophages into M1 type in the postischemic IR-S kidneys, and downregulation of C3 expression by Nx may promote polarization of macrophages into the M2 type in the IR-S kidneys. Furthermore, C3 can contribute to the accelerated fibrosis seen in the IR-S group, and the deleterious effects of C3 are reduced by contralateral nephrectomy. However, these assumptions must be thoroughly investigated in further studies.

IL-6 seemed to be a late factor of inflammation as compared to the other three proinflammatory molecules, its peak expression occurred on day 14 only. Upon the insult, tubular epithelial cells can be induced to produce IL-6, which in turn activates the expression of collagen 1 and promotes tubulointerstitial fibrosis (99). According to this mechanism, increased expressed of IL-6 may contribute to Col1a1 production, which coincidentally was most robust from day 14 in the postischemic IR-S kidneys. The reduced level of inflammatory environment observed in the IR-Nx group, in turn, downregulated the extent of ECM production.

Taken together, severe IR induced massive renal injury and substantial inflammatory responses in the postischemic kidneys, and subsequent macrophage infiltration. Contralateral nephrectomy acts against these mechanisms, which leads to functional recovery of the postischemic kidney.

6.4. Delayed nephrectomy attenuated hypoxia- and oxidative stress-related genes

It is hypothesized that HIF-1α has a role in the initial adaptation to hypoxic conditions, while HIF-2α is activated after prolonged hypoxia (100).

Indeed, increased HIF-1α expression was found in the postischemic IR-S kidneys on day 8 and again on day 28. Presumably, these changes in HIF-1α expression were not due to high energy demand of tubular epithelial cells, since renal atrophy was so extensive by day 28 that hardly any functioning nephron remained. Rather, the source of HIF-1α was leukocytes. The study conducted by Polichnowski et al. (88) also detected only low level of HIF-1α in the atrophic tubules in the postischemic kidneys 4 weeks after IR if the contralateral kidney remained intact. However, they did detect HIF-1α in the postischemic kidney if the contralateral kidney was removed 2 weeks after IR. This discrepancy can be explained by different species (rat vs. mouse) and ischemia time (60 min vs. 30 min) and the time of investigation (28 days vs. earlier and same time points). However, further research is needed to shed light on the exact cell types expressing HIF-1α in an atrophic kidney.

HIF-2α mRNA expression was markedly elevated in the postischemic IR-S kidneys on day 10 and remained upregulated up to day 28, suggesting that HIF-2α plays a more important role than in HIF-1α during this time period. Contralateral nephrectomy completely abolished the increase in HIF-1α expression, and HIF-2α was increased only on day 28, implying that no hypoxia was present in the postischemic IR-Nx kidneys already one day after Nx. However, we cannot rule out hypoxic conditions before day 7, since some signs of hypoxia was observed in the postischemic IR-S kidneys yet on day 8.

Although the role of hypoxia-inducible factors is well established in IRI, their potential function in kidney fibrosis is somewhat controversial (31). Pharmacological inhibition of prolyl-4-hydroxylase domain-containing dioxygenases, which are inhibitors of HIFs, improved renal function and reduced F4/80^{+} macrophage content, inflammation-related gene expression and collagen deposition in both the cortex and the medulla if applied before IR. On the contrary, inhibition of HIFs after IR neither improved the kidney function nor downregulated the inflammatory response nor reduced excessive ECM deposition (101). However, several studies found that HIF-1α signaling enhances kidney fibrosis. Knockout of von Hippel-Lindau (VHL) gene, a key regulator of HIF-α in tubular epithelial cells resulted in stable HIF-1α expression in mice. Upon 5/6 nephrectomy, increased interstitial fibrosis was detected in VHL KO mice compared to wild type mice and HIF-1α inhibition in UUO reduced the progression of interstitial fibrosis (102). Another study suggested that HIF-1α plays a role in fibrosis development in the early phase of UUO-induced renal fibrosis (103). Moreover, recent evidence suggests (104) that the activation of HIF-2α in the early stages of CKD can enhance kidney fibrosis, but did not worsen renal impairment. On the other hand, activation of HIF-2α at later time points can lead to amelioration of renal dysfunction and fibrosis.

Taking into account the different methods to induce renal fibrosis and to regulate HIF expression and activity, the controversial results can be explained by methodological differences. The effects of delayed contralateral nephrectomy after unilateral IR suggest that HIF-2α plays a more important role than HIF-1α in the attenuated progression of renal fibrosis, since HIF-1α expression was elevated in the postischemic IR-S kidney, but not, or just at a later time point in the IR-Nx group.

The oxidative stress marker NRF2 was more robustly elevated than HIF-1α and HIF-2α in the postischemic IR-S kidneys, and Nx markedly reduced NRF2 mRNA in the IR-Nx group. These data suggest an ongoing oxidative stress in the postischemic kidney, which markedly decreased upon contralateral nephrectomy. NRF2 is thought to be beneficial in IRI (34), so smaller expression of NRF2 in the IR-Nx than IR-S kidneys more likely reflects a decrease in oxidative stress. Curiously, the above-mentioned study of Skrypnyk et al. (87) did not address the question whether delayed contralateral nephrectomy itself may contribute to reduced level of oxidative stress. Further research is warranted to fully elucidate the mechanisms why delayed Nx results in alleviation of oxidative stress in the postischemic kidney. Regardless, both studies concluded that reduced oxidative stress leads to downregulation of renal fibrosis; hence, helps maintain the structural integrity of the kidney.

6.5. Delayed nephrectomy diminished postischemic renal fibrosis

Based on data in the literature it is not surprising that decreased inflammation, immune cell infiltration, hypoxia and oxidative stress culminated in reduced fibrosis in the postischemic IR-Nx kidneys compared to that in the IR-S group. Expression of fibrosis-related genes (α-SMA, Col1a1, FN1 and TGF-β) was elevated in the postischemic IR-S kidneys already on day 8, confirming that 30 min of IR caused AKI and, subsequently, persistent fibrosis in the mouse kidney. Although contralateral nephrectomy reduced the expression of these genes in the postischemic kidney, but only partly, as their mRNA remained higher than in the non-injured kidneys at all time points. These results suggest that constant injury persist in the postischemic kidney after severe IR, which will lead to CKD and, ultimately, end-stage renal disease.

Accordingly, Masson’s trichrome staining revealed massive ECM deposition in the tubulointerstitium in the IR-S group. It is known that the fibrotic processes are localized around the damaged tubules and further injury is necessary for progression of fibrosis (20). Indeed, based on the histological analysis, there were few functioning tubules in the postischemic kidneys without fibrotic lesions even on day 140. Upon contralateral nephrectomy the mRNA expression of Col11 and FN1 was markedly reduced from day 10 in the postischemic IR-Nx kidneys compared to the IR-S kidney, but remained elevated in comparison to the control right kidneys in all groups. This finding suggests that the downregulation of fibrosis is secondary to reduced proinflammatory processes (inflammatory mechanisms decreased already on day 8). On the other hand, this could also explain the slow deterioration of the postischemic IR-Nx kidney in the long-term study.

It is hypothesized that fibrosis was decreased in the postischemic IR-Nx kidney as the number of myofibroblasts was decreased. The rationale behind this assumption is the downregulation of TGF-β expression, a well-known regulator of fibrotic processes, in the post-ischemic IR-Nx kidney compared to the IR-S group (49). Various cell types are producing TGF-β in the injured kidney, such as tubular epithelial cells arrested in G2/M phase (50) or M2 macrophages (105). TGF-β1 induces the recruitment and proliferation of fibroblast-like cells and activates fibroblast cells (106). Less myofibroblast activation could explain the observed downregulation of FN1 and Col1a1 in the IR-Nx group from day 10. However, α-SMA expression did not show marked differences between the post-ischemic IR-Nx kidneys compared to the IR-S group before day 28. Further study is warranted to fully elucidate this contradiction.

Thus, Nx reduced kidney injury, inflammation and macrophage infiltration in the postischemic kidney, which decreased expression of profibrotic genes. In turn, this led to decreased extracellular matrix deposition, but over time, sustained ECM production induced by the sustained profibrotic signaling after severe IR still resulted in ESRD.

6.6. Ischemia-reperfusion induced profound miRNA alterations, but delayed nephrectomy caused only mild changes

It is known that miRNAs play a role in acute and chronic kidney disease (107, 108). To determine which miRNAs potentially play a role in the functional recovery of the post-ischemic kidney, a miRNA microArray analysis was performed on the samples collected on day 8 (i.e. one day after nephrectomy). It was hypothesized that based on the marked downregulation seen in inflammation and fibrogenesis already on day 8, similar changes in miRNome would be observed. On day 8 a total of 20 miRNAs was upregulated and 6 downregulated at least 2-fold in the postischemic kidneys compared to the uninjured kidneys. However, no miRNA changes were seen in response to contralateral nephrectomy.

MicroArray can yield false positive results (109), partly because of high degree homology of miRNA family members (110). Therefore, on one hand, RT-qPCR was performed for validation, and, on the other hand, to obtain a comprehensive picture of regulation of miRNAs in the post-ischemic IR-S and IR-Nx groups. Further characterization of changes in expression of miRNAs revealed that contralateral nephrectomy attenuated upregulation of several miRNAs in the post-ischemic IR-Nx kidneys later than day 8, although miRNAs remained upregulated compared to the uninjured kidneys. These effects were observed mainly 3 to 7 days after Nx, and persisted up to 21 days. No significant differences in miR-762, miR-3102-5p and miR-129-1-3p expression was found either in the post-ischemic IR-S kidneys compared to the sham-operated left kidneys, or in the IR-Nx group in comparison to the IR-S group, suggesting that the observed changes in the miRNA microArray are false for these three miRNAs. Furthermore, the expression of miR-2861 was below the detection limit, hence no data was obtained regarding this miRNA.

The expression of additional three miRNAs was also measured using RT-qPCR, which were not changed by Nx according to microArray. Mir-214-3p was chosen because it is clustered with miR-199a (111), miR-21a-3p, which is transcribed parallel with miR-21a-5p since they both origin from the pri-miR-21a gene (112) and miR-146a-5p that is implicated in IRI-induced AKI (113) and chronic kidney disease (114) in mice. Furthermore, because the effect of nephrectomy seen in the microArray was small, day 7 was included in the miRNA validation, to assess baseline expression of miRNAs on the day before Nx. The rationale behind choosing this time point is to further characterize the effects of IR and Nx on the expression of miRNAs.

In our study the validated miRNA expression patterns are in align with previously published data in C57BL/6 mice subjected to 30 min of unilateral IR without nephrectomy (115). This study found that in response to IR, the expression of miR-20a, miR-21, miR-146a, miR-199a-3p and miR-214 was upregulated, while expression of miR-187, miR-192, miR-194 and miR-805 was downregulated. They studied the role of miR-21 *in vitro*, and implicated it in the regulation of cell death and fibrosis. In was demonstrated in another study that 10 days after 30 min of IR the expression of several miRNAs increased, among others miR-21, mir-142-3p, miR-146a, miR-199a-3p and -5p, miR-214 and miR-223. In this study, miR-21 was also chosen for detailed characterization, and the authors concluded that miR-21 KO mice showed less tubular epithelial cell damage due to reduced level of cell death and decreased fibrosis. Furthermore, inhibition of miR-21 reduced albuminuria after IR and delayed nephrectomy (on day 7), suggesting retained glomerulotubular integrity already on day one after Nx (116).

No clear traits can be found in miRNA alteration patterns in our study. However, IR markedly upregulated all miRNAs investigated in the IR-S group and in the IR-Nx group apart from miR-142-5p on day 14 and miR-146a-5p on day 14 and 28. Nx did not reduced the expression of miR-21a duplex (except in case of miR-21a-3p on day 8), while a marked downregulation was found in the expression of the other 7 miRNAs from day 10 (in case of miR-142a duplex) or in the later time points investigated.

Several of the validated miRNAs have been hypothesized to have a role in the pathogenesis of AKI and in the development of renal fibrosis and CKD.

Mmu-miR-21a-5p has been shown to be beneficial in IRI. Pretreatment with pre-miR-21 improved renal function and tissue integrity 24 hours after IR. It is presumed that the beneficial effects of miR-21 upregulation in mouse IRI is due to suppression of apoptosis by downregulating the expression of programmed cell death protein 4 (PDCD4) and the caspase signaling pathway (63). A bilateral IRI study yielded similar results. IR induced the expression of miR-21 and knock-down of miR-21 with locked nucleic acid (LNA) resulted in renal function impairment through the downregulation of HIF-1α and -2α. Further characterization of the connection between miR-21 and HIFs *in vitro* revealed that miR-21 regulates the expression of HIF via the Phosphatase and Tensin homolog (PTEN)/serine threonine kinase Akt/mammalian target of rapamycin pathway. Furthermore, anti-miR-21 accelerated maturation of resident DCs through the PDCD4/ Nuclear Factor-κB (NF-κB) signaling pathway. Mature DCs responded with increased secretion of proinflammatory cytokines (TNF-α, IL-6, IL-12) upon miR-21 LNA administration before IR (117). In align with these results, the expression of miR-21a-5p markedly increased in the postischemic kidneys compared to the uninjured kidneys in our study. After Nx, the level of miR-21a-5p did not decrease, raising the possibility that the beneficial effects of miR-21a-5p contributed to the functional recovery of the postischemic IR-Nx kidney. Moreover, we also detected an increase in expression of HIF-1α and more in HIF-2α in the post-ischemic IR-S kidney. It needs further research to clarify whether increased expression of HIFs are caused by miR-21a-5p.

MiR-146a increased after IRI in both humans and mice mediated by the IL-1β/NF-κB signaling pathway. In mice, miR-146a was expressed predominantly in tubular cells and to a lesser extent in tubulointerstitial cells. MiR-146 KO mice showed increased tubular lesions, leukocyte infiltration and renal fibrosis in the postischemic kidney 14 days after IR. Further analysis indicated that miR-146a acts as an anti-inflammatory factor in tubular epithelial cells *in vitro* by suppressing the NF-κB signaling pathway (113). However, it seems that in contrast to the beneficial role of miR-146a in the early phase of AKI, miR-146a may contribute to the development of CKD (114). Indeed, our findings showed that the expression of miR-146a-5p was markedly decreased already on days 10 and 14 in the post-ischemic IR-Nx kidneys in comparison to the IR-S group and showed no difference in comparison to the uninjured right kidney from day 10. Hence, the downregulation of miR-146a-5p may contribute to the slower accumulation of ECM in the post-ischemic IR-Nx kidney. However, in contrast to changes expected, miR-146a-5p expression was markedly elevated compared to the uninjured kidney in the early time points in the IR-S group, thus more research is needed to fully elucidate the exact role of miR-146a-5p in this experimental setup.

The expression of the miR-199a duplex was higher in the postischemic than in the uninjured kidneys. However, the two strands behaved somewhat differently. MiR-199a-3p remained relatively steadily elevated up to day 28, while miR-199a-5p gradually increased and reached a peak on day 28 in the postischemic IR-S kidney compared to the right kidney. Upon Nx, the -3p strand decreased already on day 14, but the -5p strand decreased only on day 28 in comparison to the IR-S group. Based on data in human ovarian cancer, it was suggested that miR-199a regulates the proinflammatory TLR4/NF-κB-signaling pathway, specifically binding to the 3'-UTR site of the IκB kinase β (IKKβ). Since IKKβ activates NF-κB, inhibition of IKKβ by miR-199a may result in decreased level of cytokine production (118). Furthermore, miR-199a-3p was implicated in the attenuation of inflammatory processes caused by preterm labor both in humans and experimental LPS-induced preterm labor in mice. In this experimental setup, miR-199a-3p was implicated in the regulation of the non-histone DNA binding protein HMGB1 via its 3' UTR site (119). HMGB1 is able to activate TLR-receptors extracellularly, and its contribution to IR-induced kidney injury is established in mice. Treatment with neutralizing HMBG1 antibody attenuated kidney dysfunction, leukocyte infiltration and tubular epithelial cell apoptosis, presumably via TLR4-receptor signaling (120). Given that miR-199a-3p mRNA did not decrease on days 8 and 10 in the postischemic IR-Nx kidneys, it seems that miR-199a-3p similarly attenuated TLR-signaling pathways at those time points as before, so it could have contributed to reduce the activity of inflammatory processes and macrophage infiltration. Although miR-199a-3p decreased afterwards, it can be explained by the functional recovery of the kidneys after day 10. However, miR-199-3p expression was continuously elevated in the IR-S group in all time points investigated, hence further studies are warranted to resolve this apparent discrepancy in the role of miR-199a-3p in this experimental setup.

MiR-199a-5p is thought to have a beneficial effect in the early reperfusion phase of IRI via suppressing endoplasmic reticulum (ER) stress (121). It is well-known that ER stress contributes to IRI-induced AKI, renal fibrosis and CKD (122). However, since the effects of miR-199a-5p seem to be restricted to the early reperfusion phase, our model may not be suitable to investigate the role of mi-199a-5p in the Nx-induced beneficial effects on kidney function, since Nx was performed 7 days after IR. Furthermore, miR-199a-5p expression was elevated in pulmonary fibroblast after injury in *in vivo* and *in vitro*, revealing that TGF-βinduced its expression in lung fibroblast cell culture to a level, which was sufficient to activate fibroblasts (123). However, the time-related changes in TGF-β mRNA in our experiment speak against the possibility that TGF-β is the main regulator of miR-199a-5p expression in the post-ischemic IR-S and IR-Nx kidneys, because the expression of TGF-β gradually decreased from day 10 (and day 8 in the IR-Nx group), while miR-199a-5p expression peaked on day 28 in both groups. Thus, it seems that miR-199a-5p expression is regulated by factors other than TGF-β after severe IR at least at a later phase of renal IRI. Nevertheless, the elevated α-SMA expression in the post-ischemic kidney compared to the uninjured kidney suggests that increased myofibroblast activity can be mediated, at least partly, by miR-199a-5p. However, this hypothesis needs further research.

The expression of miR-142 gradually increased after IR in the IR-S kidney. After Nx, both the strands of miR-142 markedly downregulated from day 10 in the IR-Nx group.

Mice with DN showed similar pathologic alterations (e.g. tubular dilatation, macrophage infiltration, collagen deposition) to that seen in IRI-induced AKI. Furthermore, miR-142-5p was found to be increased in DN compared to controls. The increase in miR-142-5p was in conjunction with the decrease in its direct target PTEN both at mRNA and protein levels. Animals treated with oleanolic acid showed reduced level of miR-142-5p expression and renal fibrosis (124). Accordingly, miR-142-5p may be harmful and can lead to renal fibrosis. Mir-142-5p was markedly elevated in the post-ischemic IR-S kidney but was downregulated from 3 to 21 days after Nx. Thus, the observed decrease of miR-142-5p may contribute to the downregulated fibrotic processes in the post-ischemic IR-Nx kidney.

MiR-142-3p has not been studied in IRI-induced AKI. However, it is known that the expression of miR-142-3p is regulated by TGF-β. Thus, the reduced level of TGF-β expression after Nx may contribute to downregulation of miR-142-3p from day 10 in the IR-Nx group compared to the IR-S group.

The expression of miR-214-3p was increased by IR in the postischemic kidneys at all time points. Nx did not alter miR-214-3p until day 14, when a marked reduction was seen in the postischemic kidneys compared to the IR-S group. The role of miR-214 in IRI-induced AKI is somewhat controversial. MiR-214-3p was upregulated in a rat model of renal IRI and ameliorated the IRI-induced AKI during the first 72 hours by suppressing renal fibrosis and apoptosis via regulating Dickkopf 3 protein and enhancing the WNT/β-catenin-pathway (125). However, knock-out of miR-214-3p in rat proximal tubular cells *in vitro* and *in vivo* showed milder tubular damage and improved kidney function at 48 hours after IR in mice as indicated by reduced serum creatinine and urea levels compared to wild type mice. This effect was suggested to be caused by increased level of mitofusin 2, which plays a role in maintaining mitochondrial structure. Deficiency of miR-214 in IRI counteracted to the downregulation of mitofusin 2, hence decreased the extent of apoptosis (126). Different species, ischemia time or the different time points can explain these conflicting results.

Moreover, miR-214-3p was implicated in the development of CKD. Utilizing different CKD models in mice, such as UUO (7-day long experiment) and IRI (4-week long experiment) led to enhanced miR-214 expression mainly in the mitochondria of kidney cortical cells. Conditional knockout of miR-214 in the proximal tubular epithelial cells reduced apoptosis, tubular injury and proinflammatory cytokine production, such as IL-1β, TNF-α and CCL2. Furthermore, ECM deposition was reduced and TGF-β expression was markedly downregulated in UUO and IRI models (127). Another UUO study revealed that systemic knockout of miR-214 resulted in reduced renal fibrosis and expression of profibrotic genes, such as α-SMA or Col1a and Col3a in mice after IRI. However, this effect was independent of TGF-β signaling (128).

In alignment with these results, the observed increase in miR-214 in the postischemic IR-S kidneys can contribute to enhanced expression of profibrotic genes and renal fibrosis. Furthermore, the reduction of miR-214 upon Nx from day 14 may have contributed to diminish fibrosis and expression of profibrotic genes in the IR-Nx group.

Mir-223-3p expression was markedly elevated in the postischemic kidneys compared to the uninjured kidneys at all time points. Nx significantly reduced mir-223-3p expression on day 14 only in the IR-Nx group in comparison to the IR-S group. MiR-223-3p is implicated in the protection against IRI. In an experimental model, using bone marrow-derived mesenchymal stem cells (MSCs), miR-223-3p ameliorated the harmful effects of renal IRI both *in vitro* and *in vivo*. Kidney injury was ameliorated at 24 hours if MSCs were perfused immediately after bilateral IR. Hypoxic preconditioning of MSCs enhanced the protective effect. miR-223 exerted the protective effect via inhibition of nucleotide–binding oligomerization domain receptor family pyrin domain containing 3 protein, hence miR-223 repressed the activity of the inflammasome resulting in reduced level of apoptosis and renal fibrosis (129). Our results are similar to these findings, as Nx induced only a transient decrease in miR-223-3p on day 14, but otherwise miR-223-3p remained markedly increased at all time points in comparison to the uninjured right kidneys.

The miRNA-target network analysis identified 4 genes (Cd2ap, Cdk17, Crebrf, Plxna2), which could be influenced by 4 ischemia-regulated miRNAs (miR-21a-3p, miR-142a-duplex, miR-199a-duplex, miR-214-3p, miR-223-3p) and 1 gene (Plxna2) influenced by nephrectomy-regulated miRNAs (miR-142a-5p, miR-199a-5p, miR-214-3p and miR-223-3p). To our best knowledge, the role of Cdk17 and Crebrf were not investigated in the pathogenesis of IRI-induced renal fibrosis. Hence, only the CD2ap and Plxna2 protein levels were measured on day 10, when the glomerular filtration started to recover in the post-ischemic kidney after Nx.

CD2ap is expressed mainly in glomerular epithelial cells in the kidney and it plays an important role in slit diaphragm formation. Indeed, CD2ap KO mice displayed proteinuria, increased BUN and creatinine levels (130). Furthermore, in another study with a comparable experimental setup to ours, its expression and protein level inversely correlated with the duration of ischemia 28 days after IRI (3 weeks after Nx) in BALB/c mice (131). Accordingly, the upregulation of regulatory miRNAs of CD2ap should have induced its downregulation, however, the protein level of CD2ap was unchanged in the post-ischemic IR-S and IR-Nx compared to the uninjured left kidney 10 days after IR (3 days after Nx). This result suggests that regulation of CD2ap protein expression is dominated by transcriptional factors. Alternatively, the decrease of CD2ap protein expression might occur at a later time points only, which warrants further measurements to be performed later.

Plxna2 was the only predicted target of 4 Nx-regulated (and IR-regulated also) miRNAs. Plexins are the main receptors for semaphorins. In the kidney semaphorins are expressed in the podocytes, distal tubules and collecting ducts (132). It is suggested that plexin A2 is capable to transduce semaphorin 3A signaling (133). Genetic or pharmacological inhibition of semaphorin 3A resulted in decreased level of tubular injury and better preservation of kidney function 24 hours after bilateral IR. Furthermore, inhibition of semaphorin 3A likewise reduced the expression of pro-inflammatory cytokines (e.g. TNF-α or IL-6) and the level of neutrophil infiltration into the kidney (134). However, our results showed that the protein level of Plxna2 increased in the post-ischemic IR-S kidney and was not decreased by Nx in comparison to the uninjured left kidney on day 10. These findings are in contrast to the expected decrease in their expression level induced by their predicted regulatory miRNAs. Furthermore, the mRNA level of Plxna2 did not change 24 h after bilateral IR (134), however, our results suggest that its expression might be altered at later time points after IR. We hypothesize that the predicted regulatory miRNAs play role only in fine-tuning the expression of Plxna2, and other mechanisms more robustly control the expression of Plxn2 at the promoter level. Furthermore, most of the miRNAs implicated in the regulation of Plxna2 started to downregulate 7-21 days after Nx (only miR-142a-5p on day 3), hence the effect of miRNAs on the Plxna2 protein level could be confirmed on day 14 or 28. This possibility warrants further investigations.

However, the data suggest potential role of several miRNAs in kidney fibrosis, thus further studies are warranted to shed light on their contribution to acute and chronic kidney disease.

7. Conclusions

The following conclusions can be drawn from the studies performed:

1. In the presence of uninjured contralateral kidney, the post-ischemic kidney showed signs of accelerated fibrosis and atrophy.
2. We confirmed that delayed contralateral nephrectomy induced functional recovery of the post-ischemic kidney.
3. Delayed contralateral nephrectomy substantially reduced the inflammatory and fibrotic processes, while hypoxia and oxidative stress decreased to a lesser extent in the post-ischemic kidney; thus, end-stage renal failure developed over a long period.
4. Expression of numerous miRNAs was increased in the post-ischemic kidney that were downregulated by delayed contralateral nephrectomy; hence, downregulation of these miRNAs might play a role in the functional recovery of the post-ischemic kidney and/or halting its functional deterioration.

8. Summary

Acute kidney injury (AKI) is a common disease in hospitalized patients with high mortality. Chronic kidney disease (CKD) has a high prevalence and ever increasing mortality rate worldwide. Furthermore, patients with CKD often develop various co-morbidities further increasing the burden on patients and health care systems worldwide, hence the study of AKI and CKD is clinically important.

It is well-known that AKI frequently leads to CKD, although the exact pathomechanism is largely unknown. Several animal models were developed to study the pathophysiology of AKI-to-CKD transition. We utilized a model of severe unilateral renal ischemia-reperfusion injury with delayed contralateral nephrectomy one week later.

After contralateral nephrectomy the postischemic kidney hardly functioned but almost fully recovered within one to two weeks. Contralateral nephrectomy markedly reduced the expression of proinflammatory cytokines, chemokines and macrophage infiltration in the postischemic kidneys. Moreover, a marked decrease was detected in mRNAs expression of profibrotic genes and extracellular matrix accumulation. Better preservation of renal function and less interstitial fibrosis contributed to prolonged life span of mice up to 140 days, i.e. contralateral nephrectomy delayed the AKI-to-CKD transition. The performed studies indicate the pivotal role of TNF-α-CCL2-macrophage axis in the progression of AKI-to-CKD transition, while oxidative stress and hypoxia may play a smaller role in the development of CKD after AKI. MicroRNAs are implicated in the development of AKI and CKD. Indeed, severe ischemia-reperfusion injury upregulated the expression of several miRNAs. Contralateral nephrectomy counteracted these alterations with a delay of several days. Our miRNA network analysis predicted that the main targets of the differently expressed miRNAs are two podocyte slit diaphragm proteins, CD2-associated protein and Plexin A2. However, analysis of these proteins revealed no difference in their expression level in response to ischemia-reperfusion or delayed contralateral nephrectomy, suggesting, that other mechanisms may exert more substantial influence on their expression levels.

DOI:10.14753/SE.2022.2613

9. Összefoglalás

Az akut vesekárosodás egy gyakori, magas mortalitású megbetegedés a kórházi ápolást igénylő betegek esetében. A krónikus veseelégtelenség egy magas prevalenciájú, egyre növekvő mortalitási rátájú megbetegedés világszerte. A kónikus veseelégtelenségben szenvedő betegekben gyakran egyéb társbetegségek is kialakulnak további terhet róva mind a betegre, mind az egészségügyi rendszerre, így kutatásuk klinikai szempontból releváns.

Az akut vesekárosodás gyakran vezet krónikus veseelégtelenség kialakulásához, de ennek pontos patomehanizmusa jórészt ismeretlen. Több állat modellt is kidolgoztak az átmenet vizsgálatára. Kutatásaink során a súlyos egyoldali vese iszkémia-reperfúziós károsodás és egy héttel későbbi kontralaterális nefrektómia modellt alkalmaztuk.

Az ellenoldali nefrektómia után a poszt-iszkémiás vese alig volt funkcióképes, ám egy-két héten belül a működése szinte teljesen helyreállt. A kontralaterális nefrektómia nagymértékben csökkentette a proinflammatórikus citokinek, kemokinek expresszióját és a makrofág sejtek infiltrációját a poszt-iszkémiás vesében. Továbbá, jelentősen csökkent a profibrotikus génexpresszió és az extracelluláris matrix felhalmozódás. A vese funkció jobb állapotban való megőrződése és a kisebb mértékű interstíciális fibrózis hozzájárult a kísérleti egerek élethosszának a megnövekedéséhez akár 140 napig, azaz a késletett kontralaterális nefrektómia kitolta az akut vesekárosodás okozta krónikus veseelégtelenség kialakulásának idejét. Az elvégzett kísérletek alapján valószínűsíthető, hogy a TNF-α-CCL2-makrofág útvonalnak kiemelt szerepe van ezen átmenetben, míg a hypoxia és oxidatív stressz kisebb szerepet játszik benne.

A miRNS-ek szerepét több tanulmány is valószínűsíti az akut vesekárosodás és a krónikus veseelégtelenség kialakulásában. Valóban, az iszkémis-reperfúziós károsodás következtében több miRNS expressziója megemelkedett. A kontralaterális nefrektómia hatása pár nap késéssel csökkentette a miRNS expressziót. A miRNS útvonal elemzésünk alapján jósolt fő miRNS célfehérjék a podocita rés-diafragma alkotó CD-asszociált fehérje és a plexin A2 fehérje. Ám ezen fehérjék expressziója nem változott az iszkémia-reperfúziós károsodás és a késletett kontralaterális nefrektómia hatására, felvetve hogy más mechanizmusok nagyobb hatással bírnak ezen fehérjék szintjének a szabályozásában.

10. References

1. Khwaja A. (2012) KDIGO clinical practice guidelines for acute kidney injury. Nephron Clin Pract, 120: c179-184.
2. Makris K, Spanou L. (2016) Acute Kidney Injury: Diagnostic Approaches and Controversies. Clin Biochem Rev, 37: 153-175.
3. Edelstein CL. (2008) Biomarkers of acute kidney injury. Adv Chronic Kidney Dis, 15: 222-234.
4. Hoste EAJ, Kellum JA, Selby NM, Zarbock A, Palevsky PM, Bagshaw SM, Goldstein SL, Cerda J, Chawla LS. (2018) Global epidemiology and outcomes of acute kidney injury. Nat Rev Nephrol, 14: 607-625.
5. Thongprayoon C, Hansrivijit P, Kovvuru K, Kanduri SR, Torres-Ortiz A, Acharya P, Gonzalez-Suarez ML, Kaewput W, Bathini T, Cheungpasitporn W. (2020) Diagnostics, Risk Factors, Treatment and Outcomes of Acute Kidney Injury in a New Paradigm. J Clin Med, 9: 1104-1126.
6. Susantitaphong P, Cruz DN, Cerda J, Abulfaraj M, Alqahtani F, Koulouridis I, Jaber BL. (2013) World incidence of AKI: a meta-analysis. Clin J Am Soc Nephrol, 8: 1482-1493.
7. Makris K, Spanou L. (2016) Acute Kidney Injury: Definition, Pathophysiology and Clinical Phenotypes. Clin Biochem Rev, 37: 85-98.
8. Bonventre JV, Yang L. (2011) Cellular pathophysiology of ischemic acute kidney injury. J Clin Invest, 121: 4210-4221.
9. O'Connor PM. (2006) Renal oxygen delivery: matching delivery to metabolic demand. Clin Exp Pharmacol Physiol, 33: 961-967.
10. Chouchani ET, Pell VR, James AM, Work LM, Saeb-Parsy K, Frezza C, Krieg T, Murphy MP. (2016) A Unifying Mechanism for Mitochondrial Superoxide Production during Ischemia-Reperfusion Injury. Cell Metab, 23: 254-263.
11. Fischer K, Meral FC, Zhang Y, Vangel MG, Jolesz FA, Ichimura T, Bonventre JV. (2016) High-resolution renal perfusion mapping using contrast-enhanced ultrasonography in ischemia-reperfusion injury monitors changes in renal microperfusion. Kidney Int, 89: 1388-1398.

12. Sutton TA. (2009) Alteration of microvascular permeability in acute kidney injury. Microvasc Res, 77: 4-7.
13. Heyman SN, Rosenberger C, Rosen S. (2010) Experimental ischemia-reperfusion: biases and myths-the proximal vs. distal hypoxic tubular injury debate revisited. Kidney Int, 77: 9-16.
14. Kaucsar T, Godo M, Revesz C, Kovacs M, Mocsai A, Kiss N, Albert M, Krenacs T, Szenasi G, Hamar P. (2016) Urine/Plasma Neutrophil Gelatinase Associated Lipocalin Ratio Is a Sensitive and Specific Marker of Subclinical Acute Kidney Injury in Mice. PLoS One, 11: e0148043-e0148058.
15. Wei Q, Dong Z. (2012) Mouse model of ischemic acute kidney injury: technical notes and tricks. Am J Physiol Renal Physiol, 303: F1487-1494.
16. Dong Y, Zhang Q, Wen J, Chen T, He L, Wang Y, Yin J, Wu R, Xue R, Li S, Fan Y, Wang N. (2019) Ischemic Duration and Frequency Determines AKI-to-CKD Progression Monitored by Dynamic Changes of Tubular Biomarkers in IRI Mice. Front Physiol, 10: 153.
17. Cao W, Cui S, Yang L, Wu C, Liu J, Yang F, Liu Y, Bin J, Hou FF. (2017) Contrast-Enhanced Ultrasound for Assessing Renal Perfusion Impairment and Predicting Acute Kidney Injury to Chronic Kidney Disease Progression. Antioxid Redox Signal, 27: 1397-1411.
18. Chang-Panesso M, Humphreys BD. (2016) Cellular plasticity in kidney injury and repair. Nature Reviews Nephrology, 13: 39-46.
19. Kumar S. (2018) Cellular and molecular pathways of renal repair after acute kidney injury. Kidney Int, 93: 27-40.
20. Venkatachalam MA, Weinberg JM, Kriz W, Bidani AK. (2015) Failed Tubule Recovery, AKI-CKD Transition, and Kidney Disease Progression. J Am Soc Nephrol, 26: 1765-1776.
21. Rabb H, Griffin MD, McKay DB, Swaminathan S, Pickkers P, Rosner MH, Kellum JA, Ronco C, Acute Dialysis Quality Initiative Consensus XWG. (2016) Inflammation in AKI: Current Understanding, Key Questions, and Knowledge Gaps. J Am Soc Nephrol, 27: 371-379.
22. Kurts C, Panzer U, Anders HJ, Rees AJ. (2013) The immune system and kidney disease: basic concepts and clinical implications. Nat Rev Immunol, 13: 738-753.

23. Chung AC, Lan HY. (2011) Chemokines in renal injury. J Am Soc Nephrol, 22: 802-809.
24. Devarajan P. (2006) Update on mechanisms of ischemic acute kidney injury. J Am Soc Nephrol, 17: 1503-1520.
25. Li L, Okusa MD. (2010) Macrophages, dendritic cells, and kidney ischemia-reperfusion injury. Semin Nephrol, 30: 268-277.
26. Chen T, Cao Q, Wang Y, Harris DCH. (2019) M2 macrophages in kidney disease: biology, therapies, and perspectives. Kidney Int, 95: 760-773.
27. Lee S, Huen S, Nishio H, Nishio S, Lee HK, Choi BS, Ruhrberg C, Cantley LG. (2011) Distinct macrophage phenotypes contribute to kidney injury and repair. J Am Soc Nephrol, 22: 317-326.
28. McCullough JW, Renner B, Thurman JM. (2013) The role of the complement system in acute kidney injury. Semin Nephrol, 33: 543-556.
29. Zuk A, Bonventre JV. (2016) Acute Kidney Injury. Annu Rev Med, 67: 293-307.
30. Schödel J, Ratcliffe PJ. (2019) Mechanisms of hypoxia signalling: new implications for nephrology. Nature Reviews Nephrology, 15: 641-659.
31. Shu S, Wang Y, Zheng M, Liu Z, Cai J, Tang C, Dong Z. (2019) Hypoxia and Hypoxia-Inducible Factors in Kidney Injury and Repair. Cells, 8: 207-227.
32. Tomsa AM, Alexa AL, Junie ML, Rachisan AL, Ciumarnean L. (2019) Oxidative stress as a potential target in acute kidney injury. PeerJ, 7: e8046-e8066.
33. Nezu M, Suzuki N. (2020) Roles of Nrf2 in Protecting the Kidney from Oxidative Damage. Int J Mol Sci, 21: 2951-2968.
34. Liu M, Grigoryev DN, Crow MT, Haas M, Yamamoto M, Reddy SP, Rabb H. (2009) Transcription factor Nrf2 is protective during ischemic and nephrotoxic acute kidney injury in mice. Kidney Int, 76: 277-285.
35. Basile DP, Bonventre JV, Mehta R, Nangaku M, Unwin R, Rosner MH, Kellum JA, Ronco C, Group AXW. (2016) Progression after AKI: Understanding Maladaptive Repair Processes to Predict and Identify Therapeutic Treatments. J Am Soc Nephrol, 27: 687-697.
36. Coca SG, Singanamala S, Parikh CR. (2012) Chronic kidney disease after acute kidney injury: a systematic review and meta-analysis. Kidney Int, 81: 442-448.

37. Guzzi F, Cirillo L, Roperto RM, Romagnani P, Lazzeri E. (2019) Molecular Mechanisms of the Acute Kidney Injury to Chronic Kidney Disease Transition: An Updated View. Int J Mol Sci, 20: 4941-4955.
38. Xavier S, Vasko R, Matsumoto K, Zullo JA, Chen R, Maizel J, Chander PN, Goligorsky MS. (2015) Curtailing endothelial TGF-beta signaling is sufficient to reduce endothelial-mesenchymal transition and fibrosis in CKD. J Am Soc Nephrol, 26: 817-829.
39. Lech M, Grobmayr R, Ryu M, Lorenz G, Hartter I, Mulay SR, Susanti HE, Kobayashi KS, Flavell RA, Anders HJ. (2014) Macrophage phenotype controls long-term AKI outcomes--kidney regeneration versus atrophy. J Am Soc Nephrol, 25: 292-304.
40. Stevens PE, Levin A, Kidney Disease: Improving Global Outcomes Chronic Kidney Disease Guideline Development Work Group M. (2013) Evaluation and management of chronic kidney disease: synopsis of the kidney disease: improving global outcomes 2012 clinical practice guideline. Ann Intern Med, 158: 825-830.
41. Romagnani P, Remuzzi G, Glassock R, Levin A, Jager KJ, Tonelli M, Massy Z, Wanner C, Anders HJ. (2017) Chronic kidney disease. Nat Rev Dis Primers, 3.
42. Rysz J, Gluba-Brzozka A, Franczyk B, Jablonowski Z, Cialkowska-Rysz A. (2017) Novel Biomarkers in the Diagnosis of Chronic Kidney Disease and the Prediction of Its Outcome. Int J Mol Sci, 18: 1702-1718.
43. Hill NR, Fatoba ST, Oke JL, Hirst JA, O'Callaghan CA, Lasserson DS, Hobbs FD. (2016) Global Prevalence of Chronic Kidney Disease - A Systematic Review and Meta-Analysis. PLoS One, 11: e0158765-e0158782.
44. Bikbov B, Purcell CA, Levey AS, Smith M, Abdoli A, Abebe M, Adebayo OM, Afarideh M, Agarwal SK, Agudelo-Botero M, Ahmadian E, Al-Aly Z, Alipour V, Almasi-Hashiani A, Al-Raddadi RM, Alvis-Guzman N, Amini S, Andrei T, Andrei CL, Andualem Z, Anjomshoa M, Arabloo J, Ashagre AF, Asmelash D, Ataro Z, Atout MMdW, Ayanore MA, Badawi A, Bakhtiari A, Ballew SH, Balouchi A, Banach M, Barquera S, Basu S, Bayih MT, Bedi N, Bello AK, Bensenor IM, Bijani A, Boloor A, Borzì AM, Cámera LA, Carrero JJ, Carvalho F, Castro F, Catalá-López F, Chang AR, Chin KL, Chung S-C, Cirillo M, Cousin E, Dandona L, Dandona R, Daryani A, Das Gupta R, Demeke FM, Demoz GT,

Desta DM, Do HP, Duncan BB, Eftekhari A, Esteghamati A, Fatima SS, Fernandes JC, Fernandes E, Fischer F, Freitas M, Gad MM, Gebremeskel GG, Gebresillassie BM, Geta B, Ghafourifard M, Ghajar A, Ghith N, Gill PS, Ginawi IA, Gupta R, Hafezi-Nejad N, Haj-Mirzaian A, Haj-Mirzaian A, Hariyani N, Hasan M, Hasankhani M, Hasanzadeh A, Hassen HY, Hay SI, Heidari B, Herteliu C, Hoang CL, Hosseini M, Hostiuc M, Irvani SSN, Islam SMS, Jafari Balalami N, James SL, Jassal SK, Jha V, Jonas JB, Joukar F, Jozwiak JJ, Kabir A, Kahsay A, Kasaeian A, Kassa TD, Kassaye HG, Khader YS, Khalilov R, Khan EA, Khan MS, Khang Y-H, Kisa A, Kovesdy CP, Kuate Defo B, Kumar GA, Larsson AO, Lim L-L, Lopez AD, Lotufo PA, Majeed A, Malekzadeh R, März W, Masaka A, Meheretu HAA, Miazgowski T, Mirica A, Mirrakhimov EM, Mithra P, Moazen B, Mohammad DK, Mohammadpourhodki R, Mohammed S, Mokdad AH, Morales L, Moreno Velasquez I, Mousavi SM, Mukhopadhyay S, Nachega JB, Nadkarni GN, Nansseu JR, Natarajan G, Nazari J, Neal B, Negoi RI, Nguyen CT, Nikbakhsh R, Noubiap JJ, Nowak C, Olagunju AT, Ortiz A, Owolabi MO, Palladino R, Pathak M, Poustchi H, Prakash S, Prasad N, Rafiei A, Raju SB, Ramezanzadeh K, Rawaf S, Rawaf DL, Rawal L, Reiner RC, Rezapour A, Ribeiro DC, Roever L, Rothenbacher D, Rwegerera GM, Saadatagah S, Safari S, Sahle BW, Salem H, Sanabria J, Santos IS, Sarveazad A, Sawhney M, Schaeffner E, Schmidt MI, Schutte AE, Sepanlou SG, Shaikh MA, Sharafi Z, Sharif M, Sharifi A, Silva DAS, Singh JA, Singh NP, Sisay MMM, Soheili A, Sutradhar I, Teklehaimanot BF, Tesfay Be, Teshome GF, Thakur JS, Tonelli M, Tran KB, Tran BX, Tran Ngoc C, Ullah I, Valdez PR, Varughese S, Vos T, Vu LG, Waheed Y, Werdecker A, Wolde HF, Wondmieneh AB, Wulf Hanson S, Yamada T, Yeshaw Y, Yonemoto N, Yusefzadeh H, Zaidi Z, Zaki L, Zaman SB, Zamora N, Zarghi A, Zewdie KA, Ärnlöv J, Coresh J, Perico N, Remuzzi G, Murray CJL, Vos T. (2020) Global, regional, and national burden of chronic kidney disease, 1990–2017: a systematic analysis for the Global Burden of Disease Study 2017. The Lancet, 395: 709-733.

45. Webster AC, Nagler EV, Morton RL, Masson P. (2017) Chronic Kidney Disease. The Lancet, 389: 1238-1252.

46. Schelling JR. (2016) Tubular atrophy in the pathogenesis of chronic kidney disease progression. Pediatr Nephrol, 31: 693-706.
47. Meng XM, Nikolic-Paterson DJ, Lan HY. (2014) Inflammatory processes in renal fibrosis. Nat Rev Nephrol, 10: 493-503.
48. Klingberg F, Hinz B, White ES. (2013) The myofibroblast matrix: implications for tissue repair and fibrosis. J Pathol, 229: 298-309.
49. Meng XM, Nikolic-Paterson DJ, Lan HY. (2016) TGF-beta: the master regulator of fibrosis. Nat Rev Nephrol, 12: 325-338.
50. Yang L, Besschetnova TY, Brooks CR, Shah JV, Bonventre JV. (2010) Epithelial cell cycle arrest in G2/M mediates kidney fibrosis after injury. Nat Med, 16: 535-543.
51. Ruiz-Ortega M, Rayego-Mateos S, Lamas S, Ortiz A, Rodrigues-Diez RR. (2020) Targeting the progression of chronic kidney disease. Nat Rev Nephrol, 16: 269-288.
52. Gebert LFR, MacRae IJ. (2019) Regulation of microRNA function in animals. Nat Rev Mol Cell Biol, 20: 21-37.
53. O'Brien J, Hayder H, Zayed Y, Peng C. (2018) Overview of MicroRNA Biogenesis, Mechanisms of Actions, and Circulation. Front Endocrinol (Lausanne), 9: 402.
54. Racz Z, Kaucsar T, Hamar P. (2011) The huge world of small RNAs: regulating networks of microRNAs (review). Acta Physiol Hung, 98: 243-251.
55. Phua YL, Clugston A, Chen KH, Kostka D, Ho J. (2018) Small non-coding RNA expression in mouse nephrogenic mesenchymal progenitors. Sci Data, 5: 180218.
56. Marrone AK, Stolz DB, Bastacky SI, Kostka D, Bodnar AJ, Ho J. (2014) MicroRNA-17~92 is required for nephrogenesis and renal function. J Am Soc Nephrol, 25: 1440-1452.
57. Chandrasekaran K, Karolina DS, Sepramaniam S, Armugam A, Wintour EM, Bertram JF, Jeyaseelan K. (2012) Role of microRNAs in kidney homeostasis and disease. Kidney Int, 81: 617-627.
58. Brandenburger T, Salgado Somoza A, Devaux Y, Lorenzen JM. (2018) Noncoding RNAs in acute kidney injury. Kidney Int, 94: 870-881.

59. Fourdinier O, Schepers E, Metzinger-Le Meuth V, Glorieux G, Liabeuf S, Verbeke F, Vanholder R, Brigant B, Pletinck A, Diouf M, Burtey S, Choukroun G, Massy ZA, Metzinger L, European Uremic Toxin Work Group E. (2019) Serum levels of miR-126 and miR-223 and outcomes in chronic kidney disease patients. Sci Rep, 9.
60. Chung AC, Lan HY. (2015) MicroRNAs in renal fibrosis. Front Physiol, 6: 50.
61. Fan Y, Chen H, Huang Z, Zheng H, Zhou J. (2020) Emerging role of miRNAs in renal fibrosis. RNA Biol, 17: 1-12.
62. Hao J, Wei Q, Mei S, Li L, Su Y, Mei C, Dong Z. (2017) Induction of microRNA-17-5p by p53 protects against renal ischemia-reperfusion injury by targeting death receptor 6. Kidney Int, 91: 106-118.
63. Hu H, Jiang W, Xi X, Zou C, Ye Z. (2014) MicroRNA-21 Attenuates Renal Ischemia Reperfusion Injury via Targeting Caspase Signaling in Mice. American Journal of Nephrology, 40: 215-223.
64. Lorenzen JM, Kaucsar T, Schauerte C, Schmitt R, Rong S, Hubner A, Scherf K, Fiedler J, Martino F, Kumarswamy R, Kolling M, Sorensen I, Hinz H, Heineke J, van Rooij E, Haller H, Thum T. (2014) MicroRNA-24 antagonism prevents renal ischemia reperfusion injury. J Am Soc Nephrol, 25: 2717-2729.
65. Ortiz A, Sanchez-Nino MD, Izquierdo MC, Martin-Cleary C, Garcia-Bermejo L, Moreno JA, Ruiz-Ortega M, Draibe J, Cruzado JM, Garcia-Gonzalez MA, Lopez-Novoa JM, Soler MJ, Sanz AB, Red de Investigacion R, Consorcio Madrileno para investigacion del fracaso renal a. (2015) Translational value of animal models of kidney failure. Eur J Pharmacol, 759: 205-220.
66. Qiu L, Zhang ZJ. (2019) Therapeutic Strategies of Kidney Transplant Ischemia Reperfusion Injury: Insight From Mouse Models. Biomed J Sci Tech Res, 14: 002617-002623.
67. Sanz AB, Sanchez-Nino MD, Martin-Cleary C, Ortiz A, Ramos AM. (2013) Progress in the development of animal models of acute kidney injury and its impact on drug discovery. Expert Opin Drug Discov, 8: 879-895.
68. Holderied A, Kraft F, Marschner JA, Weidenbusch M, Anders HJ. (2020) "Point of no return" in unilateral renal ischemia reperfusion injury in mice. J Biomed Sci, 27: 34.

69. Hesketh EE, Czopek A, Clay M, Borthwick G, Ferenbach D, Kluth D, Hughes J. (2014) Renal ischaemia reperfusion injury: a mouse model of injury and regeneration. J Vis Exp: e51816-e51823.

70. Skrypnyk NI, Harris RC, de Caestecker MP. (2013) Ischemia-reperfusion model of acute kidney injury and post injury fibrosis in mice. J Vis Exp: e50495-e50500.

71. Ucero AC, Benito-Martin A, Izquierdo MC, Sanchez-Nino MD, Sanz AB, Ramos AM, Berzal S, Ruiz-Ortega M, Egido J, Ortiz A. (2014) Unilateral ureteral obstruction: beyond obstruction. Int Urol Nephrol, 46: 765-776.

72. Walkin L, Herrick SE, Summers A, Brenchley PE, Hoff CM, Korstanje R, Margetts PJ. (2013) The role of mouse strain differences in the susceptibility to fibrosis: a systematic review. Fibrogenesis Tissue Repair, 6: 18.

73. Franzen S, Friederich-Persson M, Fasching A, Hansell P, Nangaku M, Palm F. (2014) Differences in susceptibility to develop parameters of diabetic nephropathy in four mouse strains with type 1 diabetes. Am J Physiol Renal Physiol, 306: F1171-1178.

74. Burkholder T, Foltz C, Karlsson E, Linton CG, Smith JM. (2012) Health Evaluation of Experimental Laboratory Mice. Curr Protoc Mouse Biol, 2: 145-165.

75. Tod P, Bukosza EN, Roka B, Kaucsar T, Fintha A, Krenacs T, Szenasi G, Hamar P. (2020) Post-Ischemic Renal Fibrosis Progression Is Halted by Delayed Contralateral Nephrectomy: The Involvement of Macrophage Activation. Int J Mol Sci, 21: 3825-3842.

76. Roka B, Tod P, Kaucsar T, Bukosza EN, Voros I, Varga ZV, Petrovich B, Agg B, Ferdinandy P, Szenasi G, Hamar P. (2021) Delayed Contralateral Nephrectomy Halted Post-Ischemic Renal Fibrosis Progression and Inhibited the Ischemia-Induced Fibromir Upregulation in Mice. Biomedicines, 9: 815-833.

77. Edgar R, Domrachev M, Lash AE. (2002) Gene Expression Omnibus: NCBI gene expression and hybridization array data repository. Nucleic Acids Res, 30: 207-210.

78. Andersen CL, Jensen JL, Orntoft TF. (2004) Normalization of real-time quantitative reverse transcription-PCR data: a model-based variance estimation

approach to identify genes suited for normalization, applied to bladder and colon cancer data sets. Cancer Res, 64: 5245-5250.

79. Amann K, Koch A, Hofstetter J, Gross ML, Haas C, Orth SR, Ehmke H, Rump LC, Ritz E. (2001) Glomerulosclerosis and progression: effect of subantihypertensive doses of alpha and beta blockers. Kidney Int, 60: 1309-1323.

80. Schindelin J, Arganda-Carreras I, Frise E, Kaynig V, Longair M, Pietzsch T, Preibisch S, Rueden C, Saalfeld S, Schmid B, Tinevez JY, White DJ, Hartenstein V, Eliceiri K, Tomancak P, Cardona A. (2012) Fiji: an open-source platform for biological-image analysis. Nat Methods, 9: 676-682.

81. Chou CH, Shrestha S, Yang CD, Chang NW, Lin YL, Liao KW, Huang WC, Sun TH, Tu SJ, Lee WH, Chiew MY, Tai CS, Wei TY, Tsai TR, Huang HT, Wang CY, Wu HY, Ho SY, Chen PR, Chuang CH, Hsieh PJ, Wu YS, Chen WL, Li MJ, Wu YC, Huang XY, Ng FL, Buddhakosai W, Huang PC, Lan KC, Huang CY, Weng SL, Cheng YN, Liang C, Hsu WL, Huang HD. (2018) miRTarBase update 2018: a resource for experimentally validated microRNA-target interactions. Nucleic Acids Res, 46: D296-D302.

82. Chen Y, Wang X. (2020) miRDB: an online database for prediction of functional microRNA targets. Nucleic Acids Res, 48: D127-D131.

83. Agarwal V, Bell GW, Nam JW, Bartel DP. (2015) Predicting effective microRNA target sites in mammalian mRNAs. Elife, 4: e05005-e05042.

84. Agg B, Csaszar A, Szalay-Beko M, Veres DV, Mizsei R, Ferdinandy P, Csermely P, Kovacs IA. (2019) The EntOptLayout Cytoscape plug-in for the efficient visualization of major protein complexes in protein-protein interaction and signalling networks. Bioinformatics, 35: 4490-4492.

85. Kucsera D, Toth VE, Gergo D, Voros I, Onodi Z, Gorbe A, Ferdinandy P, Varga ZV. (2021) Characterization of the CDAA Diet-Induced Non-alcoholic Steatohepatitis Model: Sex-Specific Differences in Inflammation, Fibrosis, and Cholesterol Metabolism in Middle-Aged Mice. Front Physiol, 12: 609465-609476.

86. Motulsky HJ, Brown RE. (2006) Detecting outliers when fitting data with nonlinear regression - a new method based on robust nonlinear regression and the false discovery rate. BMC Bioinformatics, 7: 123.

87. Skrypnyk NI, Voziyan P, Yang H, de Caestecker CR, Theberge MC, Drouin M, Hudson B, Harris RC, de Caestecker MP. (2016) Pyridoxamine reduces postinjury fibrosis and improves functional recovery after acute kidney injury. Am J Physiol Renal Physiol, 311: F268-277.

88. Polichnowski AJ, Griffin KA, Licea-Vargas H, Lan R, Picken MM, Long J, Williamson GA, Rosenberger C, Mathia S, Venkatachalam MA, Bidani AK. (2020) Pathophysiology of unilateral ischemia-reperfusion injury: importance of renal counterbalance and implications for the AKI-CKD transition. Am J Physiol Renal Physiol, 318: F1086-F1099.

89. Soranno DE, Gil HW, Kirkbride-Romeo L, Altmann C, Montford JR, Yang H, Levine A, Buchanan J, Faubel S. (2019) Matching Human Unilateral AKI, a Reverse Translational Approach to Investigate Kidney Recovery after Ischemia. J Am Soc Nephrol, 30: 990-1005.

90. Chancharoenthana W, Leelahavanichkul A, Taratummarat S, Wongphom J, Tiranathanagul K, Eiam-Ong S. (2017) Cilostazol attenuates intimal hyperplasia in a mouse model of chronic kidney disease. PLoS One, 12: e0187872-e0187890.

91. Jung M, Brune B, Hotter G, Sola A. (2016) Macrophage-derived Lipocalin-2 contributes to ischemic resistance mechanisms by protecting from renal injury. Sci Rep, 6.

92. Sola A, Weigert A, Jung M, Vinuesa E, Brecht K, Weis N, Brune B, Borregaard N, Hotter G. (2011) Sphingosine-1-phosphate signalling induces the production of Lcn-2 by macrophages to promote kidney regeneration. J Pathol, 225: 597-608.

93. Furuichi K, Wada T, Iwata Y, Kitagawa K, Kobayashi K, Hashimoto H, Ishiwata Y, Asano M, Wang H, Matsushima K, Takeya M, Kuziel WA, Mukaida N, Yokoyama H. (2003) CCR2 signaling contributes to ischemia-reperfusion injury in kidney. J Am Soc Nephrol, 14: 2503-2515.

94. Kim MG, Kim SC, Ko YS, Lee HY, Jo SK, Cho W. (2015) The Role of M2 Macrophages in the Progression of Chronic Kidney Disease following Acute Kidney Injury. PLoS One, 10: e0143961-e0143977.

95. Peng Q, Li K, Smyth LA, Xing G, Wang N, Meader L, Lu B, Sacks SH, Zhou W. (2012) C3a and C5a promote renal ischemia-reperfusion injury. J Am Soc Nephrol, 23: 1474-1485.

96. Danobeitia JS, Ziemelis M, Ma X, Zitur LJ, Zens T, Chlebeck PJ, Van Amersfoort ES, Fernandez LA. (2017) Complement inhibition attenuates acute kidney injury after ischemia-reperfusion and limits progression to renal fibrosis in mice. PLoS One, 12: e0183701-e0183720.

97. Cui J, Wu X, Song Y, Chen Y, Wan J. (2019) Complement C3 exacerbates renal interstitial fibrosis by facilitating the M1 macrophage phenotype in a mouse model of unilateral ureteral obstruction. Am J Physiol Renal Physiol, 317: F1171-F1182.

98. Liu Y, Wang K, Liang X, Li Y, Zhang Y, Zhang C, Wei H, Luo R, Ge S, Xu G. (2018) Complement C3 Produced by Macrophages Promotes Renal Fibrosis via IL-17A Secretion. Front Immunol, 9: 2385.

99. Su H, Lei CT, Zhang C. (2017) Interleukin-6 Signaling Pathway and Its Role in Kidney Disease: An Update. Front Immunol, 8: 405.

100. Koh MY, Powis G. (2012) Passing the baton: the HIF switch. Trends Biochem Sci, 37: 364-372.

101. Kapitsinou PP, Jaffe J, Michael M, Swan CE, Duffy KJ, Erickson-Miller CL, Haase VH. (2012) Preischemic targeting of HIF prolyl hydroxylation inhibits fibrosis associated with acute kidney injury. Am J Physiol Renal Physiol, 302: F1172-1179.

102. Kimura K, Iwano M, Higgins DF, Yamaguchi Y, Nakatani K, Harada K, Kubo A, Akai Y, Rankin EB, Neilson EG, Haase VH, Saito Y. (2008) Stable expression of HIF-1alpha in tubular epithelial cells promotes interstitial fibrosis. Am J Physiol Renal Physiol, 295: F1023-1029.

103. Kabei K, Tateishi Y, Nozaki M, Tanaka M, Shiota M, Osada-Oka M, Nishide S, Uchida J, Nakatani T, Tomita S, Miura K. (2018) Role of hypoxia-inducible factor-1 in the development of renal fibrosis in mouse obstructed kidney: Special references to HIF-1 dependent gene expression of profibrogenic molecules. J Pharmacol Sci, 136: 31-38.

104. Kong KH, Oh HJ, Lim BJ, Kim M, Han KH, Choi YH, Kwon K, Nam BY, Park KS, Park JT, Han SH, Yoo TH, Lee S, Kim SJ, Kang DH, Choi KB, Eremina V, Quaggin SE, Ryu DR, Kang SW. (2017) Selective tubular activation of hypoxia-inducible factor-2alpha has dual effects on renal fibrosis. Sci Rep, 7: 11351.

105. Tan RJ, Liu Y. (2013) Macrophage-derived TGF-beta in renal fibrosis: not a macro-impact after all. Am J Physiol Renal Physiol, 305: F821-822.
106. Meng XM, Tang PM, Li J, Lan HY. (2015) TGF-beta/Smad signaling in renal fibrosis. Front Physiol, 6: 82.
107. Wei Q, Mi QS, Dong Z. (2013) The regulation and function of microRNAs in kidney diseases. IUBMB Life, 65: 602-614.
108. Zhao H, Ma SX, Shang YQ, Zhang HQ, Su W. (2019) microRNAs in chronic kidney disease. Clin Chim Acta, 491: 59-65.
109. Nersisyan S, Shkurnikov M, Poloznikov A, Turchinovich A, Burwinkel B, Anisimov N, Tonevitsky A. (2020) A Post-Processing Algorithm for miRNA Microarray Data. Int J Mol Sci, 21: 1228-1236.
110. Jensen SG, Lamy P, Rasmussen MH, Ostenfeld MS, Dyrskjot L, Orntoft TF, Andersen CL. (2011) Evaluation of two commercial global miRNA expression profiling platforms for detection of less abundant miRNAs. BMC Genomics, 12.
111. el Azzouzi H, Leptidis S, Dirkx E, Hoeks J, van Bree B, Brand K, McClellan EA, Poels E, Sluimer JC, van den Hoogenhof MM, Armand AS, Yin X, Langley S, Bourajjaj M, Olieslagers S, Krishnan J, Vooijs M, Kurihara H, Stubbs A, Pinto YM, Krek W, Mayr M, da Costa Martins PA, Schrauwen P, De Windt LJ. (2013) The hypoxia-inducible microRNA cluster miR-199a approximately 214 targets myocardial PPARdelta and impairs mitochondrial fatty acid oxidation. Cell Metab, 18: 341-354.
112. Kumarswamy R, Volkmann I, Thum T. (2011) Regulation and function of miRNA-21 in health and disease. RNA Biol, 8: 706-713.
113. Amrouche L, Desbuissons G, Rabant M, Sauvaget V, Nguyen C, Benon A, Barre P, Rabate C, Lebreton X, Gallazzini M, Legendre C, Terzi F, Anglicheau D. (2017) MicroRNA-146a in Human and Experimental Ischemic AKI: CXCL8-Dependent Mechanism of Action. J Am Soc Nephrol, 28: 479-493.
114. Ichii O, Otsuka S, Sasaki N, Namiki Y, Hashimoto Y, Kon Y. (2012) Altered expression of microRNA miR-146a correlates with the development of chronic renal inflammation. Kidney Int, 81: 280-292.

115. Godwin JG, Ge X, Stephan K, Jurisch A, Tullius SG, Iacomini J. (2010) Identification of a microRNA signature of renal ischemia reperfusion injury. Proc Natl Acad Sci U S A, 107: 14339-14344.

116. Chau BN, Xin C, Hartner J, Ren S, Castano AP, Linn G, Li J, Tran PT, Kaimal V, Huang X, Chang AN, Li S, Kalra A, Grafals M, Portilla D, MacKenna DA, Orkin SH, Duffield JS. (2012) MicroRNA-21 promotes fibrosis of the kidney by silencing metabolic pathways. Sci Transl Med, 4: 121ra118.

117. Song N, Zhang T, Xu X, Lu Z, Yu X, Fang Y, Hu J, Jia P, Teng J, Ding X. (2018) miR-21 Protects Against Ischemia/Reperfusion-Induced Acute Kidney Injury by Preventing Epithelial Cell Apoptosis and Inhibiting Dendritic Cell Maturation. Front Physiol, 9: 790.

118. Chen R, Alvero AB, Silasi DA, Kelly MG, Fest S, Visintin I, Leiser A, Schwartz PE, Rutherford T, Mor G. (2008) Regulation of IKKbeta by miR-199a affects NF-kappaB activity in ovarian cancer cells. Oncogene, 27: 4712-4723.

119. Peng J, Jiang J, Wang H, Feng X, Dong X. (2020) miR199a3p suppresses cervical epithelial cell inflammation by inhibiting the HMGB1/TLR4/NFkappaB pathway in preterm birth. Mol Med Rep, 22: 926-938.

120. Wu H, Ma J, Wang P, Corpuz TM, Panchapakesan U, Wyburn KR, Chadban SJ. (2010) HMGB1 contributes to kidney ischemia reperfusion injury. J Am Soc Nephrol, 21: 1878-1890.

121. Wang C, Zhu G, He W, Yin H, Lin F, Gou X, Li X. (2019) BMSCs protect against renal ischemia-reperfusion injury by secreting exosomes loaded with miR-199a-5p that target BIP to inhibit endoplasmic reticulum stress at the very early reperfusion stages. FASEB J, 33: 5440-5456.

122. Cybulsky AV. (2017) Endoplasmic reticulum stress, the unfolded protein response and autophagy in kidney diseases. Nature Reviews Nephrology, 13: 681-696.

123. Lino Cardenas CL, Henaoui IS, Courcot E, Roderburg C, Cauffiez C, Aubert S, Copin MC, Wallaert B, Glowacki F, Dewaeles E, Milosevic J, Maurizio J, Tedrow J, Marcet B, Lo-Guidice JM, Kaminski N, Barbry P, Luedde T, Perrais M, Mari B, Pottier N. (2013) miR-199a-5p Is upregulated during fibrogenic response to

tissue injury and mediates TGFbeta-induced lung fibroblast activation by targeting caveolin-1. PLoS Genet, 9: e1003291-e1003314.

124. Chen J, Cui Y, Zhang N, Yao X, Wang Z, Yang L. (2019) Oleanolic acid attenuated diabetic mesangial cell injury by activation of autophagy via miRNA-142-5p/PTEN signaling. Cytotechnology, 71: 925-933.

125. Zhu X, Li W, Li H. (2018) miR-214 ameliorates acute kidney injury via targeting DKK3 and activating of Wnt/beta-catenin signaling pathway. Biol Res, 51.

126. Yan Y, Ma Z, Zhu J, Zeng M, Liu H, Dong Z. (2020) miR-214 represses mitofusin-2 to promote renal tubular apoptosis in ischemic acute kidney injury. Am J Physiol Renal Physiol, 318: F878-F887.

127. Bai M, Chen H, Ding D, Song R, Lin J, Zhang Y, Guo Y, Chen S, Ding G, Zhang Y, Jia Z, Huang S, He JC, Yang L, Zhang A. (2019) MicroRNA-214 promotes chronic kidney disease by disrupting mitochondrial oxidative phosphorylation. Kidney Int, 95: 1389-1404.

128. Denby L, Ramdas V, Lu R, Conway BR, Grant JS, Dickinson B, Aurora AB, McClure JD, Kipgen D, Delles C, van Rooij E, Baker AH. (2014) MicroRNA-214 antagonism protects against renal fibrosis. J Am Soc Nephrol, 25: 65-80.

129. Yuan X, Wang X, Chen C, Zhou J, Han M. (2017) Bone mesenchymal stem cells ameliorate ischemia/reperfusion-induced damage in renal epithelial cells via microRNA-223. Stem Cell Res Ther, 8.

130. Shih NY, Li J, Karpitskii V, Nguyen A, Dustin ML, Kanagawa O, Miner JH, Shaw AS. (1999) Congenital nephrotic syndrome in mice lacking CD2-associated protein. Science, 286: 312-315.

131. Chen Y, Lin L, Tao X, Song Y, Cui J, Wan J. (2019) The role of podocyte damage in the etiology of ischemia-reperfusion acute kidney injury and post-injury fibrosis. BMC Nephrol, 20: 106.

132. Xia J, Worzfeld T. (2016) Semaphorins and Plexins in Kidney Disease. Nephron, 132: 93-100.

133. Sabag AD, Smolkin T, Mumblat Y, Ueffing M, Kessler O, Gloeckner CJ, Neufeld G. (2014) The role of the plexin-A2 receptor in Sema3A and Sema3B signal transduction. J Cell Sci, 127: 5240-5252.

134. Ranganathan P, Jayakumar C, Mohamed R, Weintraub NL, Ramesh G. (2014) Semaphorin 3A inactivation suppresses ischemia-reperfusion-induced inflammation and acute kidney injury. Am J Physiol Renal Physiol, 307: F183-194.

11. Publication list

9.1 Publications used for the thesis

Tod P, Bukosza EN, Roka B, Kaucsar T, Fintha A, Krenacs T, Szenasi G, Hamar P. (2020) Post-Ischemic Renal Fibrosis Progression Is Halted by Delayed Contralateral Nephrectomy: The Involvement of Macrophage Activation. Int J Mol Sci, 21: 3825-3842.

Roka B, Tod P, Kaucsar T, Bukosza EN, Voros I, Varga ZV, Petrovich B, Agg B, Ferdinandy P, Szenasi G, Hamar P. (2021) Delayed Contralateral Nephrectomy Halted Post-Ischemic Renal Fibrosis Progression and Inhibited the Ischemia-Induced Fibromir Upregulation in Mice. Biomedicines, 9: 815-833.

9.2 Additional publications

Revesz C, Wasik AA, Godo M, Tod P, Lehtonen, S, Szenasi G, Hamar P. (2021) Cold Saline Perfusion before Ischemia-Reperfusion Is Harmful to the Kidney and Is Associated with the Loss of Ezrin, a Cytoskeletal Protein, in Rats. Biomedicines, 9:30-41.

Calovi S, Mut-Arbona P, Tod P, Iring A, Nicke A, Mato S, Vizi ES, Tonnesen J, Sperlagh B. (2021) P2X7 Receptor-Dependent Layer-Specific Changes in Neuron-Microglia Reactivity in the Prefrontal Cortex of a Phencyclidine Induced Mouse Model of Schizophrenia. Front Mol Neurosci, 13: 566251-566273.

Tod P, Roka B, Kaucsar T, Szatmari K, Vizovisek M, Vidmar R, Fonovic M, Szenasi G, Hamar P. (2020) Time-Dependent miRNA Profile during Septic Acute Kidney Injury in Mice. Int J Mol Sci, 21: 5316-5332.

Roka B, Tod P, Kaucsar T, Vizovisek M, Vidmar R, Turk B, Fonovic M, Szenasi G, Hamar P. (2020) The Acute Phase Response Is a Prominent Renal Proteome Change in Sepsis in Mice. Int J Mol Sci, 21: 200-219.

Bukosza EN, Kaucsar T, Godo M, Lajtar E, Tod P, Koncsos G, Varga ZV, Baranyai T, Tu NM, Schachner H, Soti C, Ferdinandy P, Giricz Z, Szenasi G, Hamar P. (2019) Glomerular Collagen Deposition and Lipocalin-2 Expression Are Early Signs of Renal Injury in Prediabetic Obese Rats. Int J Mol Sci, 20: 4266-4282.

11. Acknowledgements

I wish to express my gratitude to my supervisors, especially Dr. Gábor Szénási, who gave me the opportunity to conduct research in the Immuno-nephrology lab at Semmelweis University and provided invaluable guidance and suggestions at all stages of the research project. I am also deeply grateful to the former chairman of Doctoral School of Theoretical and Translational Medicine Professor László Rosivall and the President of the Doctoral Council Professor Zoltán Benyó who enrolled me in the PhD program.

I would like to express my sincere thanks to late Mária Godó, who always believed in me and introduced me the basic methods in molecular biology. I am also grateful to Dr. Tamás Kaucsár for his valuable insights and help in laboratory practices and PCR measurements. Furthermore, I wish to acknowledge the help and assistance of Dr. Éva Nóra Bukosza and Beáta Róka during my PhD. Their support is greatly appreciated. I wish to express my special thanks to Ildikó Virág, without her dedicated care of the animal house and assistance, these experiments would not have been performed. It was a great pleasure to work with her.

I also wish to thank my family for their endless support, especially for the unconditional support of late Erzsébet Bácsai during my study in the Eötvös Lóránd University.

Finally, I wish express my gratitude to my collages in the Institute of Experimental Medicine, who were of great help in writing my dissertation with their helpful insights and suggestions.